AD-A166 755 DESIGN DEVELOPMENT AND INTEGRATE/INSTALL AN AIRBORNE REMOTE INSTRUMENTATI..(U) AEROJET ELECTROSYSTEMS CO AZUSA CA J J BOMMARITO ET AL. AUG 85 7921 USCG-D-27-85 1/3

UNCLASSIFIED DTCG23-80-C-20012 F/G 1/3 NL

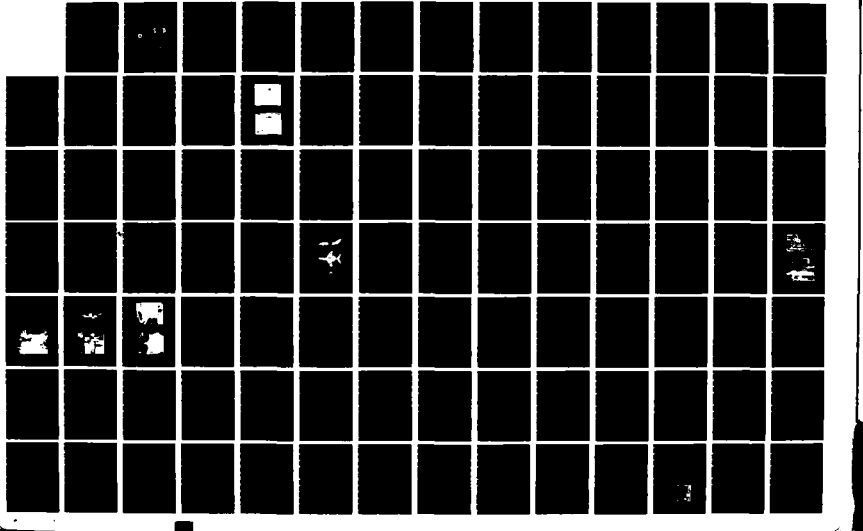

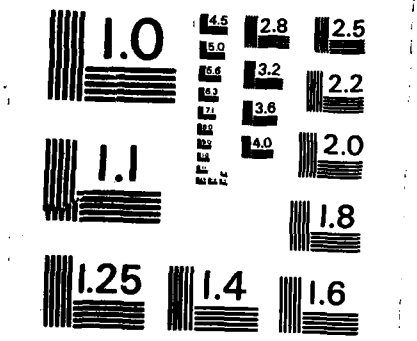

(12)

Report No. CG-D-27-85

DESIGN, DEVELOP AND INTEGRATE/INSTALL AN AIRBORNE REMOTE INSTRUMENTATION SYSTEM (AIREYE)

FINAL REPORT

AUGUST 1985

Prepared for:

U.S. Department of Transportation
United States Coast Guard

Office of Research and Development
Washington, D.C. 20593

NOTICE

This document is disseminated under the sponsorship of the Department of Transportation in the interest of information exchange. The United States Government assumes no liability for its contents or use thereof.

The contents of this report do not necessarily reflect the official view or policy of the Coast Guard; and they do not constitute a standard, specification, or regulation.

This report, or portions thereof may not be used for advertising or sales promotion purposes. Citation of trade names and manufacturers does not constitute endorsement or approval of such products.

Technical Report Documentation Page

1. Report No	2. Government Accession No	3. Recipient's Catalog No
CG-D-27-85	AD-A166 755	

4. Title and Subtitle	5. Report Date
Design, Develop and Integrate/Install an Airborne Remote Instrumentation System (AIREYE), Final Report	August 1985
	6. Performing Organization Code
	8. Performing Organization Report No
7. Author's	7921
J. J. Bommarito, L. E. Saylor	
9. Performing Organization Name and Address	10. Work Unit No. (TRAIS)
Aerojet ElectroSystems Company 1100 W. Hollyvale Street Azusa, California 91702	11. Contract or Grant No. DTCG23-80-C-20012
	13. Type of Report and Period Covered
12. Sponsoring Agency Name and Address	Final Report
Department of Transportation United States Coast Guard Office of Research and Development Washington, D.C. 20590	14. Sponsoring Agency Code

15. Supplementary Notes

16. Abstract

A prototype airborne remote instrument system, AIREYE, was developed for the U.S. Coast Guard by Aerojet ElectroSystems Company. This multisensor system permits real-time day/night, all weather detection, mapping and documentation of vessels and pollution at sea. The system was installed aboard a Coast Guard HU-25A Falcon fanjet aircraft and flight tested off the California coast. Surveillance data were obtained from natural oil seeps, known optical and radar targets, routine shipping and targets of opportunity.

The AIREYE system consists of a sidelooking radar, infrared/ultraviolet line scanner, active gated television system, aerial reconnaissance camera and a processor/display recording subsystem with real-time digital image enhancement capability.

The system reliably detected and mapped oil seeps and vessel locations for environmental conditions ranging from dense undercast to clear, windspeeds from 0 to greater than 25 knots and from daytime to total darkness. The ability to read a vessel's name and determine deck activity in total darkness was demonstrated. The AIREYE real-time digital enhancement capability provided detection, recognition and identification of targets of interest when not otherwise possible with unenhanced imagery. Test results demonstrated that the AIREYE system will provide greatly enhanced capability in the U.S. Coast Guard missions of Marine Environmental Protection (MEP), Enforcement of Laws and Treaties (ELT) and Search and Rescue (SAR).

17. Key Words	18. Distribution Statement
Surveillance, active gated TV, infrared, pollution, remote sensing, oil spill, image enhancement, radar	Document is available to the public through the National Technical Information Service, Springfield, Virginia

19. Security Classif. (of this report)	20. Security Classif. (of this page)	21. No. of Pages	22. Price
UNCLASSIFIED	UNCLASSIFIED	204	

Form DOT F 1700.7 (8-72) Reproduction of completed page authorized

CONTENTS

ILLUSTRATIONS

ILLUSTRATIONS (Continued)

ILLUSTRATIONS (Continued)

LIST OF TABLES

LIST OF ABBREVIATIONS

ADAS	Airborne Data Annotation System
AESC	Aerojet ElectroSystems Company
AGC	Automatic Gain Control
AGTV	Active Gated Television
AIREYE	Airborne Remote Instrumentation System
AOSS	Airborne Oil Surveillance
BACK	Back of the Waves
CDU	Control Display Unit
CFM	Cubic Feet Per Minute
CPU	Central Processing Unit
DIU	Display Interface Unit
DMA	Direct Memory Access
ELT	Enforcement of Laws and Treaties
EMI	Electromagnetic Interference
FAA	Federal Aviation Administration
FOV	Field-Of-View
GRSU	Geography Remote Sensing Unit
ICS	Inter-Communication System
ILS	Integrated Logistics Support
INTO	Into the Waves
IR/UV	Infrared/Ultraviolet
LRU	Line Replaceable Unit
MAC	Mean Aerodynamic Chord
MEP	Marine Environmental Protection
MPD	Multipurpose Display
NEP	Noise-Equivalent Power
NET	Noise-Equivalent Temperature
RNAV	Area Navigation
SAR	Search and Rescue
SIDE	Along the Troughs

LIST OF ABBREVIATIONS (Continued)

SLAR	Sidelooking Airborne Radar
S/N	Signal-to-Noise Ratio
SSO	Sensor System Operator
TV/VTR	Television/Video Tape Recorder
V_{mca}	Air Minimum Directional Control Speed
VTR	Video Tape Recorder

Section 1
INTRODUCTION AND SUMMARY

This document is the final report detailing activities of the development of the prototype Airborne Remote Instrumentation System (AIREYE). The AIREYE system was developed for the United States Coast Guard, Washington, D.C., by Aerojet ElectroSystems Company (AESC), Azusa, California under Contract No. DTCG23-80-C-20012. The AIREYE system is an integrated multisensor system configured to provide the Coast Guard with significantly enhanced capability to perform the Marine Environmental Protection (MEP), Enforcement of Laws and Treaties (ELT), and Search and Rescue (SAR) missions. Work summarized in this report was performed between August of 1980 and July of 1985.

The AIREYE system consists of (a) an X-band sidelooking radar system for long range, all weather ship detection and oil spill mapping; (b) an infrared and ultraviolet line scanner for pollutant detection, mapping and verification; (c) a laser-illuminated active gated television system for day or night high resolution determination of activities and identification of potential violators and (d) a high resolution aerial reconnaissance camera for photographic documentation of key events and violations. Augmenting this sensor suite is a real-time data processing display and recording subsystem that provides such features as real-time data management, digital image enhancement, absolute target position readout and sensor positioning.

The prototype AIREYE system was installed on a HU-25A Falcon fanjet and a safety-of-flight test program was conducted. This test program demonstrated the AIREYE installation to be safe with minimum impact on aircraft capabilities. AIREYE system performance test flights were also conducted. This flight test program included flights over natural oil seeps occurring in the Santa Barbara Channel, ship targets of opportunity and known sidelooking airborne radar (SLAR) and optical targets.

Flight evaluation testing consisted of 250 flight hours accumulated in approximated 130 flights. Of this total, approximately 96 hours were devoted to Mission Verification Testing during which the system was

evaluated over a broad range of environmental and operating conditions ranging from daylight to total darkness, windspeeds from 0 to 25 knots, altitudes from 200 to greater than 12,000 feet, and atmospheric conditions from clear to dense undercast.

Large ships were routinely detected and located with the AIREYE sidelooking radar at ranges greater than 65 nautical miles, and small sailing ships were detected at ranges from 30 to 40 nautical miles. The ability of the infrared/ultraviolet (IR/UV) line scanner to map and detect both very thick and extremely thin oil spills was demonstrated.

The active gated television provided good low light level performance in the reading of ship's names and low light level detection capability. The system was able to detect the light from cigarettes at ranges greater than 1.5 nautical miles. In the active mode the ability to read ship's names in total darkness was demonstrated at ranges up to 0.4 nautical miles. Silhouettes of ships were illuminated adequately to determine vessel type up to 1 nautical mile with deck details visible at ranges up to 0.6 nautical mile. Current improvements being incorporated onto the active gated television sensor, including the addition of a more sensitive image intensifier and longer focal length optics, should significantly increase these demonstrated ranges.

The ability of the KS-87B aerial reconnaissance camera to provide high resolution photographic documentation was also demonstrated.

The utility of the AIREYE data management subsystem in coupling the vast amount of available sensor and aircraft navigation data to the operator was also demonstrated. The ability of the AIREYE real-time image enhancement feature to detect, recognize and identify various targets under marginal conditions, which otherwise would have made these tasks impossible, was also demonstrated.

Throughout the test program the AIREYE system proved to be extremely reliable, thereby verifying the production and operational readiness of the system.

This report summarizes the entire AIREYE program activities. Section 2 describes key program events in terms of tasks and an overall program schedule. Section 3 contains a description of the hardware and software systems and Section 4 provides details of the flight test activities and image interpretation information. Section 5 contains conclusions and recommendations.

Section 2

PROGRAM DESCRIPTION

The AIREYE system was developed under Contract No. DTCG23-80-C-20012 "Design, Develop and Integrate/Install an Airborne Remote Instrument System (AIREYE)," during the period from 1 August 1980 to 30 July 1995. The AIREYE program consisted of two phases: Phase I - Prototype AIREYE System Development; and Phase II - AIREYE Production Options. This report documents the effort for Phase I.

2.1 TASK DESCRIPTION

Following is a summary of Phase I tasks.

Task 1 - Program/Project Management

Task 2 - System Design

Task 3 - Subsystem Design, Development and Procurement

Task 4 - Software Design and Development

Task 5 - Hot Mockup

Task 6 - Laboratory Integration and Test

Task 7 - Aircraft Installation, Integration and Ground Tests

Task 8 - System Operational Flight Tests and Evaluation

Task 9 - FAA Supplemental-Type Certificate

Task 10 - Logistics Support

Task 11 - Non-Integrated Logistics Support (ILS) Documentation

Task 12 - ILS Documentation

Task 13 - Environmental Tests

Figure 2-1 is an overall program schedule showing the major activities of the program. Task 9, FAA Supplemental Type Certificate, was changed to a military safety-of-flight program with flight testing performed by the Air Force Flight Test Center, Edwards Air Force Base, California.

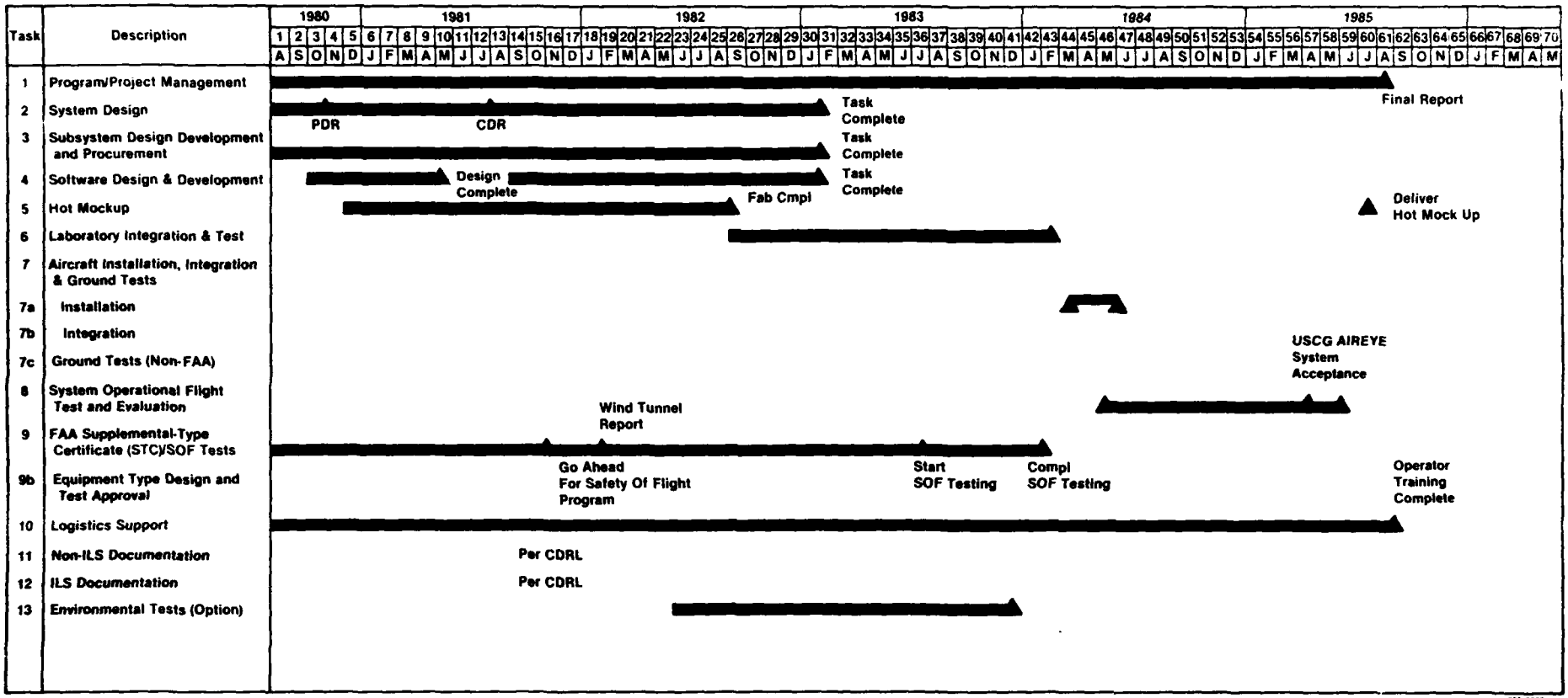

Figure 2-1. Overall Program

Section 3

AIREYE DESCRIPTION

3.1 GENERAL - SYSTEM DESCRIPTION

The AIREYE system is an integrated multisensor system configured to provide the Coast Guard with enhanced capability to perform the MEP (Marine Environmental Protection) ELT (Enforcement of Laws and Treaties), and SAR (Search and Rescue) missions.

The AIREYE system consists of the following sensor subsystems:

a. AN/APS-131 X-band Sidelooking Radar

b. RS-18C IR/UV Line Scanner

c. AN/ASQ-174 Active Gated Television (AGTV)

d. KS-87B Aerial Reconnaissance Camera

Operationally, the AIREYE system operates in two major modes: (1) the long-range detection and mapping mode, and (2) the short-range inspection, identification and mapping mode.

Figure 3-1 shows the long range operating mode. The sidelooking radar is the primary long range sensor providing ship and oil spill detection and mapping capability out to 80 nautical miles on both sides of the aircraft. Since the SLAR does not provide sensor coverage on a ±45° swath directly beneath the aircraft, this coverage is provided by the IR/UV line scanner for clear weather. In addition, for clear and adverse weather operation, the system is able to transfer target information from the aircraft's AN/APS-127 forward-looking radar to provide coverage beneath the aircraft.

In the short range identification mode (Figure 3-2), the primary sensor is the AN/ASQ-174 active gated television. This sensor provides ±220° coverage in azimuth and +15 to -70° coverage in elevation to provide day and night high-resolution real-time detection and identification capability. The KS-87B aerial camera provides high resolution daytime photographic documentation of activities directly under the aircraft and at a 30° depression angle to the left of the aircraft.

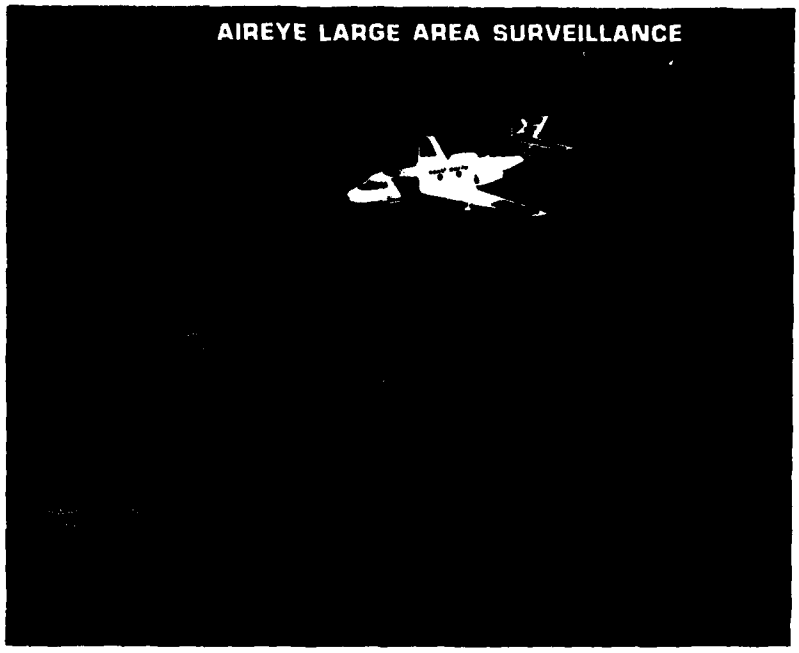

Figure 3-1. AIREYE Large Area Surveillance

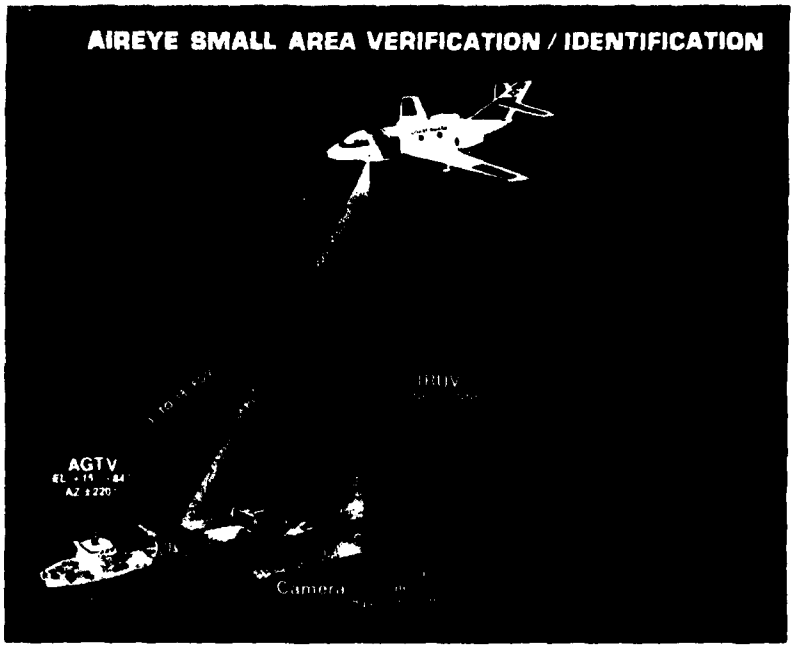

Figure 3-2. AIREYE Small Area Surveillance

The AGTV can be utilized in an automatic search mode or a computer pointed mode enabling both random and directed detection and identification. In the automatic search mode, the AGTV has a selection of three fields of view and selectable swath width to accommodate operational mission requirements.

Management of the vast amount of sensor data available and the coupling of this data to the operator is provided by the AIREYE real-time processing, display and recording subsystem.

The capability of this subsystem includes:

a. Real-time, geometrically corrected display of all sensor data with operator selectable formats and complete annotation.

b. Onboard hard copy of all sensor data with complete annotation of position and aircraft data.

c. Integrated system controls with system functions selectable by a single control and display unit utilizing a structured menu selection.

d. Computer pointing and control of the active gated television fully corrected for aircraft attitude changes.

e. Integrated map display functions providing integration of sensor and aircraft navigation data.

f. Real-time digital image processing of sensor data including data scaling, image sharpening, image smoothing and static multiframe averaging of AGTV data.

g. Continuous video tape record of annotated data with capability to enhance video tape data.

3.2 DETAILED SYSTEM DESCRIPTION

3.2.1 Overall System Specifications

Environmental	DO-160
Weight	2049 lbs
Power Requirements:	
Basic System	115 Vac, 3 phase, 400 Hz, 3296 VA 28 Vdc, 616 watts avg, 1008 watts peak
SLAR Anti-Ice	115 Vac, 3 phase, 400 Hz, 4200 VA

3.2.2 Sensor Subsystem Specifications

3.2.2.1 AN/APS-131 SLAR

3.2.2.1.1 SLAR LRU Physical Characteristics

Item	Overall Dimensions (in.) Height	Width	Depth	Overall Weight (lbs)
SLAR Control	9.00	5.75	9.00	10
Synchronizer	7.84	15.52	20.12	50
Receiver-Transmitter	7.84	15.52	20.12	75
Amplifier - Power Supply	7.84	10.26	13.12	30
Antenna	30.50	12.50	166.25	229
Recorder	21.00	14.50	27.29	103
			Total SLAR Weight	513

3.2.2.1.2 Overall System

Maximum Range	80 nmi
Resolution	
Range	30 meters (98 ft)
Azimuth	1.0°
Input Power Requirements	
AC	115 volts (line-to-neutral) 3 phase, 400 Hz, 10 A/phase
DC	+28 V, 20 A

3.2.2.1.3 Transmitter

Carrier Frequency	9250 ±1 MHz
Peak Power (at transmitter output)	185 kW (min)
Average Power	55.5 W (min at 1500 pps) 27.5 W (min at 750 pps)
Modulation	Pulse
Pulse Width	0.2 ±0.025 μs

Pulse Repetition Rate:	
Fixed Rate	750 or 1500 pps
Pseudorandom Rate	1,333.33 ±44.4 μs or 666.7 ±22.2 μs
Duty Cycle	0.015% at 750 pps 0.03% at 1500 pps

3.2.2.1.4 Receiver

Frequency	9250 ±1 MHz
IF Frequency	120 MHz
IF Bandwidth	6 ±0.25 MHz at 3 dB
Sensitivity (minimum discernible signal)	-101 dBm

3.2.2.1.5 Antenna

Beamwidth (horizontal)	0.95 ±0.05, -0.10° between half-power points
Pattern (vertical)	Cosecant squared (±1.5 dB) over a depression angle from 4° to 45°
Sidelobes:	
Azimuth	20 dB min below mainbeam peak
Elevation	25 dB min below mainbeam peak
Backlobes	34 dB min below mainbeam peak
Polarization	Vertical
Gain	31 dB min
VSWR	1.2:1 max
Operating Altitude	20,000 ft (6097 meters) max

3.2.2.1.6 SLAR Dry Silver Film

Type of Target Indicator	Modified ppi using two fiber-optic coupled CRT displays
Display Range	13.5, 27, 54, and 80 nmi
Resolution	30 lines/mm min
CRT Trace Length	39.5 ±0.05 in. (10 ±0.13 cm)
CPT Trace Correction	Correction for aircraft drift angles over +15° within ±0.65°. Correction for radar beam squint

Film Cassette Capacity	50 ft
Film Type	Cassette, photographic film LM-229A (Part No. SM-A-878294)

3.2.2.2 RS-18C IR/UV Line Scanner

3.2.2.2.1 LRU Physical Characteristics

Item	Overall Dimensions (in.) Height	Width or Diameter	Depth	Overall Weight (lbs)
Scanner (Unit 1)	-	8.75	33	53.56
Power Supply (Unit 2)	5.5	9.44	18	22.5
Control Box (Unit 3)	9.0	5.75	6.0	4.44

3.2.2.2.2 RS-18C Performance Characteristics

Scan Speed	5000 revolutions per minute	
Facets on Scan Mirror	1	
Scans per Second	83	
Optical Aperture	49.7 cm^2	
Field of View	100° (active)	
Roll Compensation	±15°	
Effective Focal Length	8.64 cm (3.4 in.)	
Spectral Region:		
Infrared	8-14 μm	
Ultraviolet	0.32-0.40 μm	
Thermal Resolution:		
Channel 1, IR Low	0.2°C (NET)	
Channel 2, IR High	0.02°C (NET)	
Channel 3, UV	1.5 mW/m^2 (NEP)	
Spatial Resolution	Across Track	Along Track
Channel 1, IR Low	2.5 mrad	2.5 mrad
Channel 2, IR High	18 mrad	2.5 mrad
Channel 3, UV	5 mrad	5 mrad

3.2.2.3 KS87B Aerial Reconnaissance Camera

3.2.2.3.1 LRU Physical Characteristics

Item	Overall Dimensions (in.) Height	Width	Depth	Weight (lbs)
Camera Body and Magazine				
with 3" lens	19.125	15.875	10.320	82.25
with 6" lens	18.5	15.875	10.320	79.75
with 12" lens	25.25	15.875	10.320	81.25
with 18" lens	32.03	15.875	10.320	96.75

3.2.2.3.2 KS87B Performance Characteristics

The performance characteristics of the KS87B aerial reconnaissance camera are shown in Table 3-1.

3.2.2.4 Active Gated Television

3.2.2.4.1 LRU Physical Characteristics

Item	Overall Dimensions (in.) Height	Width or Diameter	Depth	Weight (lbs)
Pod	25.60	15.00	108.10	381.0
Electronics	7.62	7.50	19.62	30.5
Mode Control Unit	4.50	5.74	5.25	4.8
Power Control Unit	5.62	5.74	5.25	5.5

3.2.2.4.2 Performance Characteristics

TV Output Format	RS-170
Gray Shades	10 shades on EIA test chart
Distortion	<3%
Fields of View	Selectable from 3.3° to 16° in 3 steps
Control	Via local control panels or computer control via 1553A data bus
Gimbal Freedom	Azimuth +200° to -220° Elevation +15 to -70°

TABLE 3-1 KS-87B AERIAL RECONNAISSANCE CAMERA PERFORMANCE CHARACTERISTICS

LENSES:	Focal Length and Speed - 3-inch f/4.5 6-inch f/2.8 12-inch f/4.0 18-inch f/4.0 In-Camera Resolution (Line Pairs/mm AWAR) - 60 (Pan-X) 65 (Pan-X) 85 (Pan-X) 85 (Pan-X) 40 (Plus-X) 45 (Plus-X) 60 (Plus-X) 60 (Plus-X)
FILM:	5-inch Aerial Roll Film, Any Black and White or Color Emulsion
FILM CAPACITY:	1000 feet, 2.5 mil; 700 feet, 4 mil; 500 feet, 5.2 mil
FMC FILM TRANSPORT RATE:	0.1 to 12 in/second
EXPOSURES PER SECOND (max):	6 Frames/second FMC Pulse 6 Frames/second Pulse
DATA RECORDING:	Records Flight Navigation and Fixed Mission Data BCD (Binary Coded Decimal) Annotation from Internal CRT Data Block in Corner of Each Film Frame Film Stop Period Provided Between Exposure and Recycle
POWER REQUIREMENTS:	28 Vdc, 210 W 115 Vac, 320 W, 30, 400 ± 20 Hz, 0.75 min pf
SHUTTER:	Focal Plane; Intralens Shutter in 3 and 6-inch Lens Cones for Pyrotechnics
CAMERA CONTROLS:	JANCCS or NCCS-4 with Suitable Adapter RF-4B, RF-4C, RF-101 (1181 and 1668 Mods) No Adapter Needed
FILM FLATTENING VACUUM:	1 to 8 inches Mercury with a Minimum Airflow of 0.25 cfm
FILTERS:	Interchangeable - All Types Available
EXPOSURE CONTROL:	Automatic - 12-8000 fL Brightness Range; Shutter Speed Control 1/60 - 1/3000 second Continuous Accuracy ± 1/2 f/stop
NIGHT PHOTOGRAPHY:	Focal Plane Shutter Synchronized for Electronic Flash Intralens Shutter in 3 and 6-inch Lens Cones for Use with Pyrotechnics (Synchronous Mode)

885-3941

Angular Velocity	Azimuth 60°/sec Elevation 60°/sec
Angular Acceleration	Azimuth 100°/sec Elevation 100°/sec
Position Accuracy	Drift rate <0.1°/sec
Modes	Active or passive
Laser Type	GaAs
Operational Performance	Read 1 ft high letters with 50% contrast and 50% reflectivity at an altitude of 500 ft at a minimum range of 500 meters

3.2.3 Signal Processing Display and Recording Subsystem

3.2.3.1 LRU Description

Item	Overall Dimensions (in.) Height	Width	Depth	Weight (lbs)
Computer	7.62	10.12	19.56	60.0
Scan Converter	7.62	10.12	19.56	49.0
DIU	7.8	3.68	15.0	24.8
MPD	12.50	14.00	19.50	47.5
CDU	8.88	5.74	9.75	14.7
IR/UV Film Recorder	12.0	11.75	20.50	62.3
V/H Control	3.69	5.74	7.25	3.0
VTR	6.3	10.67	14.48	28.6
Digital Tape Unit.	7.62	3.56	12.62	15.0
Camera Control Unit	5.35	5.74	7.25	4.5

3.2.3.2 Performance Specifications

1602B Processor

CPU	A single-module 20-MHz microprogrammed CPU with up to 1024-word control storage. Standard instruction set uses 440 words
Memory Address	A direct addressing capability of 64K 16-bit words of main memory

CPU Instruction Set	An extensive instruction set based on four accumulators and hardware stack pointer. Includes 81 instructions plus additional single-word instructions through the use of combinations
DMA	666,000 words/second input and 525,000 words/second output
Interrupts	16 levels of programmable priority interrupts
Power	+115 V 400 Hz power supply with electronic overvoltage and overcurrent protection
BITE	Self-diagnostic unit combined with floating-point arithmetic
Bootstrap	Hardware program bootstrap
Memory	The CPU is equipped with 32K of core memory (cycle time 1 μsec)
Environmental	MIL-E-5400, Class II and MIL-E-16400

3.2.3.2.2 Scan Converter

Functional Specifications

Equivalent Image Storage Capacity	5 x 512 x 640 x 8 bits
Graphic Capacity	8 overlays, each 512 x 640 x 1 bit
TV Sync (output)	RS-170-compatible composite
Access Time to Any Picture Element (read or write)	2 μs
Image Scaler Capacity	8-bit data in; 8-bit data out
Cursors	4; defined by 16 preprogrammed shapes (16 x 16 matrix)
Brightness Control	Annotation, graphics, and cursor independently programmable to 256 brightness levels
Processing Capabilities	Externally controllable from host computer for alphanumeric annotation (internal ASCII character generator), graphics, cursor control, image processing features include:

	• Zoom • Edge enhancement • Contrast enhancement • Convolution (3 x 3 kernel) (sharpen, smooth, general purpose) • Static multiframe average
Environmental	DO-160

3.2.3.2.3 **DIU**

Designation	Converter, signal data CV-3722/ASD-6; AESC P/N 1315619-1
Functions	TV/VTR synchronization, SLAR data integration, IR/UV data integration, BITE interface, A-scope interface, scan converter interface, scan converter timing, IR/UV film recorder interface, analog conditioning and switching, SSO console data interface
TV Signal Input/Output Format	RS-170 (VTR and AGTV)
Scan Converter Interface Format	16-bit bidirectional data bus; 8-bit high-speed unidirectional data bus; control bus; BITE status
A-Scope Video Switching	Selects video and synchronization signals to A-scope for viewing. Options - VTR in, VTR out, SLAR in, integrated SLAR, IR/UV in, integrated IR/UV
BITE Inputs	SLAR, IR/UV, KS87B camera, film recorder, DIU
Film Recorder Outputs	Image video, synchronization, annotation, film speed
SLAR Integrator	
Type	Range-gated digital filter
Sample Period	200 ns
Effective Integration Time	Programmable based on ground speed
IR/UV Integrator	
Type	Scan-to-scan digital filter
Sample Rate	Variable based on scan angle for tangential sweep geometric correction
Effective Integration Time	Programmable based on V/H ratio

Analog Inputs	VTR, AGTV, scan converter annotation, IR1, IR2, UV, SLAR
Analog Outputs	MFD, A-scope, VTR
SSO Console Digital Interface	Video tape control out, video tape counter in, degraded mode control in, digital velocity and altitude from V/h control thumbwheel switches in, KS87B camera status in, SLAR mode switch position in
Power	115 V, 3 phase, 400 Hz
Environmental	DO-160

3.2.3.2.4 **MPD**

Per AESC specification AE-23704F (summarized below).

Performance Requirements

Video Input	EIA RS-170 compatible
Video Bandwidth	14 MHz ±3 dB
Brightness Contrast	Brightness: 100 FL Contrast: 30:1 in low ambient lighting
Resolution	600 TV lines
Linearity	±2% of picture height
Phosphor	P43
Input Power	115 V, 400 Hz, 3 phase
Power Consumption	100 W
Screen Size	11 x 8.25 in. (13.8 in. diagonal)
Mounting Provisions	SSO console
Built-In Test	Operator-activated test pattern viewed on monitor

3.2.3.2.5 **CDU**

Type	Collins 813H-ID
Interface	MIL-STD-1553A multiplex bus
Modes	Alphanumeric, map, test
1553A Terminal Address	Selectable via jumpers on power connector

Manual Input	Alphanumeric keyboard with special function keys and 12 line select keys
Display Update Rate	5 Hz
Display Refresh Rate	80 Hz nominal; 60 Hz min
Display Brightness	Green phosphor; readable in ambient lighting of 10,000 footcandles
Alphanumeric Format	13 lines of 22 characters each - six label lines, six data lines and one scratchpad line
Alphanumeric Character Size	Label lines - 0.093 inch square, data and scratchpad lines - 0.140 inch high by 0.093 inch wide
Number of Alphanumeric Characters	63
Environmental	DO-160
Power	115 Vac, 400 Hz

3.2.3.2.6 **IR/UV Film Recorder**

Per AESC Specification No. AE-23703E and Amendment 1 (summarized below).

Performance Requirements

Video Input	0.5 Vdc; 5 Vdc = maximum exposure
Horizontal Resolution	Spot size 0.003 in. + 0.005 in. - 0.002 in.
Passband	DC to 455 kHz
Recording Media	Selectable utilizing 2 cassettes:
Dry Silver cassette	Dry silver film or dry silver paper
Wet-Process Film Cassette	Kodak 2496 film
Takeup Spool	Takeup spool provided for both dry silver and wet-process film
Dry Silver Development.	Development by heat, temperature controlled as a function of V/h input
Image Format	2 adjacent 2 in. images; 0.5 in. for annotation
Media Annotation	Internally performed by image CRT and annotation circuitry
Annotation Format	8 x 8 character matrix identical to that produced by the ADAS

Film Media Speed	0.25 in./s (V/h - 0.3) to 0.0125 in./s (V/h - 0.015)
Horizontal Sweep	Linear sweep initiated by T^2L triggered pulse provided by AIREYE system
Recording Media Capacity	250 ft of 3.5-mil dry silver film
Sweep Speed	3.3 to 8.67 ms (internally adjustable): nominally 5 ms
Input Power Source	115 V, 400 Hz, single phase
Power Consumption	125 VA at V/h - 0.3; 90 VA at V/h = 0.015; 200 VA heater surge
Built-In Test	Constant monitoring of yoke current, motor current, CRT grid voltage, and heater temperature. Failure mode activates an indicator on front panel.

3.2.3.2.7 **V/h Control**

Designation	AESC P/N 1315650-1
Modes	Automatic or manual
Signal Input	RNAV V/h; E(V/h) = 11.83 (V/h) ±5%
Signal Outputs	Scaled V/h signal to film recorder, camera control panel, and computer
Manual Inputs	Velocity - 0 to 999 knots; altitude - 0 to 99,9999 feet
Front Panel Controls	Velocity (KTs) - thumbwheel switch Altitude (ft) - thumbwheel switch Lamp Test - pushbutton Power On/Off - pushbutton Auto/Man - pushbutton
Power	28 Vdc
Environmental	DO-160

3.2.3.2.8 VTR/VTR Control

Type	TEAC V-1000 AB-F
Tape Type	3/4 in. video cassette
Video Input	EIA RS-170 compatible (525 lines)
Bandwidth	10 Hz to 5 MHz within -5 dB
Video Output	EIA RS-170 compatible (525 lines)
Signal-to-Noise Ratio	>40 dB
Amplitude Linearity	20 gray scales minimum
Horizontal Resolution	>400 lines
Level Control	Automatic gain control
Record Time	>71 min
Audio Tracks	Two channels of record and reproduce audio
Operating Modes:	
Record	
Slow Play (Fwd/Rev)	Variable from still to normal in either position
Fast Play (Fwd/Rev)	Variable from normal to seven times normal in either direction
Rewind	
Fast Forward	
Still Play (Stop Motion)	
Remote Controls	For the above operating modes plus power on/off, event mark record
Remote Indicators	Ready (tape threaded), record mode, end of tape, tape address counter, event marker detection
Power Requirements	
Input Power Sources	28 Vdc per MIL-STD-704B

3.2.3.2.9 Digital Tape Recorder

Type	Genisco Model ECR10
Tape Size	1/2 in. by 450-ft cartridge
Recording Track	9 track, 800 bpi, NRZ1, ANSI-compatible, 12K bytes/s at 15 ips
Environmental	MIL-E-5400 qualified
Power Source	28 Vdc

3.2.3.2.10 Camera Control Unit

Designation	AESC P/N 1315635
Front Panel Controls	Power-off-ready-operate, focal length selector (3, 6, 12 and 18 inch), cloud cover switch (25%, 0%, 50%), maximum rate, lamp test
Front Panel Indicators	System ready, operate/fail, mount position (30° left/90° vertical), film remaining counter
Input Signals	Mount vertical, mount 30°, dc power, camera door open, V/h, camera fail, film remaining, data demand, auxiliary camera operate (cockpit)
Output Signals	FMC (K V/h signal), camera door command, camera fail, cycle pulse (day mode), ready power (day mode)
Intervalometer Operation	
Input Signal Format	11.83 (V/h) ±5.0%
Input Signal Range	0.0067 to 2.00 knots per foot
Output Frequency Range	*0.08 Hz to 6 Hz*
Compensation	Focal length, camera depression angle
Output Pulse Width	75 ±25 milliseconds
Output Pulse Amplitude	28 volts nominal
Power	28 Vdc
Environmental	DO-160

3.2.4 System Block Diagram

Figure 3-3 is a detailed block diagram of the AIREYE system. The major AIREYE processing units are the Rolm 1602B computer, Signal Data Converter CV-3721/ASD-6 (referred to hereafter as the scan converter) and signal data converter CV-3722/ASD-6 (referred to hereafter as the Display Interface Unit (DIU)). The DIU accepts analog video and synchronization signals from the SLAR, IR/UV line scanner, active gated television (AGTV) and video tape unit. These data are converted to digital format in the DIU and transferred to the scan converter for formatting for real time display, recording or subsequent digital enhancement processing.

The DIU and scan converter are normally controlled by the AIREYE Operating Program resident on the Rolm 1602B computer. Operator control of program and system functions is facilitated by a menu-driven Control and Display Unit (CDU) coupled to the Rolm computer using one of the two system 1553 interfaces.

In the event of a Rolm computer failure, DIU and scan converter functions may be controlled by the degraded mode control unit,which provides limited system functions adequate to allow the completion of a mission as well as providing local control of video tape recorder functions.

The Rolm 1602B computer contains interfaces to the aircraft systems as summarized in Table 3-2

3.2.4.1 Display and Recording Functions

MPD

All sensor data and video tape recorded data may be displayed on the Multipurpose Display (MPD) in operator selectable formats. AGTV and video tape data are normally displayed directly on analog format unless further processing is required for enhancement or permanent record. For subsequent processing the AGTV or VTR data are digitized and stored in the scan converter. Up to five TV frames of data may be stored.

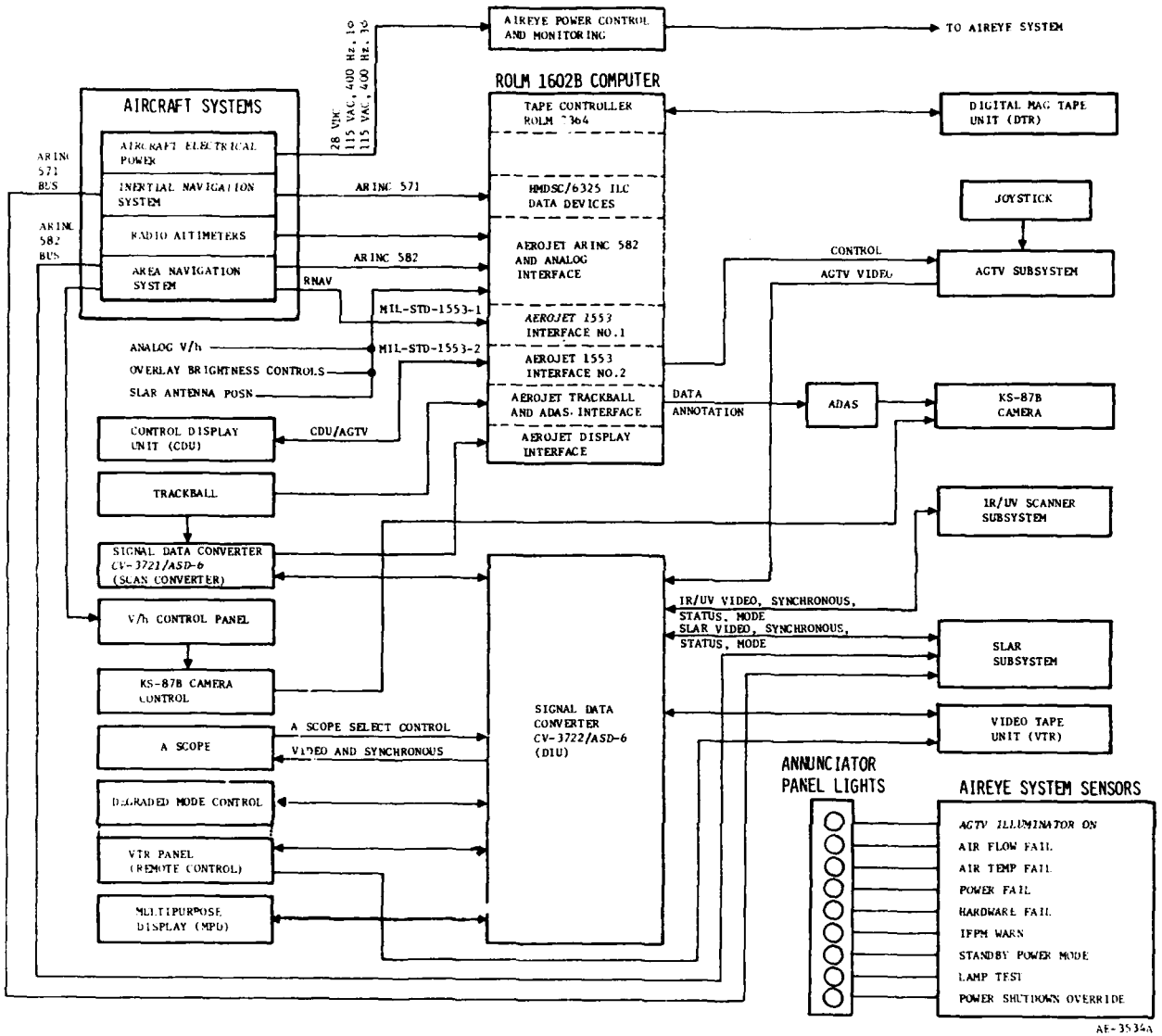

Figure 3-3. AIREYE Detailed Block Diagram

TABLE 3-2 ROLM 1602B COMPUTER INTERFACES

Interface Name	Aircraft System	Key Parameters
ARINC 571	Aircraft Inertial Sensor	Synchro roll, pitch drift angle, heading
ARINC 582	RNAV	Drift angle, present position, heading, barometric altitude
Analog	Altimeters, RNAV	Radar altitude, analog V/h
1553 No. 1	RNAV	Aircraft waypoints, search radar targets

The remaining interfaces in the computer perform the following functions:

Interface Name	Unit Interfaced to	Function
Analog	SLAR	Antenna position
	MPD	Overlay brightness control positions
1553 No. 2	AN/ASQ-154 AGTV	Gimbal position input and output Mode control input and output Laser range output BITE input
	CDU	Menu or map data out, pushbutton commands in
Trackball	Trackball	x and y trackball position data
Tape controller	Digital tape deck	Program or image data in and out
ADAS	Airborne Data Annotation System	Aircraft and position annotation data to be recorded on KS-87B film
Display	Scan Converter	Digital image and control data in and out to scan converter

SLAR and IR/UV data are digitized in the Display Interface Unit and converted to a TV compatible format in the scan converter for display on the MPD. The operator may select the desired display format utilizing the CDU or the Degraded Model Panel.

Annotation containing current aircraft parameters, system operating modes, sensor pointing angle position and target information is displayed on the right-hand edge of the MPD display for all sensors. The brightness and shade of the annotation are operator selectable by controls on the MPD. The MPD is a Conrac Model 61417, IP-1408/ASD-6.

VTR

The MPD presentation may be recorded on the video tape recorder (VTR) at any time. Video switching circuitry in the Display Interface Unit also permits operator viewing of AGTV data while recording scan converted data (IR/UV or SLAR) or viewing of scan converted data while recording the AGTV. Control of the VTR is accomplished either in the remote mode using the CDU or in the local mode using controls on the VTR control panel. Control of the VTR is accomplished either in the remote mode using the CDU or in the local mode using controls on the VTR control panel. Control and status information from the VTR for the remote mode are routed from the VTR control panel to the DIU and ultimately through the scan converter to the Rolm computer. Video switching and signal formatting for the VTR is accomplished in the DIU. Tape recorded data may be viewed on the MPD or digitized in the DIU and stored digitally in the scan converter for subsequent processing. The video tape recorder is a TEAC model V-1000 AB-F.

Digital Tape Recorder

The AIREYE program is resident in core memory. An Airborne Cassette Digital Tape Recorder is provided to permit loading and reloading of the program if required. In addition digital image data may be recorded on digital tape and later loaded onto the scan converter memory for further processing. This feature permits high quality storage of important image data for subsequent processing without the slight degradation incurred with video recording. The digital tape recorder is a Genisco Model ECR-10 and interfaces to the computer using the tape control interface.

Dry Silver Film Recorder

Hard copy of IR/UV scanner data or the current MPD presentation may be recorded on the AIREYE dry silver film recorder. In the IR/UV scanner recording mode, the IR/UV scanner data are scan corrected, digitized, integrated and formatted into analog format and transferred to the film recorder in the DIU. A signal proportional to V/h ratio commands the film speed of the recorder to maintain the proper aspect ratio of the scanner imagery.

In the normal (automatic) mode this signal originates into the RNAV system, is formatted by the V/h control panel, and transferred to the film recorder in the DIU. In the degraded mode,the signal originates in the V/h control panel as a function of thumbwheel velocity and altitude controls and is transferred to the film recorder through the DIU.

In the MPD hard copy mode the film recorder records an exact hard copy of the image presented on the MPD including MPD annotation and any data enhancement. In this mode the original image is stored in the scan converter refresh memory. Upon command, the digital data is transferred to the DIU, converted to analog format and recorded on the film recorder. For MPD hard copy a fixed speed command signal is sent to the DIU to present the proper aspect ratio.

Annotation in identical format to the KS-87B (ADAS) annotation block is recorded in the right-hand margin of the film record. This data is generated in the Rolm computer, and is transferred to the film recorder through the DIU.

The film recorder can utilize dry silver paper, dry silver film or wet processed film. In the dry silver mode a built-in heater provides near-real-time viewing. The heater temperature is programmed to provide uniform development over a wide range of media speeds and corresponding V/h ratios. The recorder is an Edo Western Model 722, per AESC Specification AE-23703E.

SLAR Film Recorder

The SLAR subsystem provides a continuous hard copy of the SLAR data with geographic references and annotation. The SLAR film recorder is a Motorola Model RO 525 and is part of the SLAR subsystem.

3.2.4.2 Miscellaneous Controls and Indicators

A-Scope

The A-scope is a small modified Tektronix oscilloscope used to monitor key functions within the AIREYE system. Key functions monitored are VTR video in and out, AGTV video, MPD (displayed) video, raw SLAR data, raw IR (3 channels), integrated SLAR or IR data. Selection is via pushbutton switches mounted on the A-scope panel and actual switching of video and sync signals is accomplished in the DIU.

V/h Control Panel

The V/h control panel provides V/h signals to the camera control panel, the IR/UV film recorder and the sensor computer. The unit operates in a totally automatic mode or, in the event of RNAV failure, in a manual mode with manual operator velocity and altitude inputs from front panel thumbwheel switches.

In the automatic mode the V/h control panel accepts an analog V/h signal directly from the RNAV computer and appropriately scales it for the various units. The scaled V/h signal for the IR/UV film recorders is routed through the DIU to provide switching to the proper film recorder speed for MPD hard copy operations.

In the manual mode system operation is exactly the same as above except the V/h data are input from the thumbwheel switches on the V/h control panel instead of the RNAV V/h output.

Camera Control Panel

The camera control panel provides the signals to operate and monitor status of the KS-87B aerial reconnaissance camera. In the normal mode, upon operator demand, a series of trip pulses (camera exposure commands) are sent to the camera. The interval between exposures is computed in the camera control panel as a function of aircraft V/h ratio, lens size, and camera mounting angle to provide a 40% frame overlap. An analog V/h signal from the V/h control panel is used to perform the computation. An alternate mode provides maximum camera exposure rate on pushbutton command.

Status of the camera BITE is processed through the camera control panel and sent to the DIU for master system BITE processing. A film-remaining indicator operated from the exposure pulse in the camera provides a positive indication of remaining film.

VTR and Degraded Mode Control

The VTR and degraded mode control are physically enclosed in a single unit. The VTR control provides local control of VTR functions and interfaces the VTR to the DIU for control via the CDU. The tape counter may be read on the VTR control panel or remotely using the CDU.

The degraded mode control provides the system with adequate capability to complete basic mission requirements should the AIREYE computer fail. This unit interfaces to the DIU which in turn transfers selected display commands to the scan converter for processing. Since the normal MPD annotation will not be present if the AIREYE computer fails, the degraded mode has a thumbwheel switch that selects a number that appears on the lower right corner of the MPD that can be correlated with flight logs to provide backup documentation.

Annunciator Panel

The annunciator panel provides the operator with an instantaneous indication of system health. Major warnings include air flow fail, overheat, power fail, hardware fail, and IFPM Warn 1. The IFPM is a software BITE indication that indicates that a timing problem has been sensed in the AIREYE program. The power shutdown override may be activated to override the normal system shutdown in the event of cooling air failure for limited time periods.

Trackball

The trackball is the system X-Y input device used for a variety of processing functions and AGTV positioning. Trackball X-Y data is input to the scan converter and to the AIREYE computer.

Power Control and Monitoring

The AIREYE power subsystem consists of the power distribution unit, the power control unit and the system power meter panel. The power distribution unit accepts aircraft power (28 Vdc and 115 Vac, 3 phase, 400 Hz) from the aircraft sensor power bus and distributes the voltages to the AIREYE subsystems. The power distribution unit provides power protection features including overcurrent and reverse phase, and formats aircraft power to provide voltage and current monitoring via the AIREYE meter panels. The power control unit provides system power switching as well as power-on and power-fail indicators.

3.3 SYSTEM OPERATION AND PROCESSING

The AIREYE system is operated entirely from the SSO console. After system power-up, the SSO CDU becomes the major interactive device through which the SSO operates the AIREYE system. The use of a structured menu using software labeled function select switches provides a logical path of operation requiring minimum operator training. Figure 3-4 is the AIREYE menu hierarchy. Following is a brief discussion of each menu function included to provide a summary of system capabilities.

Master Select

This menu appears at system power-up and anytime through the CDU keyboard "IDX" pushbutton. It selects the general category of control or information desired by the operator.

Sensor

The sensor menu selects the sensor to be set up or modified. Selections are SLAR, IR/UV, or the AGTV surface search or surface track mode.

SLAR

The two SLAR menus set up the parameters for SLAR display and processing. The RANGE/DELAY/ANTENNA menu sets up the basic SLAR display mode. Special processing functions including SLAR full resolution zoom are selected from the DISPLAY MODE selections.

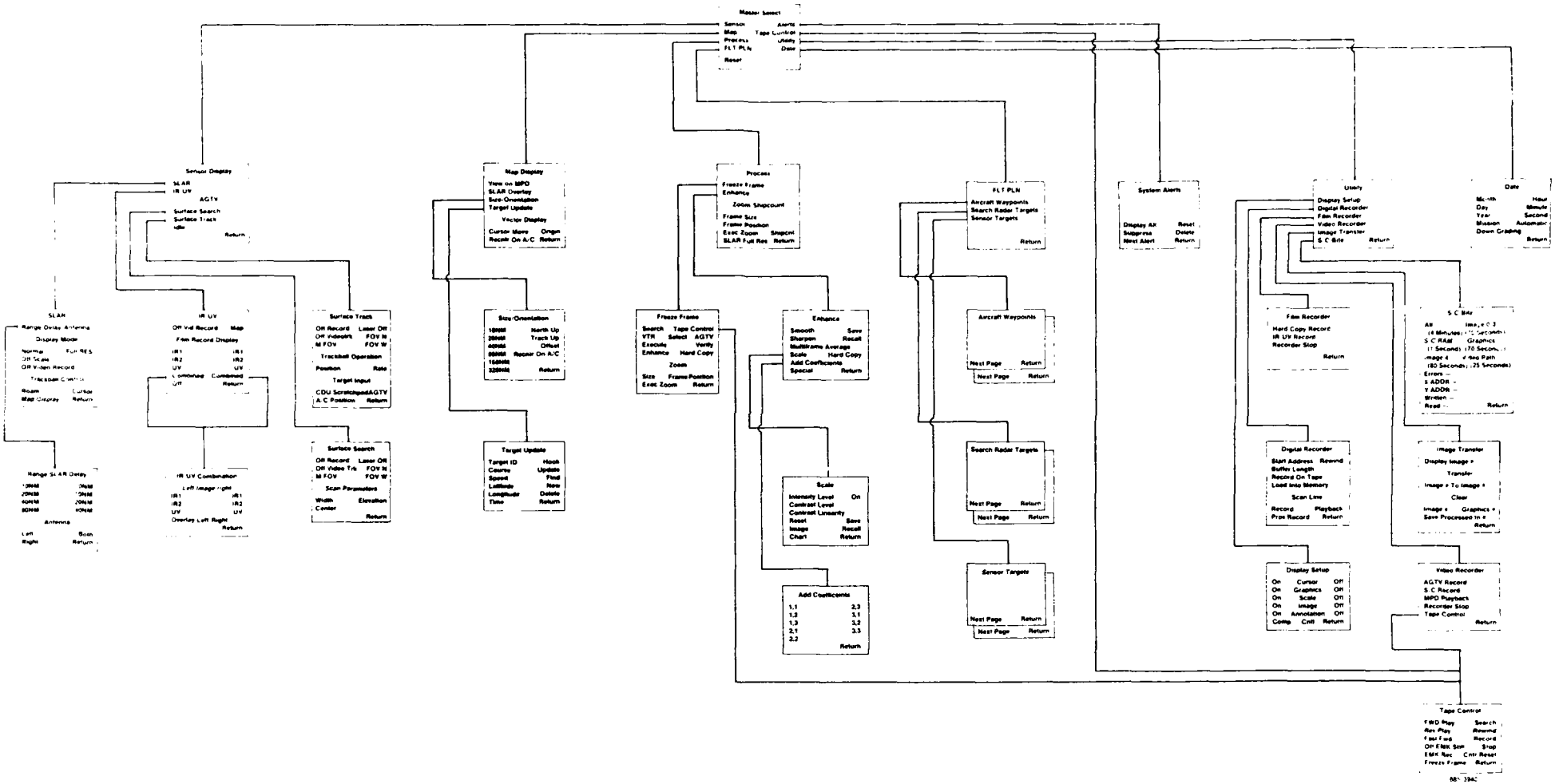

Figure 3-4. AIREYE Menu Hierarchy

IR/UV

This menu selects the setup and IR/UV channel selection for the display and IR/UV film recorder. If desired to display two IR/UV channels side by side or overlay two channels, the operator selects the IR/UV COMBINATION menu.

IR/UV Combination

This menu sets up the channels to be combined for MPD display or IR/UV film recording.

AGTV Surface Track

This menu selects the surface track functions for the active-gated television. Functions available include FOV selection, video track selection, laser control, VTR record, trackball function (position or rate update) and target input selection (CDU SCRATCHPAD in which the AGTV points to selected target name or AIRCRAFT POSITION in which the AGTV points to and maintains the current aircraft position).

Surface Search

The surface search mode parameters of scan width, scan center and scan elevation are selected in this menu. In addition, supporting selection of VTR record, FOV selection, laser control and video track functions are available.

Map Display

Selection of map on the master select menu activates this menu. Either the normal map display or the SLAR overlay may be selected for view on the MPD. In addition, setup selections are available for map size and orientation and vector functions.

Size/Orientation

This menu selects the map scale, orientation (north up or track up) and map offset.

Target Update

This menu provides update or entering of target parameters and may be used in map or SLAR overlay mode.

Process

Selection of process on the master select activates this menu. Selections available include freeze frame functions, zoom and ship count setup, and AIREYE image enhancement functions.

Freeze Frame

Selection of this menu permits execution of the AIREYE digital freeze frame function from the VTR or directly from the AGTV. Direct access to the video tape control menu is available to facilitate freeze frame from the VTR. Zoom parameters are also included.

Enhance

This menu selects the AIREYE enhancement process. Available selections are:

SMOOTH - provides reduction in noise from any sensor data

SHARPEN - accentuates high frequency spatial detail

MULTIFRAME AVERAGE - averages four sequential AGTV or VTR frames to improve image signal-to-noise ratio

SCALE - selects menu that sets up brightness enhancement functions

ADD COEFFICIENTS - selects menu that enables operator to insert special enhancement functions into convolution kernel coefficients

SPECIAL - performs the image enhancement using the special coefficients above

Scale

This menu sets up the brightness enhancement transformation parameters. Included are intensity level, contrast level, and contrast linearity. Selection of the CONTRAST LINEARITY function permits setup of nonlinear brightness enhancements. Selection of the CHART function provides a graphic representation of the brightness transformation parameters in use. The SAVE and RELEASE functions can be used to store and recall previous brightness enhancement functions.

Add Coefficients

This menu is used for inserting special convolution processing functions (3 x 3 matrix).

Flight Plan

This menu selects viewing of aircraft waypoints, search radar targets, or sensor targets.

Aircraft Waypoints

This function provides a list of aircraft navigation waypoints from the RNAV system.

Search Radar Targets

This function provides a list of search radar targets from the RNAV system.

Sensor Targets

This function provides a list of the sensor targets entered in the map function.

Date

Selection of this menu from the master select menu allows entering of the current date.

System Alerts

Selection of this function from the master select menu allows viewing of the system hardware and software health and status. This page is also available by selecting the STAT key on the CDU keyboard.

Utility

Selection of this menu from the master select menu provides access to general utility functions. Functions available are display setup, digital recorder setup, film recorder setup, video recorder setup, special purpose image transfer and special purpose scan converter BITE.

Film Recorder

Selection of this menu allows selection of the film recorder function (hard copy or IR/UV recording) and film recorder on/off command.

Digital Recorder

Sets up the digital recorder function. Setup of Start Address and Buffer Length followed by selection of record on tape records a specific section of Rolm memory on the magnetic tape. Selection of load memory loads magnetic tape data to a specific area of core memory. Selection of scan line record will record the current image being displayed from the scan converter onto the digital tape. Selection of scan line playback will load digital image data from magnetic tape to the scan converter for processing/display. Selection of PROG RECORD records the entire AIREYE program on magnetic tape.

Display Setup

This menu allows special display presentation different from that automatically selected by the program.

Scan Converter BITE

This menu runs specific scan converter self-test routines and displays the results.

Image Transfer

This menu, to be used by the advanced operator, saves and transfers image and graphic data in the scan converter. It also provides the ability to clear image and graphic data.

Video Recorder

Selection of this menu allows control of video tape recorder input and output and provides access to the tape control menu.

Tape Control

This menu provides control of the video tape recorder from the CDU. Search mode speed is controlled by the trackball. This menu is also accessible from the master select and freeze frame menus.

3.4 AIREYE SYSTEM AIRCRAFT INSTALLATION

(The prime reference document for aircraft installation is Aerojet Drawing No. 1315760-1, titled Surveillance System, Multisensor, Airborne AN/ASD-6 installation.)

The AIREYE system is installed on board an HU-25A aircraft. Figure 3-5 shows the location of the various sensors and associated equipment, both external to the aircraft and within the fuselage interior. The external sensors consisting of the active gated television (AGTV) pod, the sidelooking airborne radar (SLAR) antenna pod and the infrared/ultraviolet (IR/UV) line scanner pod are located under the left wing, the fuselage and the right wing, respectively. The KS-87B aerial camera is located within the fuselage, aft of the cockpit on the left side. The major subassemblies located within the fuselage consists of the equipment rack assembly, the Surveillance Systems Operator (SSO) control console assembly, the auxiliary fuel cell equipment assembly, and the left side SLAR assembly. Interconnecting cables are routed between these assemblies and secured to existing aircraft structure. Additional controls (pod jettison and SLAR pod anti-icing) are located in the cockpit on the pilot's left-side console.

3.4.1 Aircraft Preparation for AIREYE Installation

In order to accept the AIREYE system, the HU-25A aircraft must be modified in the following manner:

1. Rerouting of the camera power and control cabling in the fuselage overhead and SSO console area.
2. Rerouting of aircraft systems cabling in the SSO console area.
3. Modification of the 115 Vac 3 phase power box to accept the SLAR anti-icing power cable.
4. Installation of the pod jettison cables in the left and right wing leading edges, and in the wing root under the floor area.
5. Installation of the pod jettison and SLAR anti-icing cables from the left-side pilot's console, center console, and circuit breaker panel to the sensor distribution panel.

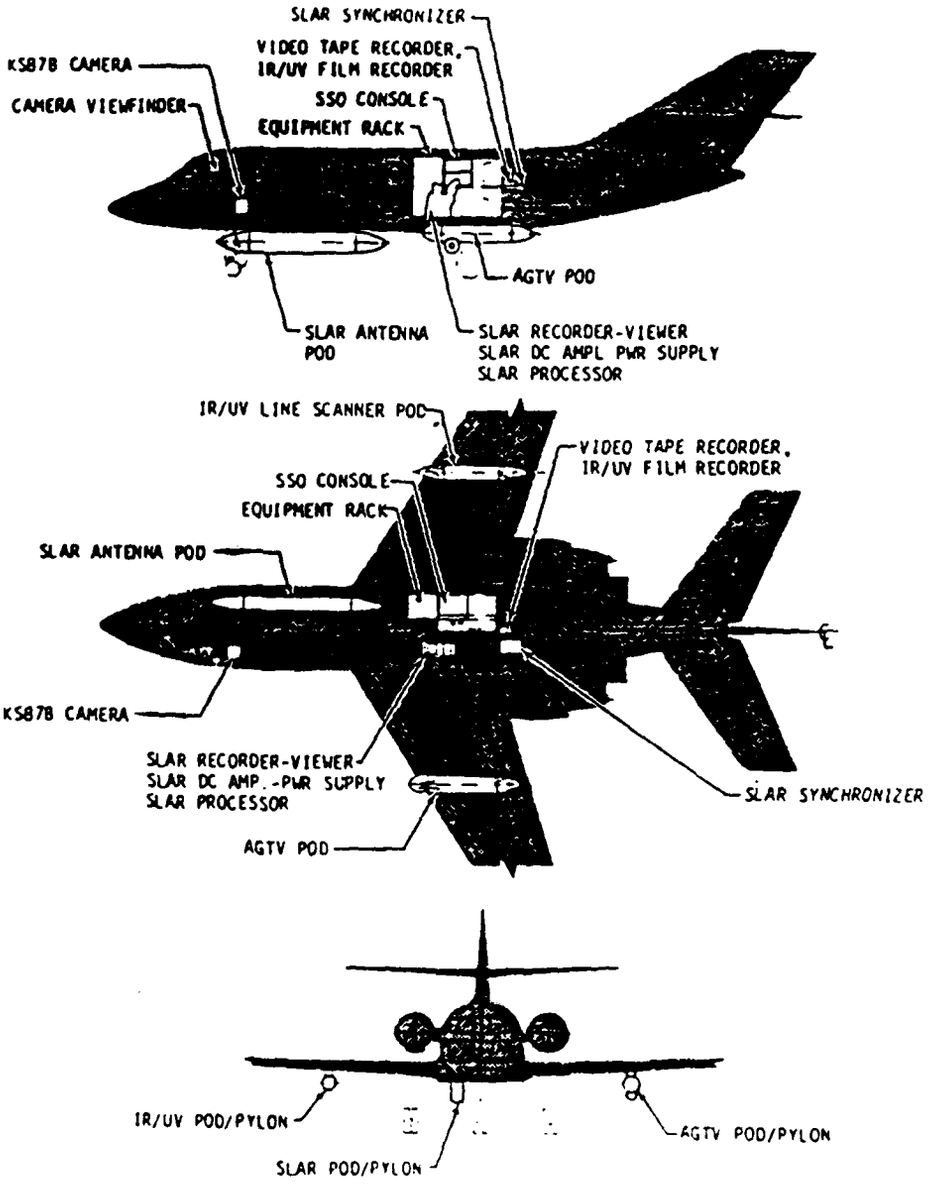

Figure 3-5. AIREYE System Installation

3.4.2 Interior Equipment Installation

Figure 3-6 shows the interior equipment installation and cable routing. All equipment mounts to existing hardpoints and requires no structural modifications to the airframe.

3.4.2.1 Equipment Rack Assembly

The equipment rack assembly is rigidly mounted to the existing seat rails at the base (four places) and to existing hardpoints located in the upper right-hand fuselage structure as shown in Figure 3-7. The rack is collapsible to permit it to be moved intact through the narrow confines of the fuselage during transfer and installation. The rack contains integral wiring/cable harnesses, cooling ducts/fans and equipment support trays and houses the following AIREYE components:

1. SLAR receiver/transmitter
2. Computer
3. AGTV electronics
4. Scan converter
5. Airborne Data Annotation System (ADAS)
6. Power distribution box
7. Display interface unit (DIU)
8. Digital tape recorder
9. Power meter panel.

Location of the rack is between aircraft stations F.S.290.75 and F.S. 319.13 (aft of the escape hatch) on the right-hand side of the aircraft. The exterior of the forward and inboard sides of the rack are covered by a decorative wood grain aluminum/balsa wood laminate which matches the HU-25A interior decor. Access to the electronic boxes is provided by hinged panels. All components, with the exception of the SLAR receiver/transmitter and power meter panel are removable from the forward side. The radar receiver/transmitter extends out into the aisle for removal.

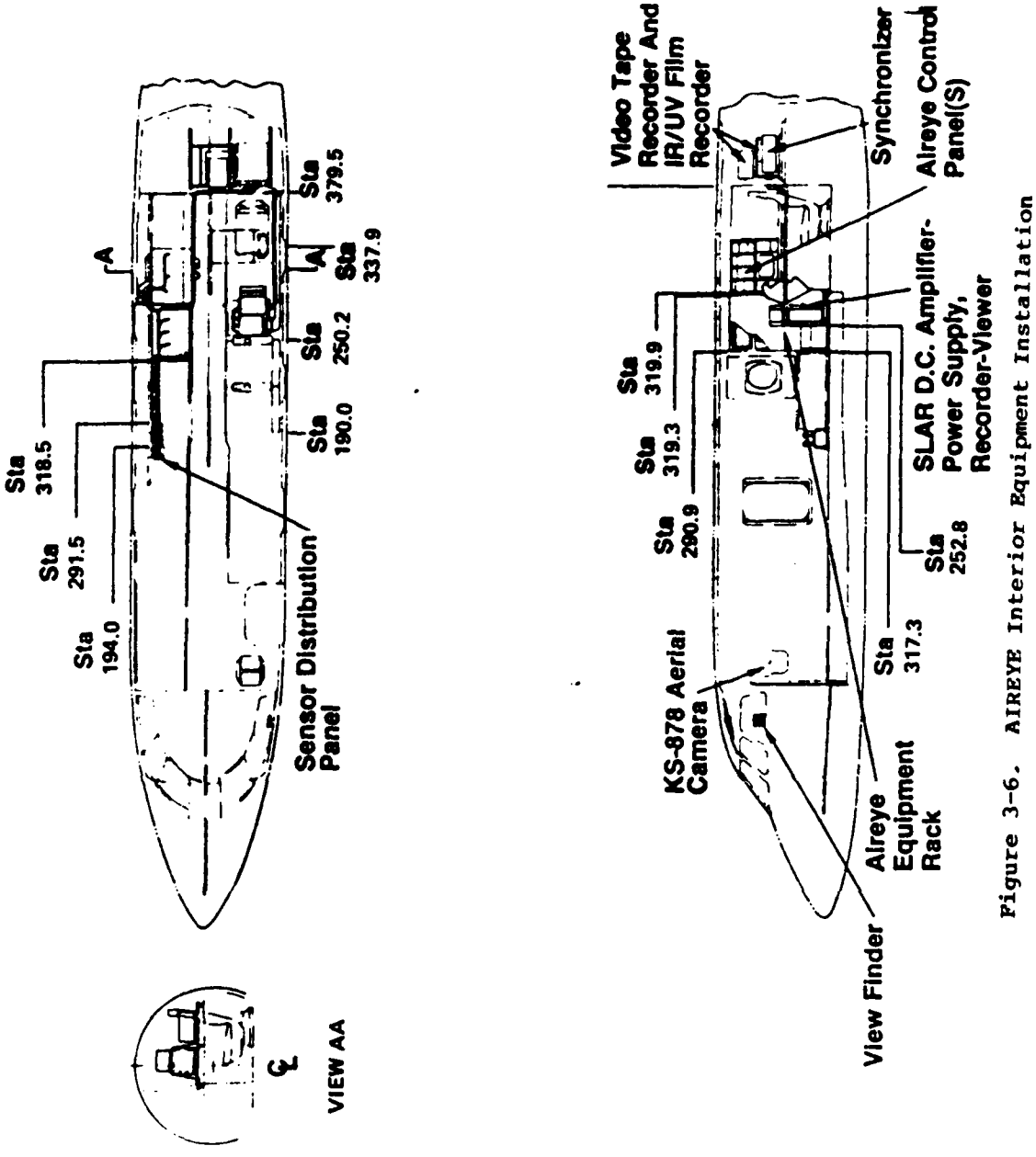

Figure 3-6. AIREYE Interior Equipment Installation

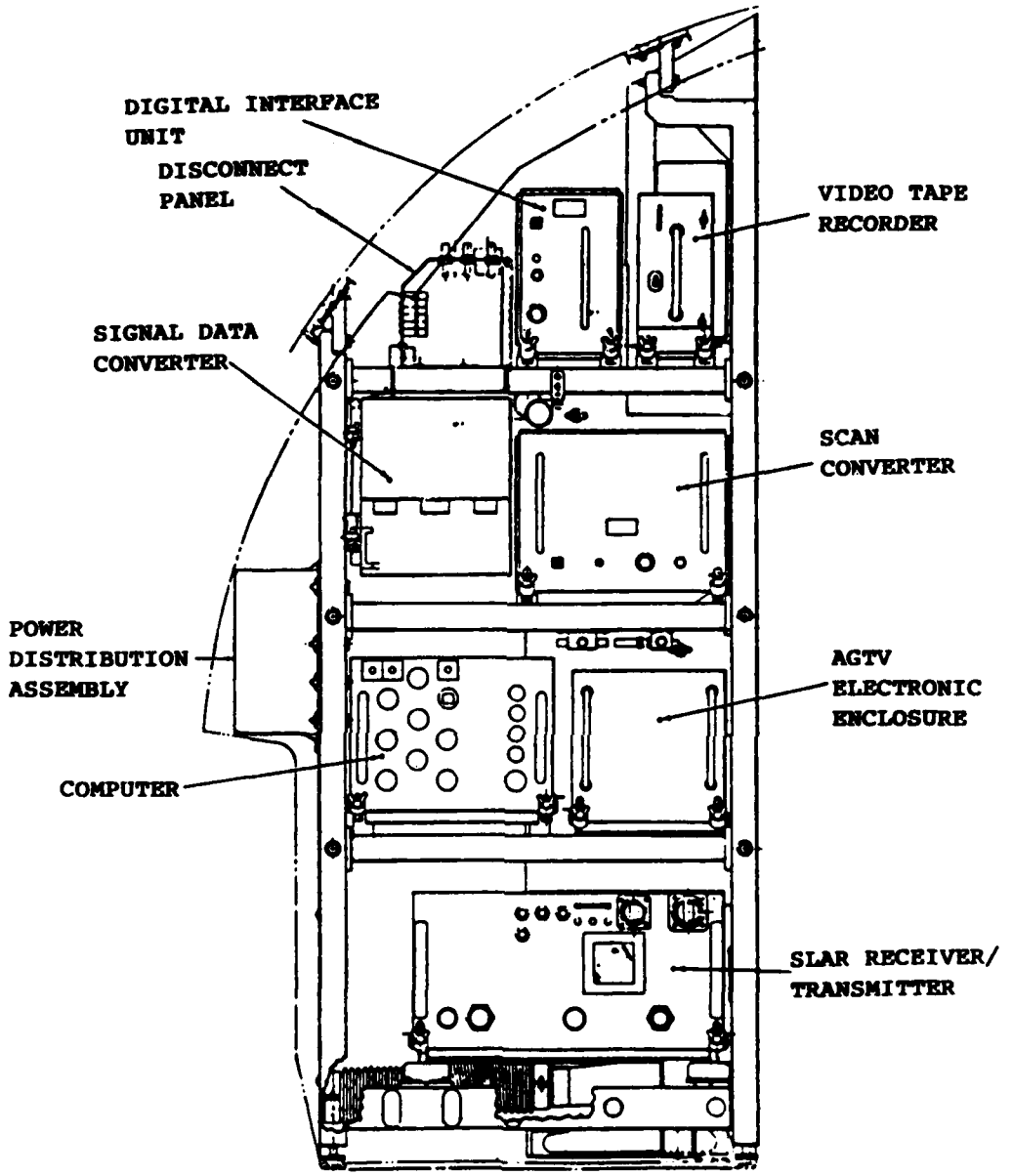

Figure 3-7. Equipment Rack

3.4.2.2 SSO Console Installation

The SSO console installation consist of the mounting of the exhaust blowers, installation of the various cooling air ducts and plenums, and the mounting of the A-scope, CDU and MPD support structures. The control panel locations are shown in Figure 3-8. All control panels are fastened to the console with standard 1/4 turn Dzus fasteners. The standard aircraft desk is modified to accept the trackball and joystick assembly. (The prime reference document for the SSO console is Aerojet Drawing No. 1315750-1, titled Console, situation display QJ-519/ASD-6.)

3.4.2.3 Auxiliary Fuel Cell Equipment

Figure 3-9 shows the equipment arrangement on the auxiliary fuel cell. The IR/UV film recorder and the video tape recorder share a common shock-mounted support structure and the SLAR synchronizer is shock-mounted on a separate support structure. Each structure is mounted to seat rails, provided by the airframe manufacturer, on top of the auxiliary fuel cell. Since the synchronizer is behind the aft fuselage partition, the partition must be removed for access to this unit.

3.4.2.4 Left-Side SLAR Equipment

As shown in Figure 3-10, the SLAR recorder viewer, processor and dc amplifier-power supply are mounted to a common unitized assembly. The recorder viewer is attached to a sliding plate which allows the SSO operator to either move it towards the center of the aircraft for easier viewing during operation or stow it in the position shown in Figure 3-10 for landing and takeoff. Provisions have been made which allow the total assembly to be moved from its standard position, adjacent to the SSO operator (third passenger seat area) forward to the first passenger seat area, F.S. 252.8 up to F.S. 192.8. The flexibility of this movement was Coast Guard requested to aid in SSO operator training. The left-side SLAR unit is mounted to the aircraft seat rails in the identical manner as the equipment rack, but requires no overhead securing. Exhaust air from the unit is directed to the auxiliary fuel cell area via ducting routed along the fuselage side wall, and through the partition.

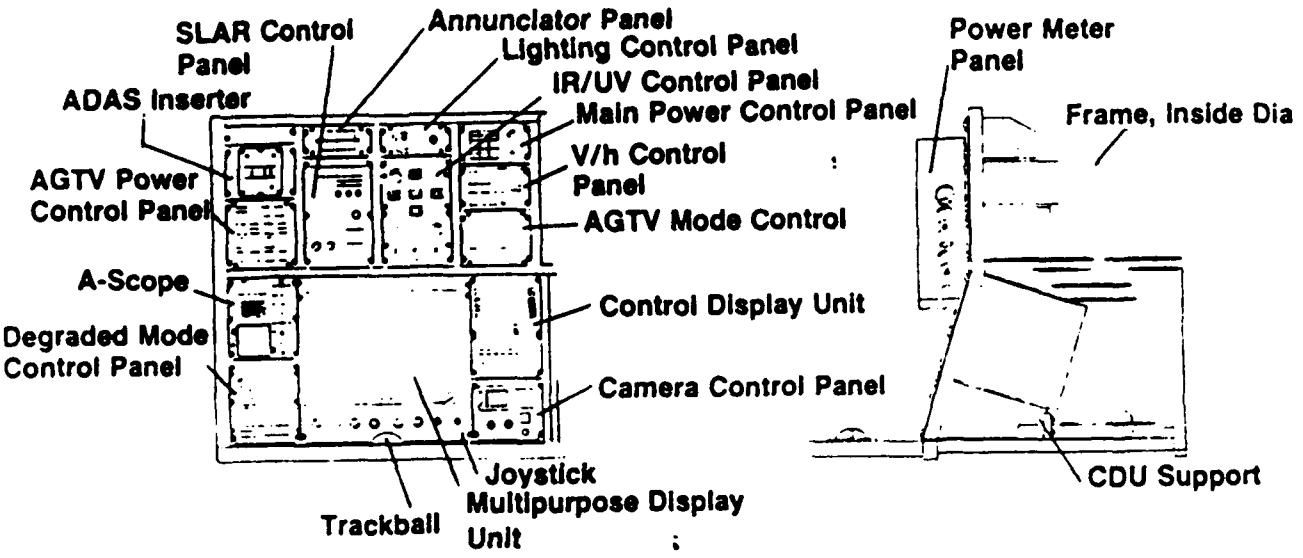

Figure 3-8. SSO Console

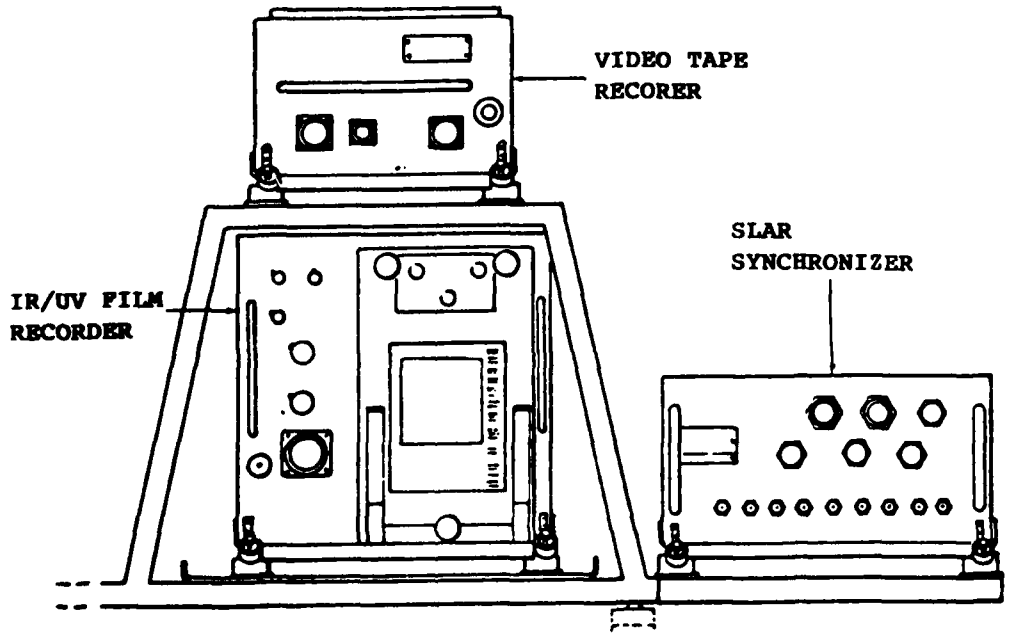

Figure 3-9 Auxiliary Fuel Cell Equipment

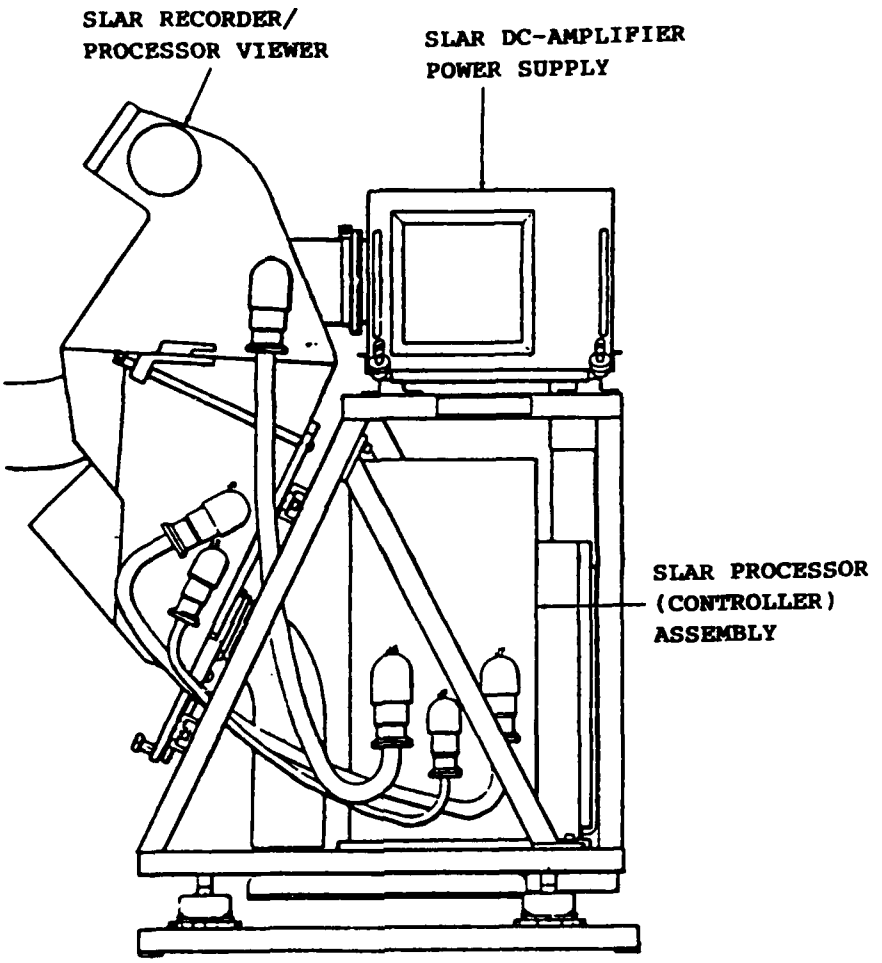

Figure 3-10. Left Side SLAR Equipment

3.4.2.5 Sensor Interface and Ancillary Equipment

The primary sensor electrical interface occurs at the sensor distribution panel located on the floor (right-hand side) between F.S. 239.8 and F.S. 258.4. It is from this distribution panel that all external sensor power and signal cables and radar waveguide runs are directed to the interior equipment. Waveguide pressurization is provided by a 3000 psi dry nitrogen bottle/regulator system, mounted on the forward edge top of the life raft compartment at F.S. 252.8. The pod jettison control panel and the SLAR anti-icing are located on the pilot's left side console at F.S. 85.0 and F.S. 89.0, respectively. Each unit is fastened to the console by four 1/4 turn Dzus fasteners.

3.4.3 AIREYE System Environmental Control

The AIREYE system utilizes ambient cabin air as a source of cooling air. The cooling cycle of the system is as follows:

1. Equipment Rack - Cabin air is drawn in at the base of the rack by a 160 CFM blower, and directed through the scan converter and DIU duct. Two (2) 60 CFM fans circulate the ambient air within the equipment rack.

2. SSO Console - Two (2) 240 CFM blowers draw cabin air into the SSO console area through gaps between the control panels and also create a low pressure area within the upper portion of the equipment rack.

3. The warm air from the equipment rack and the SSO console is expelled into the SSO console exhaust ducts by the 240 CFM blowers to the auxiliary fuel cell area and dumped adjacent to the outflow valves. The exhaust duct also contains the thermal and flow monitoring sensors.

4. The left-side SLAR draws in ambient cabin air and exhausts it into the auxiliary fuel cell area adjacent to the outflow valves.

5. The SLAR synchronizer draws in cabin air and exhausts it adjacent to the outflow valves.

3.4.4 Sensor Pod(s) Installation

3.4.4.1 AGTV and IR/UV Pods

The AGTV and IR/UV pod/pylon assemblies are mounted under the left and right wing, respectively, 146.8 inches outboard of the aircraft longitudinal centerline. The attachment of the pod/pylon assemblies consists of two 1/2 x 20 UNF bolts fastening the forward pylon support to the wing spar hardpoints, and a precision 1/2-inch-diameter pin supports the aft portion of the pylon. This rather unorthodox method of attachment was required due to the load handling characteristics of the hardpoints and the airframe manufacturer's recommendation. Electrical interfaces for power, signal and pod jettison are made via connectors located in the leading edge of the pylon assembly. AESC has provided ground handling fixtures to both position the pod assemblies for mating and demating with the aircraft as well as transportation between the aircraft. Photographs of the test pods and associated ground handling fixtures are shown in Figure 3-11.

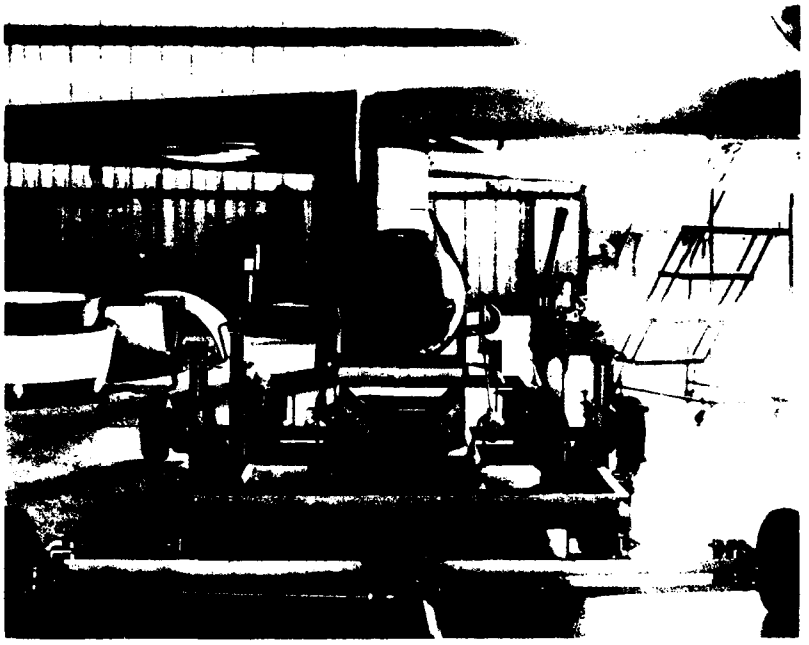

Test IR/UV Pod Installation and Handling Fixture

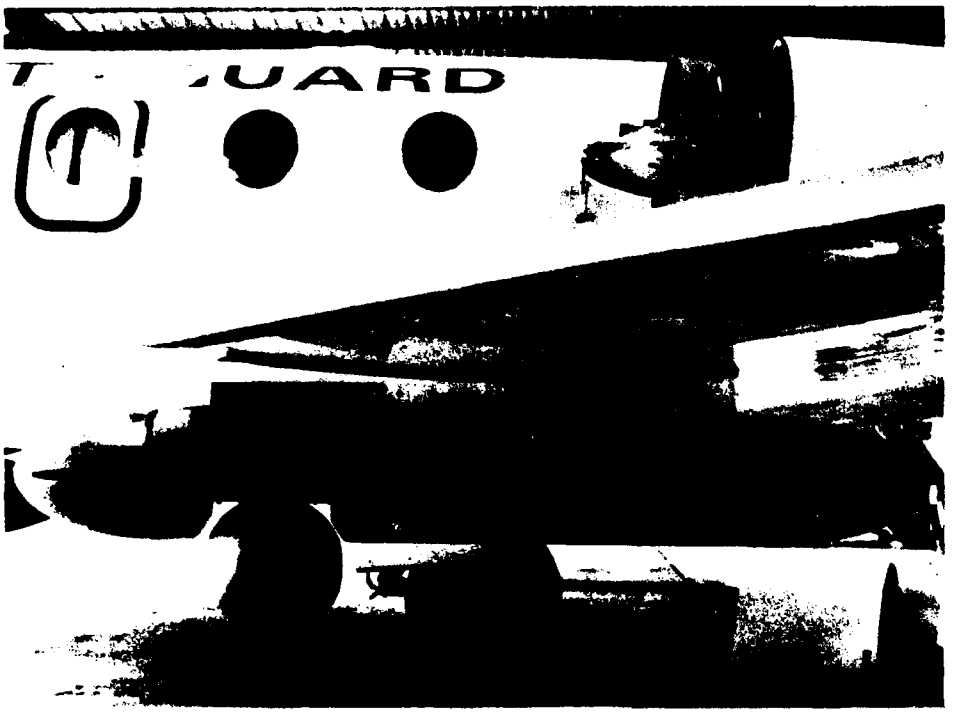

Test AGTV Pod Installation

Figure 3-11. Wing-Mounted Pod(s) Installation

3.4.4.2 SLAR Antenna Pod

The SLAR antenna pod is mounted to the right-side under-fuselage area with the centerline of the antenna offset 22.05 inches. The center of gravity of the antenna is at F.S. 183.8. Attachment of the antenna pod is accomplished as follows. Adapter plates are mounted to the fuselage hardpoints. These adapter plates pick up the aircraft hardpoints and provide the mounting surface for pylon-to-aircraft interface. After attachment of the pylon-to-aircraft interface mounting hardware, the antenna-to-aircraft waveguide hardware is installed as well as the electrical interface connectors mated. As in the case of the wing-mounted pods, a ground handling fixture is provided which both positions the antenna pod for mounting and transporting the unit between aircraft. Photographs of the test pod and ground handling fixture are shown in Figure 3-12. Additional photographs of the overall AIREYE installation are shown in Figure 3-13 (external sensor installation) and Figures 3-14 through 3-16 (interior equipment installation).

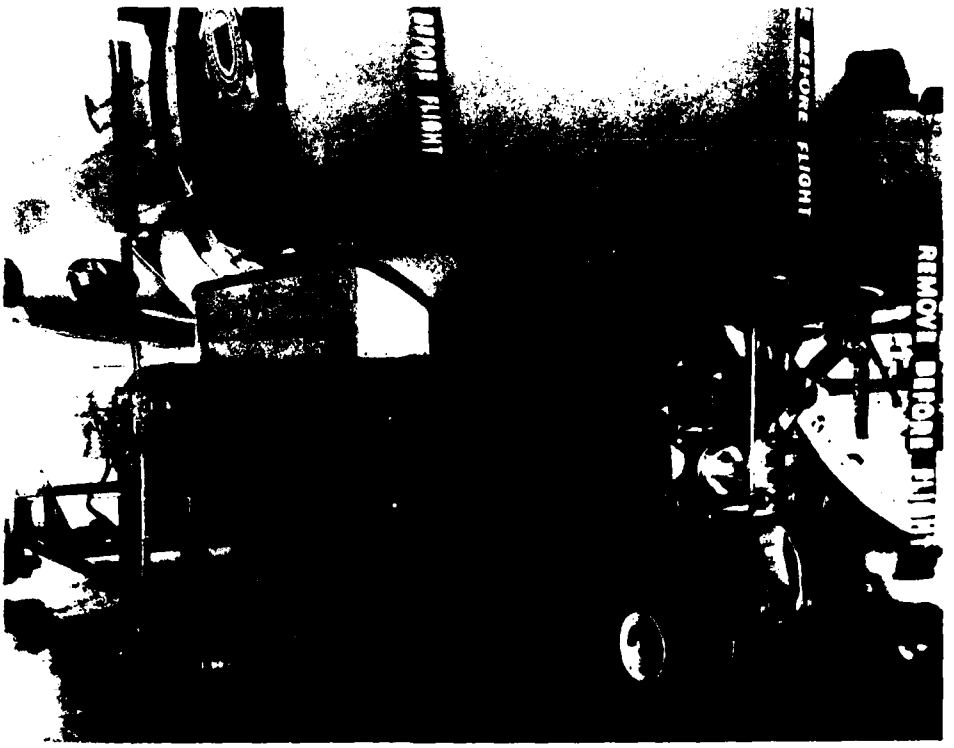

Figure 3-12. SLAR Pod Installation and Handling Fixture

Figure 3-13. AIREYE External Sensor Installation

Figure 3-14. Interior, Looking Aft, Equipment Rack Left Side Foreground, Left Side SLAR Right Side Foreground, SSO Console Left Side, and Auxiliary Fuel Cell Equipment

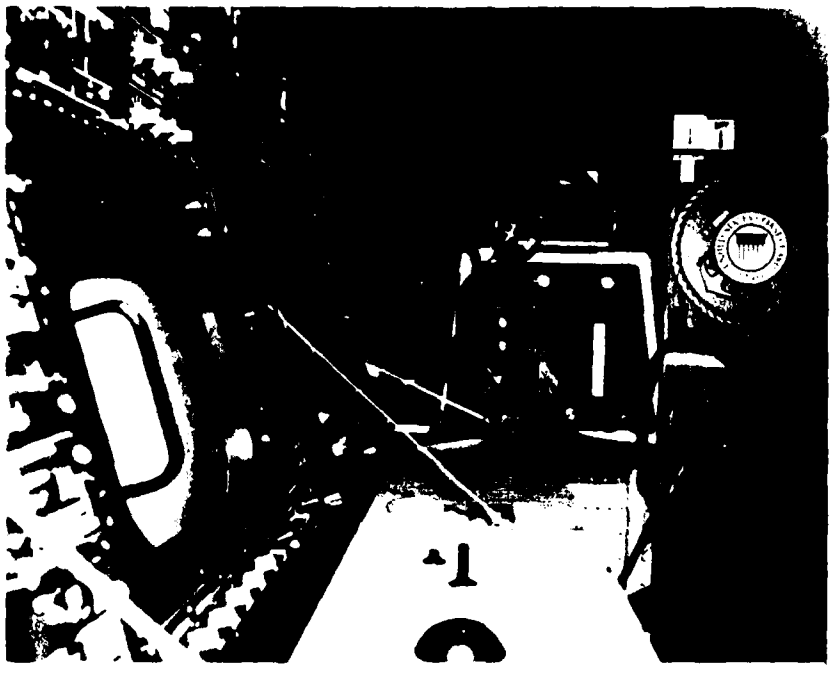

Figure 3-15. Interior Looking Aft, SSO Console on Left and Auxiliary Fuel Cell Equipment

Figure 3-16. Interior Looking Forward, Left Side SLAR Equipment Located at F.S. 192.8

3.4.5 AIREYE System/HU-25A Weight and Balance

As shown in Figure 3-17, the balance envelope of the HU-25A can vary from 19% to 30% mean aerodynamic chord (MAC). During the design phase of the program, particular attention was devoted to maintaining accurate weight data for the various AIREYE subsystems and components. The locations of the major subsystems were dictated by the Coast Guard and the airframe manufacturer. As can be seen in Figure 3-17, all the interior components as well as the wing-mounted sensors are located about the balance zone, the camera and the SLAR pod being the only sensor units located forward. The final AIREYE configuration and installation weight table is shown in Table 3-3. Figure 3-18 is a summary of weight and balance.

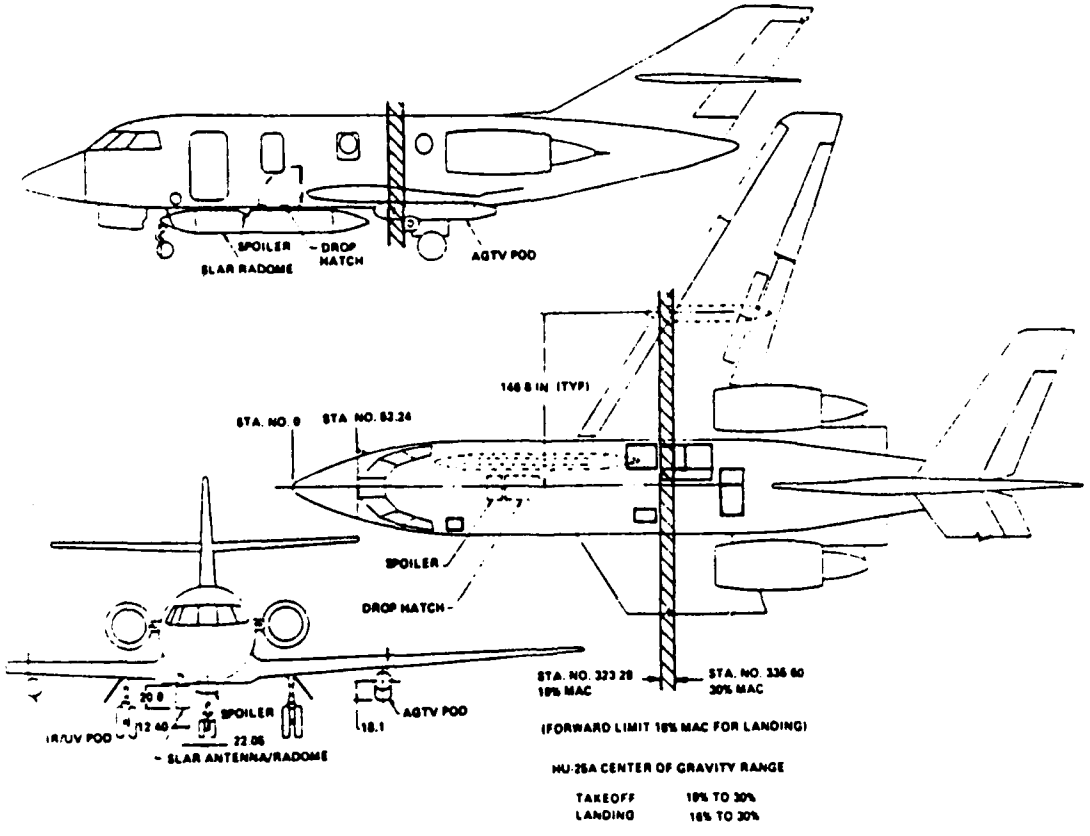

Figure 3-17. AIREYE/HU-25A Weight and Balance

TABLE 3-3 AIREYE WEIGHT TABLE

DESCRIPTION	WEIGHT (lbs)	ARM (in.)	MOMENT (in.-lbs.)	REMARKS
Basic Aircraft	20,033.0	334.4		S/N 2118
Survival Kit	505.0	262.2		Per FJC
Crew Flt. Deck (2)	360.0	112.2		
Observers (2)	360.0	214.9		
SSO Operator (1)	180.0	348.2		
Droppable Stores	225.0	179.2		Per FJC & USCG
Empty Operating Wt.	21,663.0			Per FJC & USCG
Less ARC Divan Seat, Armrest & Drawer	-30.7			
	21,632.3	325.5	7,041,932.12	A/C Empty For AIREYE
AIREYE Equip. Installation				
Cockpit				
Pod Drop Control	2.25	85.0	191.25	
Anti-Icing Control	1.6	89.0	142.4	
Circuit Breaker	.1	120.0	12.0	
Circuit Breaker	.1	120.0	12.0	
Connectors, Cable & Wire	4.3	180.0	774.0	
Cockpit sub-total	8.35			
Camera (KS-87B)	79.0	131.2	10,364.8	
Distribution Panel				
Waveguide Pressure Regulator/Gauges	5.0	264.2	1,321.0	
Connectors, Cables	8.0	268.5	2,149.0	
Dist. Panel sub-total	13.0			
Equipment Pack				
SLAR Receiver Transmitter Unit	74.5	305.5	22,759.75	
Scan Converter	49.7	305.3	14,959.7	
Computer	60.0	304.8	18,288.0	

TABLE 3-3 AIREYE WEIGHT TABLE (Continued)

DESCRIPTION	WEIGHT (lbs)	ARM (in.)	MOMENT (in.-lbs.)	REMARKS
Equipment Rack (cont)				
Display Interface Unit	24.8	305.8	7,583.8	
AGTV Electronics	30.5	304.7	9,293.4	
ADAS Unit	22.25	303.6	6,755.1	
Digital Tape Recorder	15.0	301.5	4,522.5	
Power Meter Panel	3.49	319.2	1,114.2	
Power Distribution Box	25.5	305.	7,777.5	
Equip. Rack W/ATR's, Harness, Plenums, Panels & Conn. Panel	124.0	305.0	37,820.0	
System Cables	75.5	305.0	22,875.0	
Equip. Rack sub-total	504.54			
SSO Console				
ADAS Inserter Panel	1.75	323.7	566.48	
AGTV Power Panel	5.52	323.7	1,786.8	
A-Scope Panel	11.51	323.7	3,725.79	
Degraded Mode Panel	5.52	323.7	1,786.8	
Annunciator Panel	1.6	330.2	528.3	
SLAR Control Panel	7.04	330.2	2,324.61	
Multipurpose Display	47.5	333.5	15,841.3	
Track Ball	3.0	333.5	1,000.5	
Joystick	2.0	340.1	680.0	
Lighting Control Panel	2.04	336.5	686.5	
IR/UV Control Panel	3.79	336.5	1,275.34	
Control Display Unit	14.66	343.7	5,038.64	
Camera Control Panel	4.51	343.7	1,550.1	
Power Control Panel	2.24	343.7	769.1	
V/H Control Panel	2.97	343.7	1,020.8	
AGTV Mode Panel	4.83	343.7	1,660.7	
Equipment Support Structure	4.6	333.5	1,534.1	
Blower	5.0	323.7	1,618.5	
Blower	5.0	343.7	1,718.5	
Ducting & Baffles	8.0	333.5	2,669.6	
System Cabling	50.1	333.5	16,708.4	
SSO Console sub-total	193.18			

TABLE 3-3 AIREYE WEIGHT TABLE (Continued)

DESCRIPTION	WEIGHT (lbs)	ARM (in.)	MOMENT (in.-lbs.)	REMARKS
Left-Side SLAR Equipment				
SLAR Rec/Viewer	62.9	322.0	20,253.8	
SLAR Processor	35.0	312.7	10,944.5	
SLAR Power Supply	26.1	310.7	8,109.3	
Structure With Blower	35.0	312.7	10,944.5	
Connectors and Cables	16.7	312.7	5,222.1	
L. Side SLAR sub-total	175.7			
Auxillary Fuel Cell Equipment				
IR/UV Film Recorder	62.3	391.2	24,371.8	
Video Tape Recorder	27.5	390.2	10,730.5	
SLAR Synchronizer	49.25	394.0	19,404.5	
Equipment Support Structure	22.0	394.0	8,668.0	
Connectors and Cables	16.7	382.0	6,379.4	
Anti-Icing Controller	7.0	391.2	2,738.4	
Aux. F.C. Equip. sub-total	184.75			
IR/UV Pod	120.6	333.6		
IR/UV Pod Pylon	35.1	333.6		
IR/UV Pod/Pylon sub-total	155.7		51,941.5	
AGTV Pod	381.0	338.4		
AGTV Pod Pylon	32.1	338.4		
AGTV Pod/Pylon sub-total	413.1		139,793.04	
SLAR Ant./Pod	227.0	183.8	41,722.6	
SLAR Pod Pylon	57.1	183.8	10,495.0	
Anti-Icing Heaters	2.4	124.8	299.5	
SLAR Pod/Pylon sub-total	286.5			
Pod Drop Cabling	8.9	274	2,438.6	
SLAR Anti-Icing Cabling	17.85	274	4,891.0	
	8.9	325	2,892.5	
Sub-Total	35.65			
TOTAL AIREYE SYSTEM WEIGHT WITH CABLES	2,049.5			
TOTAL	23,681.8		7,655,[illegible]1.32	

C. G. @ EMPTY A/C W/AIREYE WITH CREW OF 5 = 323.27 in. (18.995% MAC)

NO FUEL CONDITION

	Weight (lbs)	Arm (in.)	Moment (in.–lbs)	Center of Gravity Inches	Center of Gravity % MAC
BASIC AIRCRAFT (5)	21,632.3	325.5	7,041932.12	325.5	20.99
AIREYE SYSTEM	2,049.5		613728.9		
TOTAL	23,681.8		7,655661.02		
	7,655661.02 ÷		23,681.8 =	323.3	18.99

AT MAX. GROSS TAKEOFF WEIGHT (32,000 LBS)

AIRCRAFT WITH AIREYE	23,681.8	323.3	7,655661.02		
FUEL (WINGS)	7,820	331.08	2,589000		
FUEL (FEEDERS)	498	433.48	215,873		
TOTAL	31,999.8		10,460534.02		
	10,460534.03 ÷		31,998.8 =	326.9	22.23

Figure 3-18. AIREYE/HU-25A Weight and Balance Summary

Section 4

FLIGHT TEST PROGRAM

The AIREYE flight test program consisted of four categories of flights:

1. Safety of flight tests
2. Engineering evaluation tests
3. Acceptance test
4. Mission verification tests

Safety of flight tests were performed to establish the effects of external AIREYE stores on aircraft safety and performance, verify the integrity of the pod release mechanisms and pod release trajectories, and verify the performance of the SLAR anti-icing. Engineering evaluation tests were performed to verify AIREYE aircraft interfaces and AIREYE operation under flight conditions prior to performing the formal AIREYE flight acceptance test. Mission verification tests were performed to document AIREYE system performance against a variety of target and environmental scenarios. The safety of flight tests were performed from 5-27-83 to 4-3-84. The remainder of AIREYE system flight tests were performed from May of 1984 to May of 1985.

4.1 SAFETY OF FLIGHT

The overall objective of the safety of flight test program was to qualify the HU-25A as airworthy and safe for flight with the AIREYE external pods installed. The original certification intent was to obtain FAA certification of the aircraft with the AIREYE system installed. Due to a multitude of problems, however, it was decided to redirect the effort to a safety-of-flight test program, to be conducted by the Air Force Flight Test Center, Edwards Air Force Base. To provide a level of safety equivalent to the basic aircraft, the test program used, wherever applicable, current FAA regulations and military specifications. Test flights were conducted in accordance with the joint AFFR/AESC AIREYE HU-25A Safety of Flight (Flight Test) Plan dated 1 April 1983. Two additional flights were conducted at the completion of the basic safety-of-flight test program to verify the function of the SLAR pod anti-icing system.

Specific objectives of the test program were:

1. Evaluate the changes in the aircraft's flight characteristics and performance due to the installation of the AIREYE external pods and to develop manual changes applicable to the AIREYE-configured HU-25A.

2. Verify function of the pod release mechanism, and verify pod release trajectories.

3. Verify the function of the SLAR anti-icing system.

All performance and flying qualities test objectives were satisfied. The following is a summary of key findings:

1. The pod release system was safe and functional.

2. The addition of the AIREYE pods changed both the pilot and copilot position error contained in the flight manual.

3. The terminal area climb performance was degraded by the installation of the AIREYE pods.

4. The climb and cruise performance of the HU-25A was degraded with the aircraft pods.

5. Vmca was increased by 10 knots due to the installation of the AIREYE pods. The flight manual was modified to reflect time change.

6. The installation of the AIREYE pods required rudder and aileron trim changes with changes in airspeed. This was not found objectionable.

7. The aircraft exhibited a reduction in directional static stability with the installation of the AIREYE pods. Departure from controlled flight was observed from a steady-heading sideslip, using full rudder and opposite aileron deflection in cruise configuration. The flight manual was modified to prohibit full rudder with the AIREYE pods installed except in an engine-out emergency.

8. The flight manual procedure for emergency free fall and extension of the landing gear required application of full rudder and opposite aileron. Due to 7 (above), the flight manual was modified to require jettison of the AIREYE pods prior to applying full rudder.

9. The takeoff trim settings specified for the clean aircraft were not adequate for the AIREYE-equipped HU-25A. The flight manual was modified to reflect the new takeoff trim settings established during the test program.

10. The AGTV pod reduced ground clearance of the left wing. The flight manual was revised to include a note to use caution during left wing low landings.

11. The SLAR anti-icing system reduced ice buildup to less than that observed on other critical aircraft structures.

Table 4-1 is a summary of the flight test activity.

4.2 AIREYE SYSTEM FLIGHT TESTS

Table 4-2 is a chronological tabulation of all AIREYE system flight tests broken down by test category and flight duration. For completeness, support flights such as aircraft ferry, avionics repair, aircraft check flights, etc are also shown.

The total number of flights and flight hours for each category of AIREYE flight test are summarized below:

	Flights	Total Time
Aircraft Tests or Avionics Repair	16	22.2
AIREYE Engineering Evaluation/Test	42	78.8
AIREYE Acceptance Test Procedure	18	34.9
AIREYE Mission Verification	46	95.6
Misc (Pilot Familiarization, Ferry, etc)	8	23.8
Total	130	255.3

4.2.1 Engineering Evaluation Tests

Engineering evaluation flight tests were performed throughout the flight test period, to evaluate system performance and/or evaluate changes or corrections implemented in hardware or software. The tests can be categorized by major activities into several time intervals as shown in Table 4-2.

TABLE 4-1 SAFETY OF FLIGHT TEST FLIGHT SUMMARY

Flight No.	Date	Loading	Test
GVT	5-21-83	1	Aileron Stiffness/Damping Characteristics
1	5-27-83	1	Flutter and Loads
2	6-2-83	1	Flutter and Loads
3	6-10-83	2	Flutter and Loads
4	6-15-83	2	Flutter and Loads
5	6-17-83	2	Flutter and Loads
6	6-29-83	2	Pitot-Static Calibration
7	7-1-83	2	Pitot-Static Calibration
8	7-6-83	1	Pitot-Static Calibration
9	7-7-83	1	Pitot-Static Calibration
10	7-8-83	1	Pitot-Static Calibration
11	7-11-83	3	Taxi Flutter
12	7-19-83	3	Taxi Flutter
13	7-22-83	3	Taxi Flutter
14	7-25-83	3	Taxi Flutter
15	7-26-83	3	Taxi Flutter
17	7-29-83	3	Taxi Flutter
18	7-29-83	3	Taxi Flutter
19	8-3-83	3	Flutter
20	8-5-83	3	Flutter
21	8-9-83	1	Pitot-Static Calibration
22	8-10-83	1	Pitot-Static Calibration
23	8-10-83	1	Ferry to Sacramento - Maintenance

Flight No.	Date	Loading	Test
24	8-11-83	1	Ferry Return to Edwards AFB
25	8-16-83	2	Pitot-Static Calibration
26	8-17-83	2	Pitot-Static Calibration
27	8-20-83	3	Pitot-Static Calibration
28	8-24-83	2	SLAR Loads
29	8-25-83	1	Pitot-Static Calibration
30	8-26-83	1	Stability and Control Stalls
31	8-29-83	1	Stability and Control Stalls
32	8-31-83	4	AGTV Flutter/Loads
33	9-2-83	4	Flutter
34	9-7-83	1	Performance and Flying Qualities (P&FQ)
35	9-8-83	2	P&FQ (Stalls)
36	9-9-83	2	P&FQ Cruise Performance
37	9-10-83	1	P&FQ Climb Performance
38	9-12-83	2	P&FQ Climbs
39	9-15-83	2	P&FQ Overwater Performance
40	9-16-83	1	P&FQ Overwater Performance (No Data)*
41	9-17-83	4	P&FQ Stalls
42	9-19-83	4	P&FQ Low Altitude Cruise
43	9-20-83	4	P&FQ Climbs
44	9-21-83	4	P&FQ Cruise
45	9-22-83	3	P&FQ Climbs
46	9-23-83	3	P&FQ Overwater Cruise
47	9-24-83	3	P&FQ Cruise
48	9-26-83	1	P&FQ Overwater Cruise
49	9-27-83	1	P&FQ Firing Qualities
50	9-28-83	1	P&FQ Stability and Control

Flight No.	Date	Loading	Test
51	9-29-83	4	Pitot Static
52	10-4-83	4	Ferry aircraft from FSI/Mojave to Edwards AFB
53	10-5-83	4	AGTV pod drop
54	10-11-83	2	SLAR pod drop
55	10-13-83	3	AGTV pod drop
56	10-18-83	4	AGTV pod drop
57	10-21-83	2	SLAR pod drop
58	10-21-83	1	Ferry aircraft from Edwards AFB to FSI/Mojave
*	10-25-83	1	Ferry aircraft from FSI/Mojave to Edwards AFB
59	10-25-83	3	IR/UV pod drop
60	10-27-83	4	AGTV pod drop
*	10-31-83	4	Ferry aircraft from Edwards AFB to FSI/Mojave
61	11-4-83	4	Aircraft ferry flight FSI/Mojave to Edwards AFB
62	11-5-83	2	Flying Quality Tests
63	11-5-83	2	Flying Quality Tests
64	11-7-83	2	Flying Quality Tests
65	11-8-83	1	Flying Quality Tests
66	11-8-83	2	Quality Tests
67	11-9-83	3	Flying Quality Tests
68	11-9-83	4	Wing Pod Icing Test
*	11-10-83	4	Deflated both left tires and strut to determine AGTV turret ground clearance
69	11-11-83	4	Flying Quality Tests
70	11-11-83	4	Flying Quality Tests
71	11-12-83	3	Flying Quality Tests
72	11-12-83	4	Flying Quality Tests
73	11-14-83	4	Flying Quality Tests

Flight No.	Date	Loading	Test
73	11-15-83	1	Aircraft ferry flight to Garrett/LAX for engine inspection/nozzle replacement
*	11-19-83	1	Aircraft ferry flight Garrett/LAX to Edwards AFB
74	11-19-83	1	Flying Quality Tests
75	11-21-83	1	Flying Quality Tests
76	11-21-83	1	Flying Quality Tests
77	11-22-83	3	Flying Quality Tests
78	11-22-83	2	SLAR pod drop
79	11-22-83	1	Flying Quality Tests
80	11-23-83	4	Flying Quality Tests
81	11-28-83	2	Flying Quality Tests
82	11-28-83	2	Flying Quality Tests
83	11-29-83	3	Flying Quality Tests
84	11-29-83	3	IR/UV Separation
85	11-30-83	2	Flying Quality Tests
86	12-1-83	1	Flying Quality Tests
87	12-1-83	1	Flying Quality Tests
88	12-2-83	1	Flying Quality Tests
89	12-2-83	1	Flying Quality Tests
90	12-3-83	4	Flying Quality Tests
91	12-5-83	4	Flying Quality Tests
92	12-5-83	3	Flying Quality Tests
93	12-6-83	1	Flying Quality Tests
94	12-6-83	2	Flying Quality Tests
95	12-6-83	4	Flying Quality Tests
96	12-6-83	3	Flying Quality Tests
97	12-7-83	2	Flying Quality Tests
98	12-7-83	3	Flying Quality Tests

Flight No.	Date	Loading	Test
99	12-8-83	4	SALVO Pod Drop Test
Anti-Ice *	1-11-84	2	SLAR Anti-Ice Performance
Anti-Ice *	4-3-84	2	SLAR Anti-Ice Performance

*No flight number assigned in log.

POD LOADINGS

1 = No Pods

2 = SLAR Pod

3 = SLAR & IR/UV Pod

4 = SLAR, IR/UV, and AGTV

TABLE 4-2 AIREYE SYSTEM FLIGHT TESTS

Date	Location	Purpose	Duration (hrs)	Aircraft (S/N)
5-2-84	Local area	Engr evaluation	2.1	2118
5-3-84	Local area	Aircraft check	0.3	2118
5-4-84	Sacramento and return	FLR repair	2.5	2118
5-7-84	Local area - Catalina	Engr evaluation	3.3	2118
5-9-84	Local area - Catalina	Engr evaluation	2.3	2118
5-11-84	Local area - Catalina	Engr evaluation	2.4	2118
5-15-84	Local area - Catalina	Engr evaluation	2.5	2118
5-16-84	Local area - Catalina	Engr evaluation	2.1	2118
5-17-84	Local area - Catalina	Engr evaluation	2.0	2118
5-22-84	Local area	Engr evaluation	2.3	2118
5-22-84	Local area	Engr evaluation	1.0	2118
5-23-84	Local area	Engr evaluation	1.9	2118
5-24-84	Local area	Pilot familiarization	1.9	2118
5-25-84	Local area - Barstow	ATP	2.2	2118
5-25-84	Local area	ATP	1.8	2118
5-29-84	Local area	ATP	2.0	2118
5-30-84	Local area - Corona	ATP	1.9	2118
5-30-84	Local area - Corona	ATP	2.3	2118
5-31-84	Local area	ATP	2.2	2118
5-31-84	Local area	ATP	1.8	2118
6-1-84	Local area	ATP	1.9	2118
6-2-84	Local area	ATP	1.9	2118
6-6-84	Santa Barbara	Engr evaluation & area familiarization	1.9	2118
6-7-84	So. Cal area	Pilot area familiarization	3.2	2118
6-13-84	So. Cal area	Engr evaluation	1.1*	2118
6-15-84	Local area - Catalina	Engr evaluation	2.1	2118
6-18-84	Local area - Catalina	Engr evaluation	1.4	2118
6-29-84	Santa Barbara channel	Engr evaluation	1.9	2118
7-2-84	Sacramento and return	FLR repair	2.3	2118

TABLE 4-2 AIREYE SYSTEM FLIGHT TESTS (Continued)

Date	Location	Purpose	Duration (hrs)	Aircraft (S/N)
7-6-84	Santa Barbara channel	Engr evaluation	2.0	2118
7-10-84	Santa Barbara channel	Engr evaluation	2.2	2118
7-12-84	Santa Barbara channel	Engr evaluation	2.2	2118
7-13-84	SBA	Engr briefing for UCSB personnel	1.5	2118
7-17-84	Santa Barbara channel	Engr evaluation	0.2*	2118
7-25-84	So. Cal area	Aircraft check	0.3	2118
7-27-84	So. Cal area	Aircraft check	1.5	2118
7-30-84	Santa Barbara channel	Engr evaluation	0.8	2118
7-30-84	Santa Barbara channel	Engr evaluation	2.3	2118
8-1-84	Santa Barbara channel	Engr evaluation	2.3	2118
8-3-84	So. Cal area	Aircraft check	0.6	2118
8-4-84	Santa Barbara channel	Engr evaluation	1.5	2118
8-6-84	Local area	Aircraft check	0.7	2118
8-8-84	To Tinker AFB	On route to Griffiss AFB	4.5*	2118
8-10-84	Tinker local area	Aircraft check	0.9	2118
8-11-84	To Griffiss	Complete flight to Griffiss	4.1	2118
8-18-84	Griffiss local area	Aircraft check	2.4	2118
8-19-84	Griffiss local area	AGTV engr eval	2.0	2118
8-19-84	Lake Ontario	AGTV engr eval	2.4	2118
8-21-84	Griffiss local area	AGTV engr eval	2.0	2118
8-23-84	To Cape Cod	Aircraft repair	1.1	2118
8-26-84	To Ontario, CA	Return aircraft	7.0	2118
8-30-84	Santa Barbara channel	Engr evaluation	2.3	2118
8-31-84	Santa Barbara channel	Engr evaluation	1.7	2118
9-8-84	Local area	ATP	1.8	2118
9-10-84	Santa Barbara channel	Mission Verification	2.0	2118

TABLE 4-2 AIREYE SYSTEM FLIGHT TESTS (Continued)

Date	Location	Purpose	Duration (hrs)	Aircraft (S/N)
9-10-84	Santa Barbara channel	Mission verif	1.5	2118
9-13-84	Santa Barbara channel	Mission verif	0.8	2118
9-13-84	Santa Barbara channel	Mission verif	3.0	2118
9-17-84	Santa Barbara channel	ATP	2.1	2118
9-18-84	Santa Barbara channel	Mission verif	1.9	2118
9-18-84	Santa Barbara channel	Mission verif	2.0	2118
9-19-84	Sacramento and return	FLR repair	2.4	2118
9-20-84	Santa Barbara channel	Mission verif	1.7	2118
9-20-84	Santa Barbara channel	Mission verif	2.0	2118
9-24-84	Santa Barbara channel	Mission verif	2.0	2118
9-24-84	Santa Barbara channel	Mission verif	0.8	2118
9-25-84	Santa Barbara channel	Mission verif	1.6	2118
9-25-84	Santa Barbara channel	Mission verif	1.3	2118
9-27-84	Santa Barbara channel	Mission verif	2.0	2118
9-27-84	Santa Barbara channel	Mission verif	2.2	2118
9-28-84	Santa Barbara channel	Mission verif	2.2	2118
9-28-84	Santa Barbara channel	Mission verif	2.3	2118
10-16-84	Local area	ATP	1.7*	2118
10-17-84	Santa Barbara channel	Mission verif	2.0	2118
10-17-84	Santa Barbara channel	Mission verif	2.3	2118
10-18-84	Santa Barbara channel	Mission verif	1.5	2118
10-18-84	Santa Barbara channel	Mission verif	1.1	2118
10-19-84	Santa Barbara channel	Mission verif	1.9	2118
10-19-84	Santa Barbara channel	Mission verif	1.9	2118
10-22-84	Santa Barbara channel	Mission verif	2.0	2118
10-22-84	Santa Barbara channel	Mission verif	2.5	2118
10-23-84	Santa Barbara channel	Mission verif	1.1	2118
10-23-84	Santa Barbara channel	Mission verif	4.0	2118
10-26-84	Santa Barbara channel	Mission verif	2.7	2118

TABLE 4-2 AIREYE SYSTEM FLIGHT TESTS (Continued)

Date	Location	Purpose	Duration (hrs)	Aircraft (S/N)
10-26-84	Santa Barbara channel	Mission verif	2.8	2118
10-29-84	Santa Barbara channel	Mission verif	2.0	2118
10-29-84	Santa Barbara channel	Mission verif	2.3	2118
10-30-84	Santa Barbara channel	Mission verif	1.9	2118
10-30-84	Santa Barbara channel	Mission verif	2.4	2118
10-31-84	Santa Barbara channel	Mission verif	2.0	2118
10-31-84	Santa Barbara channel	Mission verif	2.2	2118
11-9-84	Santa Barbara channel	ATP	1.8	2118
11-9-84	Santa Barbara channel	Engr evaluation	2.0	2118
11-14-84	Santa Barbara channel	ATP	1.7	2118
11-15-84	San Francisco area	Mission verif	2.5	2118
11-15-84	San Francisco area	Mission verif	1.9	2118
1-16-85	Local area	Aircraft check	0.3	2122
1-17-85	Local area	Aircraft check	2.9	2122
1-17-85	Local area	Aircraft check	2.2	122
1-18-85	Local area	Aircraft check	2.1	2122
1-28-85	Local area	Aircraft check	0.4	2122
1-29-85	Local area	Aircraft check	0.4	2122
1-31-85	Local area	Air data comp, ATP	2.6	2122
2-1-85	Santa Barbara channel	Mission verif	1.9	2122
2-2-85	Santa Barbara channel	ATP	1.8	2122
2-5-85	Local area	ATP	1.5	2122
2-28-85	Santa Barbara channel	Mission verif	2.0	2122
4-2-85	Newport Beach	Engr evaluation	1.6	2118
4-9-84	Local area - desert	Engr evaluation	1.7	2118
4-11-85	Local area - desert	Engr evaluation	1.5	2118
4-11-85	Local area - desert	Engr evaluation	2.1	2118
4-15-85	Local area - desert	Engr evaluation	1.8	2118
4-15-85	Local area - Long Beach	Engr evaluation	2.0	2118

TABLE 4-2 AIREYE SYSTEM FLIGHT TESTS (Continued)

Date	Location	Purpose	Duration (hrs)	Aircraft (S/N)
4-16-85	Local area - desert	Engr evaluation	1.6	2118
4-18-85	Santa Barbara channel	Engr evaluation	2.3	2118
4-18-85	Santa Barbara channel	Engr evaluation	1.9	2118
4-24-85	Santa Barbara channel	Engr evaluation	1.5	2118
4-24-85	Santa Barbara channel	Engr evaluation	1.5	2118
4-25-85	Santa Barbara channel	Engr evaluation	1.4	2118
5-8-85	Santa Barbara channel	Engr evaluation	1.7*	2118
5-10-85	To Ontario	Return aircraft	0.5	2118
5-12-85	Santa Barbara channel	Mission verif	3.0	2118
5-13-85	Santa Barbara channel	Mission verif	2.8	2118
5-14-85	Santa Barbara channel	Mission verif	2.2	2118
5-14-85	Santa Barbara channel	Mission verif	2.1	2118
5-15-85	Santa Barbara channel	ATP	1.9	2118
5-15-85	Santa Barbara channel	Mission verif	2.5	2118
5-16-85	Santa Barbara channel	Mission verif	2.1	2118
5-19-85	Santa Barbara channel	Mission verif	2.4	2118
5-19-85	Santa Barbara channel	Mission verif	2.3	2118

*Major aircraft problem

TABLE 4-3 ENGINEERING EVALUATION FLIGHT BREAKDOWN

Start Date	End Date	Flights	Purpose
5-2-84	5-23-84	10	Initial system checkout and debug
6-13-84	8-4-84	12	AGTV checkout; SLAR overlay correction
8-19-84	8-21-84	3	AGTV test flights at Griffiss AFB
8-30-84	8-31-84	2	SLAR overlay correction
4-2-85	5-8-85	13	AGTV checkout

4.2.2 AIREYE Functional Flight Tests (Formal Acceptance Test Procedure)

The AIREYE Acceptance Test Procedure was run utilizing AESC Procedure No. AE-24434/094. Initially, the entire procedure was run in a period from 25 May 1984 to 2 June 1985. Rerun of portions of the procedure to verify correction of problems were run as the schedule permitted throughout the remainder of the flight test program. AGTV gimbal problems and associated AGTV problems required rerun of the entire AGTV section of the Acceptance Test Procedure when these problems were corrected.

4.2.3 AIREYE Mission Verification Tests

Mission verification flight tests were performed to document AIREYE system performance over a wide range of environmental and operating conditions, and to determine the optimum operational parameters for utilization of the AIREYE system. The majority of the flight tests were conducted over the Santa Barbara channel and surrounding area. The AIREYE system was exercised against targets involving natural oil seeps, ships of various sizes, vessel wakes, thermal discharges and kelp. Tests were conducted under as wide a range of environmental conditions as possible during the testing time frame, under flight conditions ranging from 200 ft to 10,000 ft in altitude, and from airspeeds ranging from less than 150 KIAS to greater than 250 KIAS.

The Geography Remote Sensing Unit of the University of California, Santa Barbara was utilized for several AIREYE mission verification tests to collect ground truth data and perform specific data reduction tasks.

4.2.3.1 Data Reduction Techniques

The principal sources of data utilized in data reduction are shown on Table 4-4.

TABLE 4-4 DATA SOURCES

Sensor	Data Source
SLAR	Videotape, SLAR film record, IR/UV film record (hard copy mode); UCSB ground truth
IR/UV	Videotape, IR/UV film record, UCSB ground truth
AGTV	Videotape, IR/UV film record (hard copy mode), UCSB ground truth
KS-87B	KS-87B film record

Detailed flight log sheets containing salient data for each data run including aircraft parameters, environmental parameters, and target parameters were combined with the image data and associated AIREYE annotation data from the recording media analyzed. Voice recordings of the ICS recorded on the audio track of the videotape recorder were used extensively to augment other data.

From the combined data sources, a data reduction record was generated for all data runs. This record combined all available data with reduced target detection parameters (detection range, orientation, etc). The data summaries subsequently presented in this report were obtained from analyses of the data reduction record.

4.2.3.2 SLAR Data

4.2.3.2.1 Detection Principles

For a point target, the classical radar equation is

$$P_r = \frac{P_t G^2 \sigma_T \lambda^2}{(4\pi)^3 R^4} \qquad (4\text{-}1)$$

where P_r = power received

P_t = peak power transmitted

G = one-way antenna gain

σ_T = radar target cross section

λ = operating wavelength

R = slant range to the target

This equation expresses the power received at the radar as a function of radar operating parameters, target reflection characteristics and range.

There are two limiting cases that limit a radar's ability to detect a target:

1. The noise limited case, in which the return from the desired target is masked by the radar's internal noise
2. The clutter limited case, in which the return from the desired target is masked by return from features surrounding the target (clutter).

For the noise limited case, the receiver noise equivalent power N, is defined as

$$N = KTBNF \tag{4-2}$$

where

K = Boltzmann's constant

T = equivalent receiver temperature

B = radar noise bandwidth

NF = radar receiver noise figure

For reliable detection, the signal from the target must exceed the receiver noise by a value defined as the signal-to-noise ratio (S/N). A larger signal-to-noise ratio produces a higher probability of detection, and a lower false alarm rate. Substituting the relationship for the noise power and required signal-to-noise ratio for the received power, P_r, in Equation (4-1) yields

$$KTBNF(S/N) = \frac{P_t G^2 \sigma_T \lambda^2}{(4\pi)^3 R^4} \tag{4-3}$$

or

$$R = \left[\frac{P_t G^2 \sigma_T \lambda^2}{(4\pi)^3 KTBNF(S/N)}\right]^{1/4} \tag{4-4}$$

Equation (4-4) therefore gives the detection range for a point target for the noise limited case. The parameter σ_T is a measure of a point target's ability to reflect radar energy. The numerical value of the radar cross section, σ_T , depends on a variety of functions including the target material, physical configuration, wavelength and viewing angle.

The radar cross section, σ_T , is used for definition of the radar return from a point target, such as a ship at long range. For an extended target, such as the ocean, a normalized radar cross section, σ_o (cross section per unit area) is used. The total radar cross section, σ , for an extended target is obtained by the product of the normalized radar cross section and the area of a resolution element on the ground.

$$\sigma = G_o A \tag{4-5}$$

where

σ_o = normalized radar cross section

A = area of the radar's resolution element on the ground.

For a sidelooking radar, the area of the resolution element, A , is given by

$$A = \frac{R \gamma \tau c \sec\theta}{2} \tag{4-6}$$

where R = slant range to target

τ = pulse width

c = speed of light

θ = depression angle

γ = antenna 3-dB azimuthal beamwidth

Substituting Equation (4-6) into Equation (4-5) yields

$$\sigma = \frac{\sigma_o R \gamma \tau c \sec\theta}{2} \tag{4-7}$$

For an extended target the detection range is given by substituting the relationship given by Equation (4-7) into Equation (4-4)

$$R = \left[\frac{P_t G^2 \lambda^2 \sigma_o \gamma \tau c \sec\theta}{2(4\pi)^3 KTBNF(S/N)}\right]^{1/3} \tag{4-8}$$

For the clutter limited case, the signal-to-clutter ratio is given by

$$S/C = \frac{2\sigma_t}{\sigma_o R \gamma \tau c \sec\theta} \tag{4-9}$$

The mechanism for the detection of oil by a side-looking radar is the reduction of backscatter resulting from the calming effect of oil films on small-scale water waves. Oil films significantly damp or attenuate the capillary and small-scale gravity waves which cause much of the normal sea backscatter at radar frequencies. The damping action manifests itself in a reduction of the normalized cross section of the ocean, and, hence, oil-covered areas in SLAR images appear dark relative to the grainy brighter returns from an undisturbed sea surface.

Detection of oil on the ocean surface requires that the return from the undisturbed (i.e., oil free) ocean be detectable by the radar. Ocean return as defined by σ_o or normalized radar cross section is a function of windspeed, viewing angle, and viewing aspect. For example, Figure 4-1 is data obtained by AESC during AOSS I flight tests showing the values for ocean return as a function of windspeed for depression angles of 2, 5 and 10 degrees, for crosswind and upwind viewing respectively. Figure 4-2 shows the variation on ocean-normalized radar cross section, σ_o, as a function of depression angle for upwind and crosswind data for a 2-6 knot wind, 0-ft sea, and 1-ft swell. Figure 4-3 shows the same data for 2 to 15-knot winds, 2-ft seas and 5-ft swells. The expected maximum oil spill detection may be calculated by inserting the value of σ_o as obtained from these curves into Equation (4-8) and using the AN/APS-131 radar characteristics.

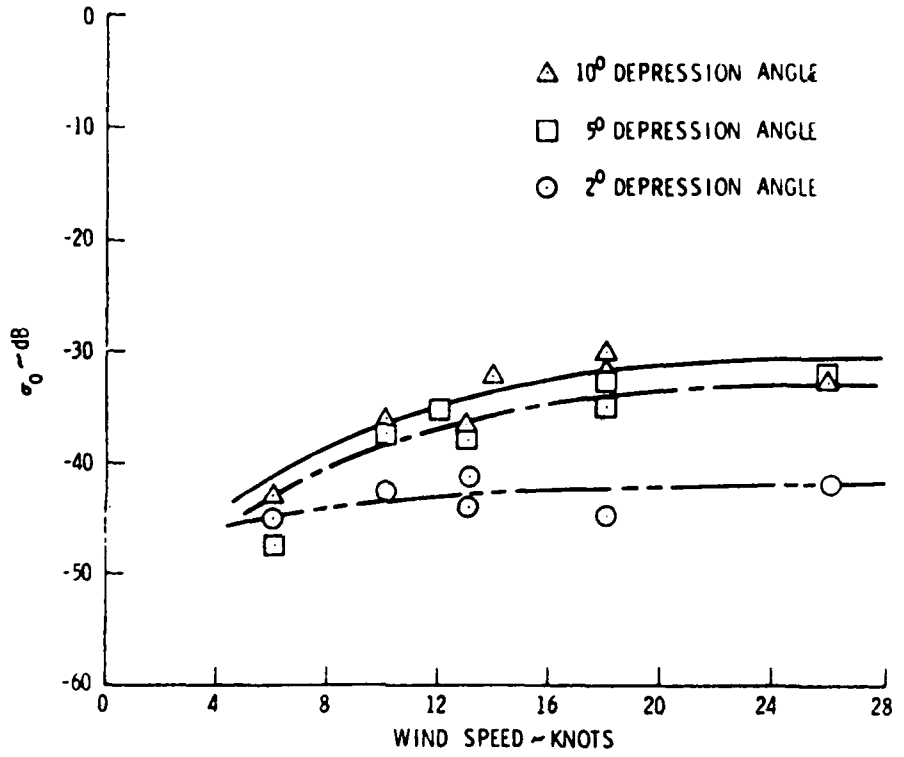

Figure 4-1a. Normalized Radar Cross Section for Ocean Returns (Crosswind)

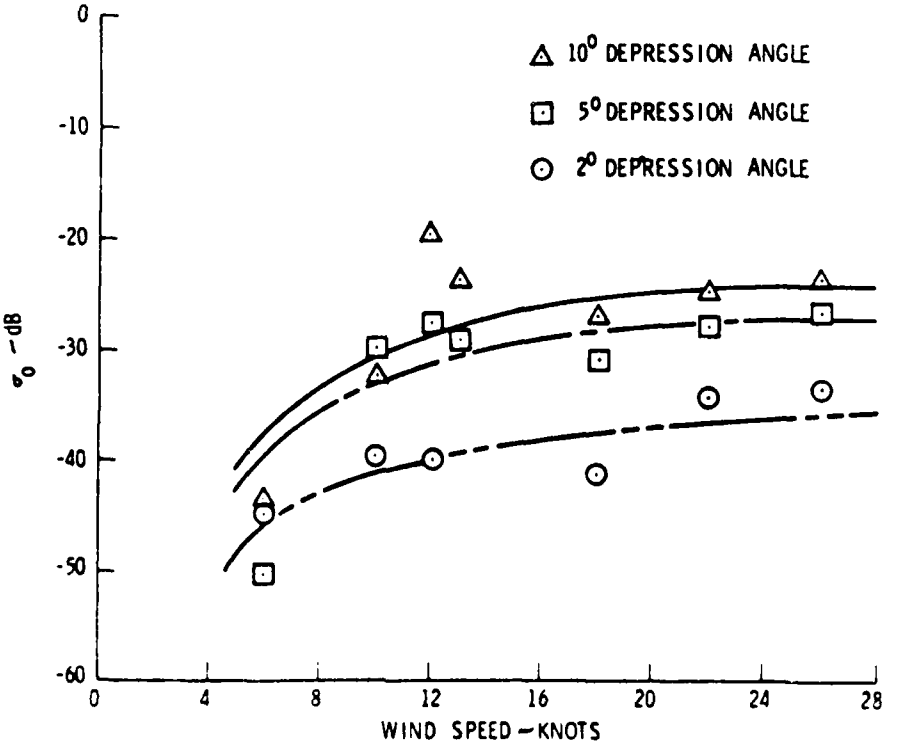

Figure 4-1b. Normalized Radar Cross Section for Ocean Returns (Upwind)

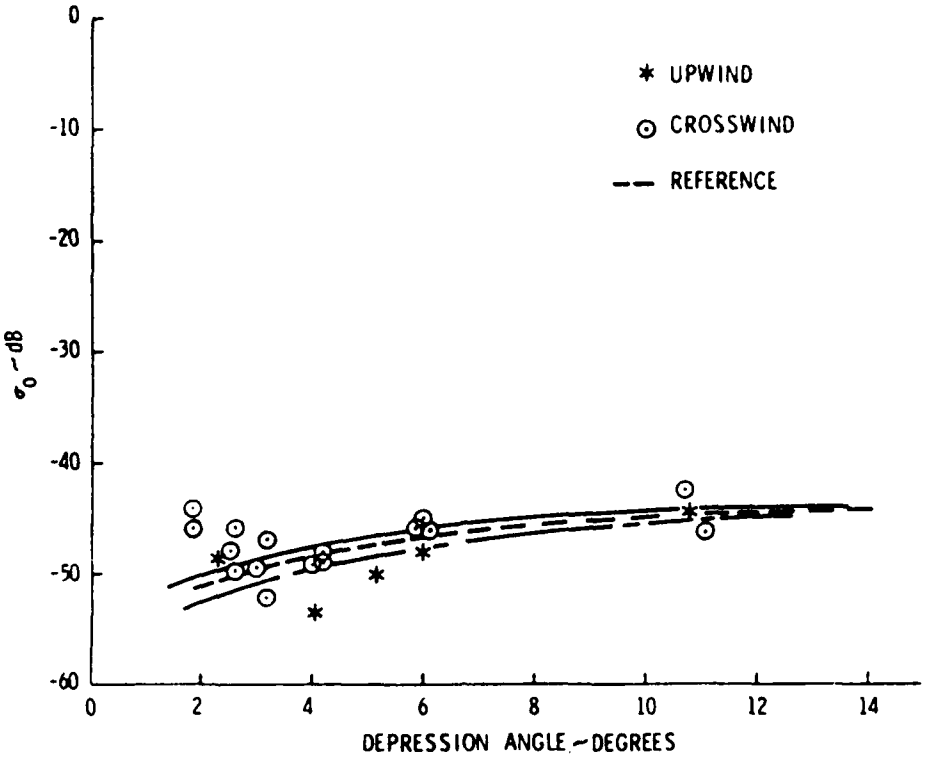

Figure 4-2. Normalized Radar Cross Section for Ocean Returns, 2-6 Knot Wind, 0 ft Sea, 1 ft Swell (Sea State = 0-1)

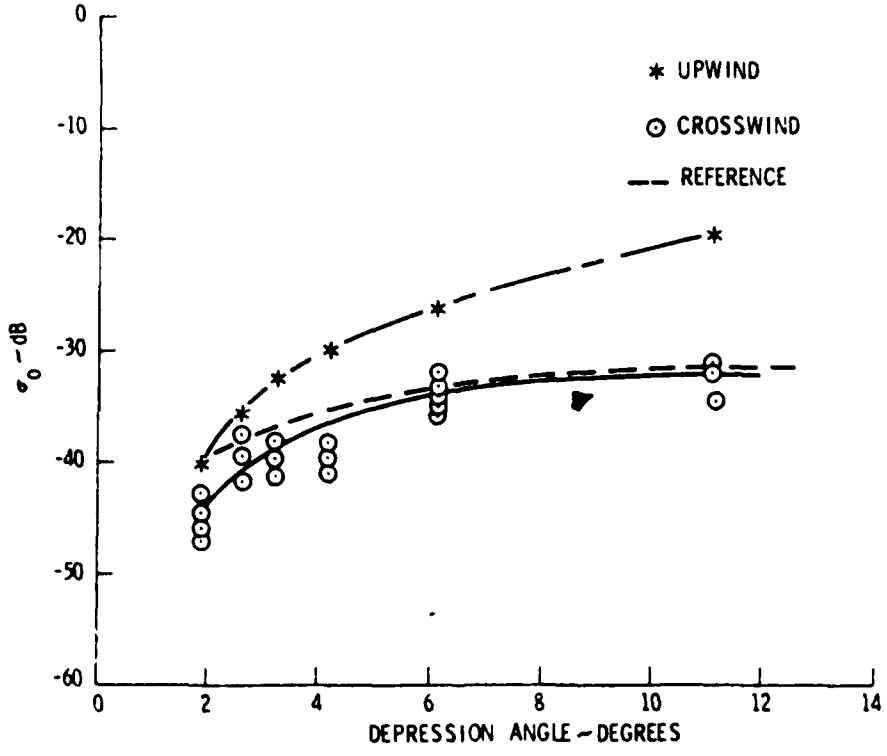

Figure 4-3. Normalized Radar Cross Section for Ocean Returns, 12-15 Knot Wind, 2 ft Sea, 4 ft Swell (Sea State = 3)

In general, the ocean return is highest for upwind data, i.e., with the SLAR antenna looking "into" the front of the waves and smallest for crosswind aspects, i.e., with the SLAR antenna looking parallel to the troughs of the waves. Ocean return is highest for larger depression angle and is highest for higher wind speeds.

Although some reduction in the ocean return from the damping action by oil occurs for all viewing (depression angles), data obtained on the AOSS-I measurement program indicates that maximum suppression (and hence higher contrast imagery) will occur at approximately eight degrees of depression.

The AIREYE SLAR utilizes a vertically polarized antenna to maximize return from the ocean to provide maximum detection range of oil spills. Optimum ship detection occurs with horizontal polarization since ocean return is minimized. However, the selection of vertical polarization represents the best tradeoff for optimum overall system performance.

The optimum operating conditions for ship detection occur when the return from the ocean surface is minimized providing a lower clutter return. Hence lower windspeeds, minimum depression angle, and crosswind viewing aspects will generally provide maximum ship detection range.

4.2.3.2.2 Flight Test Results

Table 4-5 is a summary of the environmental and operational parameters existing for data taken for the determination of SLAR ship detection capability. Table 4-6 is a similar summary for data taken for the determination of SLAR oil slick detection.

4.2.3.2.2.1 Ship Detection Data Results

Table 4-7 is a summary of the demonstrated detection ranges for known ship targets obtained during the flight test program. It should be noted that in some cases the given ranges do not represent absolute maximum detection ranges but rather maximum observed ranges. Although extensive effort was expended to determine the maximum range, the logistics of the required flight paths required were extremely time consuming. In addition,

TABLE 4-5 SLAR SHIP DETECTION DATA RUN SUMMARY

SLAR

Target (Ships Unless Specified)	Nominal Altitude	Wave Direction*			Seas			Time			Gnd Speed		Atmosphere		
		Into Waves	Back Of Waves	Sides Of Waves	Calm	Medium	Rough	AM	PM	Night	Low	High	Clear	Overcast	Undercast
<30 Ft	10,000	X	X	X	X			X				X		X	
30-150		X			X				X			X		X	
150-600			X	X			X	X	X			X			X
150-600		X	X	X			X		X			X			X
600-1000															
Corner Reflector				X			X		X			X	X		
	7500														
<30 Ft			X	X		X		X				X	X		
30-150			X	X		X		X				X	X		
150-600															
600-1000															
Corner Reflectors				X			X	X				X	X		
<30 Ft	5000	X	X		X			X				X		X	
30-150		X			X				X			X		X	
30-150		X				X			X			X	X		
150-600		X	X	X		X		X				X	X		
150-600		X				X			X			X	X		
600-1000															
Corner Reflectors		X	X	X			X		X				X	X	
Corner Reflectors				X		X		X					X	X	
⩽30 Ft	2500														
30-150															
150-600															
600-1000															
⩽30 Ft	1000		X		X			X			X			X	
30-150															
150-600															
600-1000															

Seas

Cat	Calm	Medium	Rough
Wind (kts)	0-5	5-12	12

Ground Speed

Low ⩽ 200kts
High > 200kts

*Refers To Direction That SLAR Antenna Is Viewing

885-39.1

TABLE 4-6 SLAR OIL DETECTION DATA RUN SUMMARY

SLAR

Target	Nominal Altitude	Wave Direction: Into	Wave Direction: Back	Wave Direction: Side	Seas	Time: AM	Time: PM	Time: Night	Gnd Speed: Low	Gnd Speed: High	Atmosphere: Clear	Atmosphere: Overcast	Atmosphere: Undercast
Oil	10,000	X	X	X	Rough	X				X	X		
	7500		X			X				X	X		
		X					X			X	X		
	5000	X	X				X			X	X		
	10,000	X	X		Meduim	X				X	X		
		X		X			X			X	X		
	7500		X			X				X	X		
				X		X	X			X	X		
	5000		X			X				X	X		
				X			X			X	X		
	2500			X			X			X	X		
	10,000				Calm								
	7500	X				X				X	X		
	5000												
	2500												

Seas			
CAT	Calm	Medium	Rough
Wind	0-5	5-12	> 12

Ground Speed

Low ⩽ 200kts
High > 200kts

TABLE 4-7 SUMMARY OF DEMONSTRATED SLAR BOAT DETECTION RANGES

Vessel Description	Wind (KTS)	Seas (ft)	Wave Angle	Detection Range (nautical miles)
30 ft Sailboat	7	2-3	Side	15
35 ft Sailboat	7	2-3	Side	15
90 ft Sailboat	7	2-3	Side	15
25 ft Sailboat	8	2	Side	5
"	20-25	6	Side	10
"	20-25	6	Back	3
500 ft Cargo	20-25	6	Side	5
"	10	5	Into	18.6
"	10	5	Into	35.3
"	10	5	Back	48
"	10	5	Back	65.3
"	10	5	Back	66.6
"	10	5	Side	49.3
300 ft Work Boat	10	5	Into	48
"	10	5	Into	60
50 ft Fishing Boat	10	5	Into	10
"	10	5	Into	16
"	10	5	Into	29
"	10	5	Into	42
450-500 ft Tanker	15	8	Side	61,3
"	15	8	Back	37.3
"	15	8	Back	68
"	15	8	Back	25.4
"	15	8	Back	53.3
"	15	8	Back	34.6
"	15	8	Into	34.6
"	15	8	Back	25.3
"	15	8	Into	45
25-30 ft Fishing Boat, Fiberglass	4	2	Into	5.3
"	4	2	Into	11.3

TABLE 4-7 SUMMARY OF DEMONSTRATED SLAR BOAT DETECTION RANGES (Continued)

Vessel Description	Wind (KTS)	Seas (ft)	Wave Angle	Detection Range (nautical miles)
"	4	2	Into	16
"	4	2	Into	22
"	4	2	Into	25.3
"	4	2	Into	12.6
"	4	2	Into	22.5
55 ft Wood Boat	4	2	Into	20.25
"	4	2	Into	30.6
"	4	2	Into	50.7
20-22 ft Open Boat, Fiberglass	2	2	Back	15
"	2	2	Back	25
"	2	2	Back	30
"	2	2	Back	40

geographic constraints and restricted flying zones frequently prohibited flying the patterns required to determine maximum range.

It should also be noted that many more ships than are listed were routinely detected during the flight test program. It was impossible however to fly to each ship and document the vessel's characteristics due to the limited time available for each flight.

Figures 4-4a, 4-4b and 4-4c are the data in Table 4-5 presented in graphic form for vessel sizes of ≤30 ft, 30-150 ft, and >150 ft respectively. Detection ranges are plotted as a function of wind speed for wave viewing angles of into the waves (INTO), back of the waves (BACK) and along the troughs (SIDE).

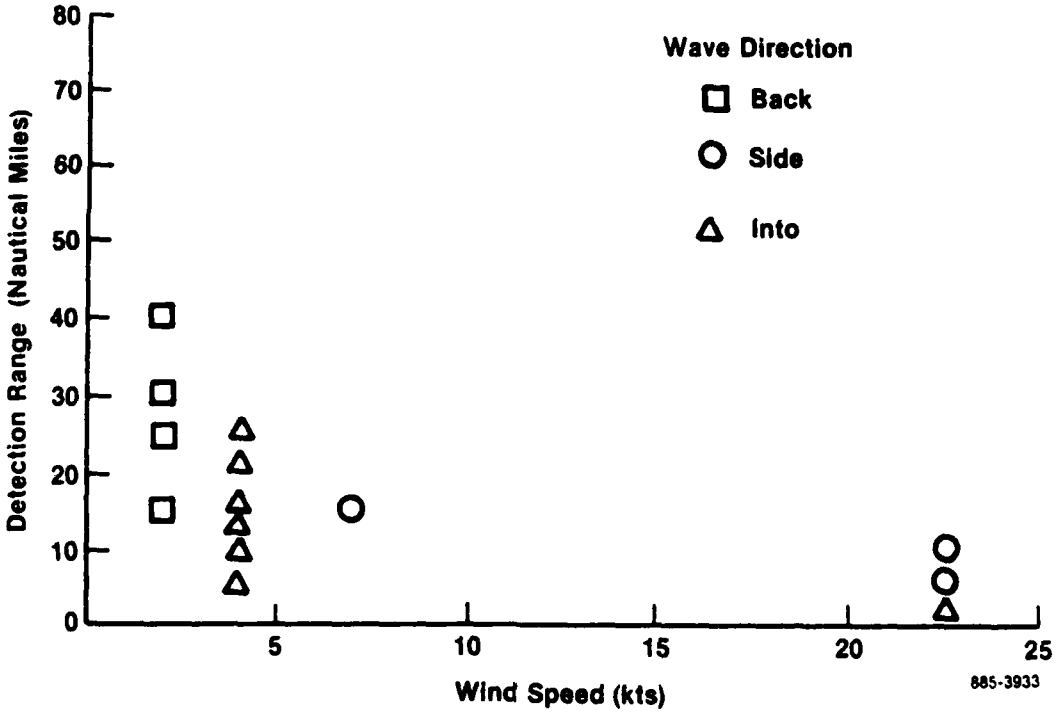

Figure 4-4a. Demonstrated Ship Detection Ranges Vessel Size ≤30 ft

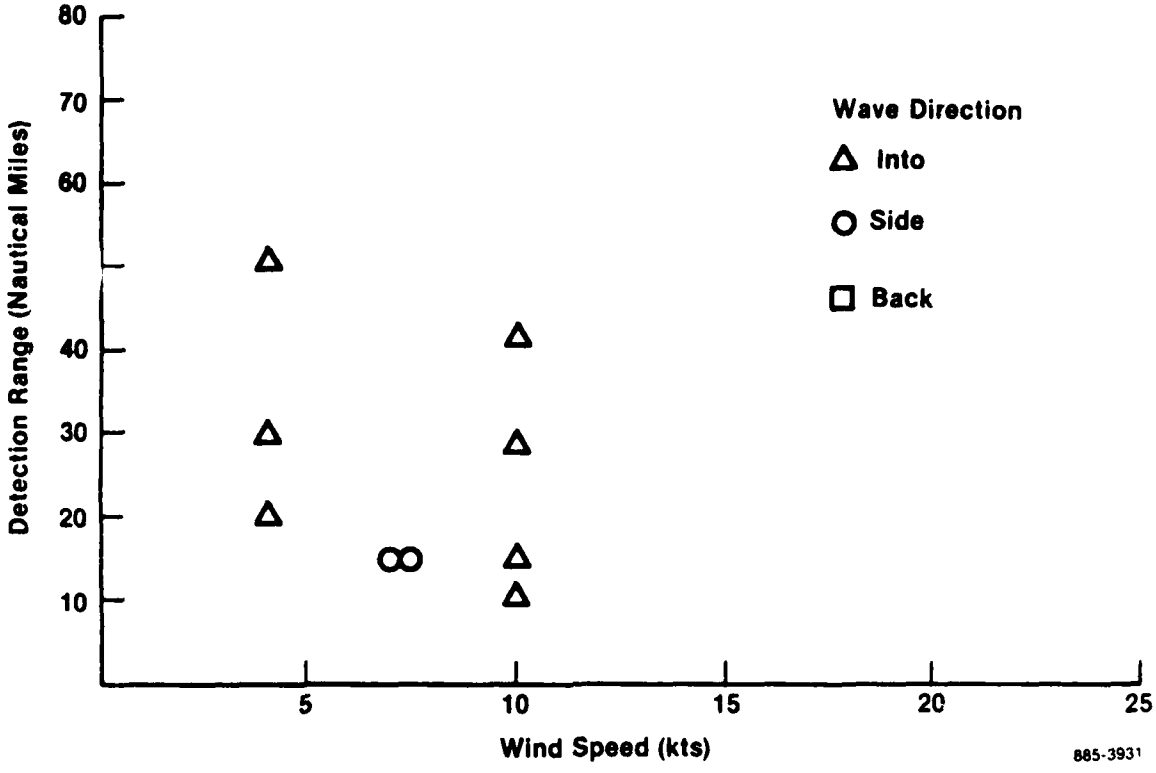

Figure 4-4b. Demonstrated Ship Detection Ranges
Vessel Size 30-150 ft

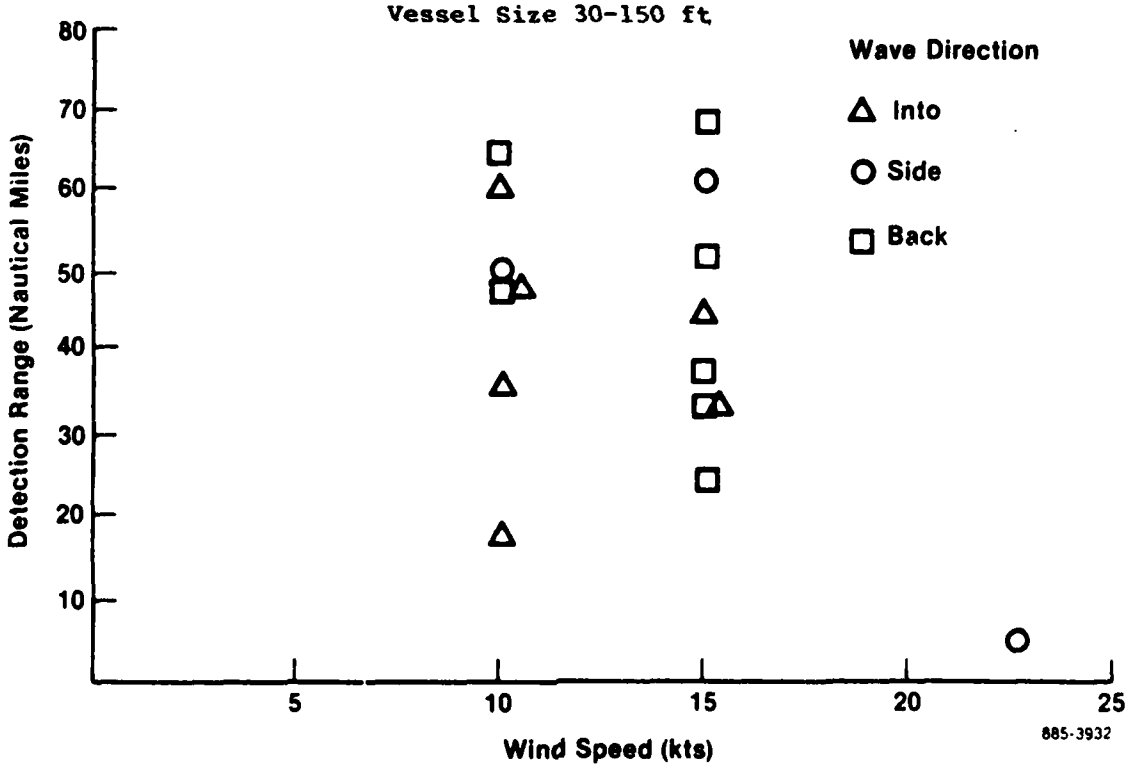

Figure 4-4c. Demonstrated Ship Detection Ranges
Vessel Size >150 ft

4.2.3.2.2.2 Oil Detection Data Results

Table 4-8 is a summary of demonstrated oil detection ranges for the SLAR. As in the case of ship detection data, some of the ranges are not necessarily the maximum detection ranges due to the same constraints of available flying time and other logistics problems. No differentiation is made between oil thicknesses since it has been demonstrated in AOSS flight tests that no significant differences in the oil signature exist as a function of oil thickness. All data were obtained using the natural oil seeps in the Santa Barbara channel. Figure 4-5 is a graphic representation of the same data contained in Table 4-8, with oil detection ranges plotted as a function of windspeed for the three wave viewing angles.

As demonstrated in a variety of test programs including AOSS I, for oil spills with an areal extent greater than the resolution element of the SLAR (100 ft x R ft), spill detection will be possible if the ocean return is detectable. This is because the detection phenomena noted is the reduction of ocean return due to the damping action of the oil on the wave fine structure. Hence a legitimate extrapolation of the actual oil detection range may be obtained by determining the maximum range at which sea clutter is detectable. Table 4-9 is a plot of the clutter return limits obtained from review of the various SLAR data sources, and Figure 4-6 is a graphic representation of the same data. Maximum clutter detection range is plotted as a function of windspeed for three different wave viewing angles. Note the general increase of detectable clutter ranges as wind speed increases, the higher detection ranges for detection looking into the front of the waves, and lowest detection ranges looking into the troughs (side). The upward arrows on the 20-knot windspeed indicate that the clutter was visible and still strong at ranges extending to the maximum display range setup at the time the data was taken.

TABLE 4-8 DEMONSTRATED SLAR OIL DETECTION RANGES

Wind (KTS)	Seas (ft)	Wave Direction			Demonstrated Detection Range (nautical miles)
		Into	Back	Side	
7	2-3			X	15
5	1-2	X			17
12	2-3	X			18
12	2-3	X			20
12	2-3	X			35
7	1-2		X		10
7	1-2		X		4
7	1-2		X		5
8	1-2			X	5
20	5-8		X		7½
20	5-8		X		17
20	5-8	X			7
20	5-8		X		20
20	5-8	X			18
20	5-8		X		17
20	5-8			X	15
20	5-8	X			7½
20	5-8		X		20
20	5-8	X			8
20	5-8		X		20
20	5-8	X			20
20-25	6			X	20

TABLE 4-9 CLUTTER RETURN LIMITS

MSN No.	Date	Wind (KTS)	Seas (ft)	Max Clutter Detection Range (nautical miles)		
				Into	Back	Side
007	9-24	7	2-3		25	20
008	9-25	3-4	2			15
009	9-27	5	1-2	18		
010	9-27	12	2-3	37		
011	9-28	7	1-2	20+		16
012	9-28	8	1-2			7-10
014	10-17	20	5-8	40	20	40
015	10-17	20	5-8	>40	>40	
016	10-18	8	2-3			16-20
017	10-19	25	>6			>20
018	10-19	25	>6	-	-	-
021	10-23	10	5	30	20	15
023	10-26	15	8	40	30	25
025	10-29	4	2	10@5KTS 15@10KTS	5	
026	10-29	2	flat	0		
027	10-30	5	2	15	0	
029	10-31	15	8			25

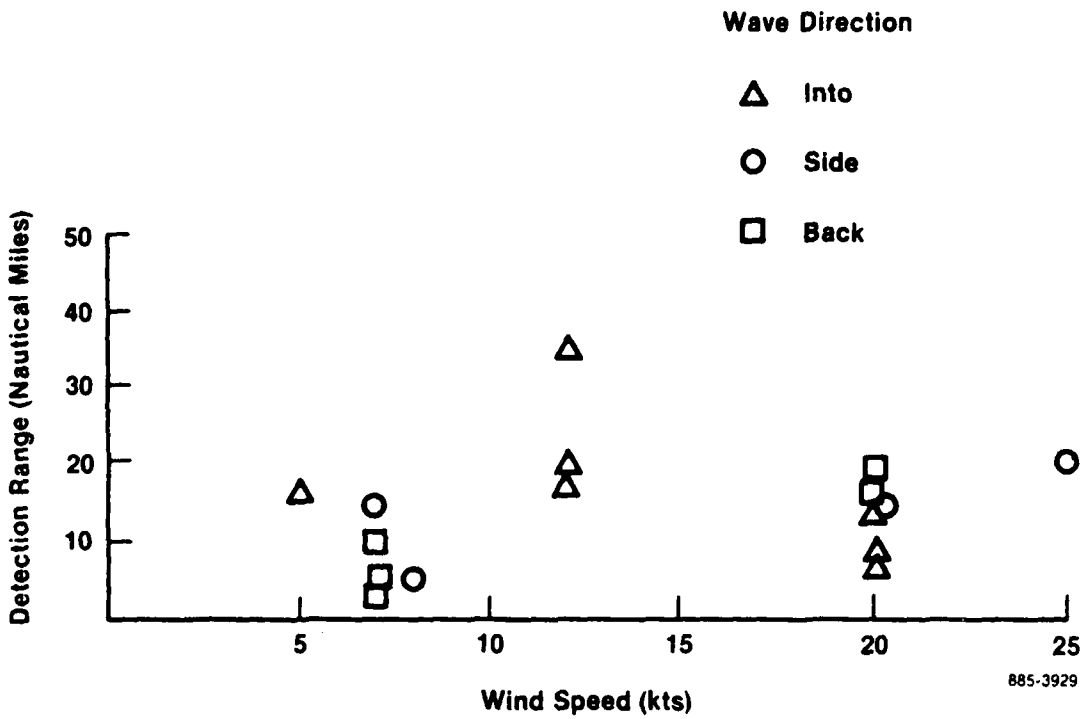

Figure 4-5. Demonstrated SLAR Oil Detection Ranges

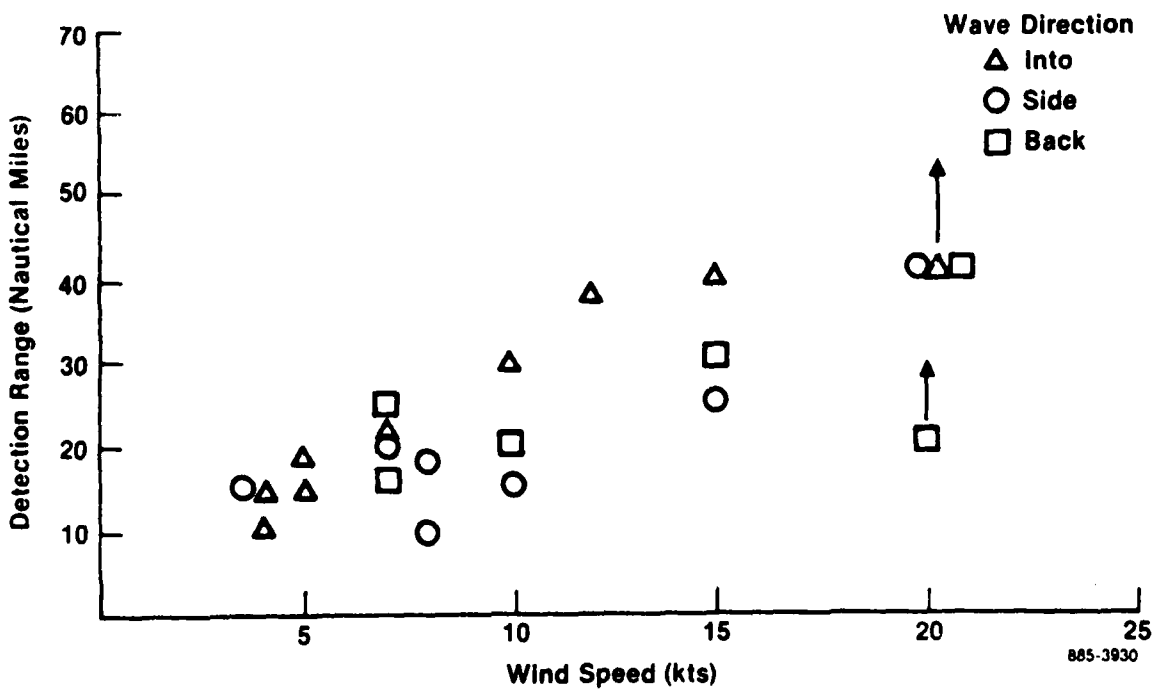

Figure 4-6. Maximum Sea Clutter Detection Range

4.2.3.2.3 SLAR Data Interpretation and False Alarm Potential

SLAR data on the MPD is presented in a sense such that bright or light areas represent higher signal returns. Data from the SLAR dry silver film record is presented such that dark or black areas represent areas of higher signal returns and clear areas represent no signal return. Figure 4-7 is a SLAR image of the Santa Barbara channel photographed directly from the MPD. The dark, well-defined area in the vicinity of Platform Holly is oil from the natural oil seep in that area. This dark area represents reduced radar backscatter and hence reduced signal return than that obtained from the surrounding undisturbed (i.e., no oil) ocean surfaces.

Platform Holly appears as a bright spot representing a large signal return characteristic of large metallic structures. The smaller bright spots are boats of various sizes in the area. Land masses produce a large signal return and hence are very bright compared to the ocean surface.

Oil on the ocean surface has a unique signature that is easily recognized by an operator with minimum training. An oil slick appears as a well defined area of less signal return observable as a dark area on the MPD presentation or light area on the SLAR dry silver film record.

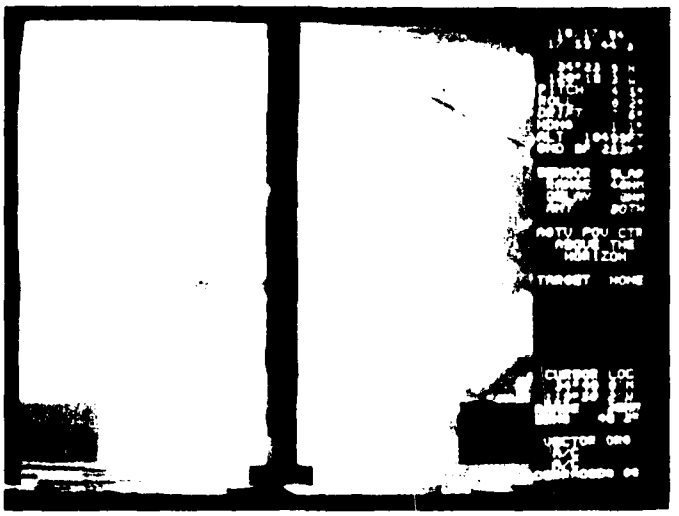

Figure 4-7. SLAR Image of Santa Barbara Channel

The only other observed phenomena which may appear as an oil slick "false alarm" is an area of local absence or reduction of surface wind caused by a geographic feature or local wind characteristic. These areas, however, are not generally as sharply defined as oil on the ocean surface and can frequently be identified by relating them to the geographic feature causing the wind disturbance.

Ships appear as small bright dots or bright extended lines on the MPD depending on the range. Although return from any point target such as an oil rig, buoy, etc, can be mistaken for a ship in SLAR image interpretation, these features generally appear on charts and can be readily eliminated as potential false alarms. For example, on an initial surveillance mission, features on the imagery can be compared to local charts and, utilizing the AIREYE SLAR overlay capability, can be assigned an identification name. After the initial setup, the imagery from subsequent surveillance of the same area will automatically superimpose the known target identification labels on the SLAR imagery. This capability was frequently used during the Mission Verification tests to label the key oil drilling platforms.

The wake of a vessel, if large enough to significantly disturb the ocean surface, will produce a larger return than that obtained from the surrounding ocean surface. If the disturbance is significant, the wake may be long enough to directly estimate the vessel's approximate direction of travel.

4.2.3.3 IR/UV Line Scanner Data

4.2.3.3.1 Detection Principles

This section is extracted in part from the UCSB Final Report entitled "Aerojet ElectroSystems Oil Sampling Test." The entire report is contained as Appendix A to this final report.

Thermal infrared imagery sensed in the 8-14μm portion of the electromagnetic spectrum of oil slicks has been found to be an effective tool for the identification of oil on sea water. Thermal IR sensors are passive and respond to emitted rather than reflected radiation. As a result, the

sensor does not depend upon reflected energy from the sun facilitating the system both day and night surveillance capabilities.

A thermal infrared sensor measures thermal radiation, which is electromagnetic radiation in the wavelength range of 4 to 20 μm. The intensity of the thermal radiation emitted by a target depends on the kinetic temperature, and on the emissivity of the object. Emissivity (ϵ) is the ratio of the exitance of a body of kinetic temperature T to the blackbody (perfect radiator) exitance at the same temperature. The exitance of a blackbody ($M_{bb}(\lambda,T)$) is described by Planck's equation (Equation (4-10)):

$$M_{bb}(\lambda,T) = \frac{2\,hc^2}{\lambda^5[e^{(hc/k\,T)} - 1]} \qquad (4\text{-}10)$$

where

c = speed of light (ms^{-1})

h = Planck's constant (js)

λ = wavelength (m)

k = Boltzmann's constant ($j\ deg^{-1}$)

T = temperature (degrees Kelvin)

The spectral emissivity of a given target can be defined as:

$$(\epsilon) = \frac{M_r(\lambda,T)}{M_{bb}(\lambda,T)} \qquad (4\text{-}11)$$

where

$M_r(\lambda,T)$ = exitance of a real material at a certain wavelength and temperature.

Therefore, the radiant temperature recorded by a remote sensor will be less than the kinetic temperature of the object.

By the Kirchoff radiation law, the spectral emissivity of an object equals its spectral absorptance $\alpha(\lambda)$. This means that good absorbers are also good emitters. The energy balance equation (Equation (4-12) can be modified as follows:

AD-A166 755 DESIGN DEVELOPMENT AND INTEGRATE/INSTALL AN AIRBORNE 2/3
REMOTE INSTRUMENTATI (U) AEROJET ELECTROSYSTEMS CO
AZUSA CA J J BONNARITO ET AL. AUG 85 7921 USCG-D-27-85
UNCLASSIFIED DTCG23-80-C-20012 F/G 1/3 NL

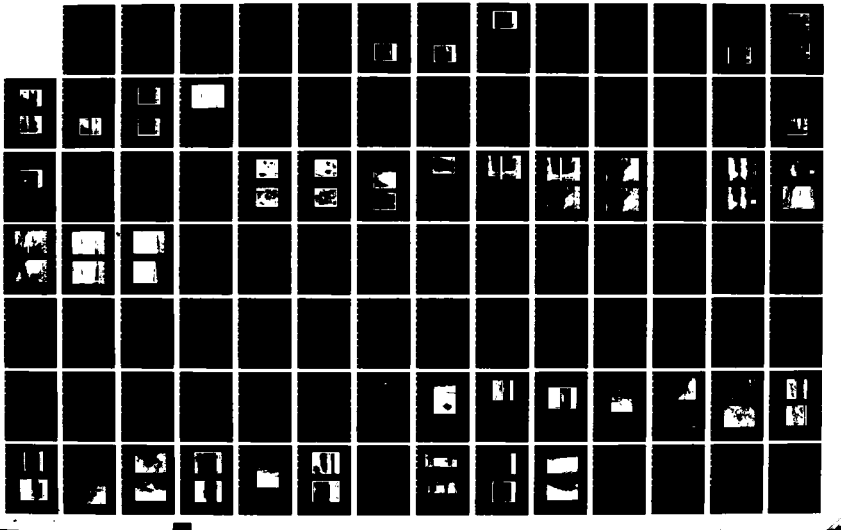

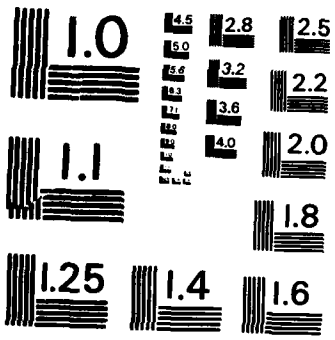

$$\alpha(\lambda)+\rho(\lambda)+\tau(\lambda) = 1 \qquad (4\text{-}12)$$

where

α = absorptance

ρ = reflectance

τ = transmittance

and

$$\alpha(\lambda) = \epsilon(\lambda) \qquad (4\text{-}13)$$

Equation (4-12) becomes:

$$\epsilon(\lambda)+\rho(\lambda)+\tau(\lambda) = 1 \qquad (4\text{-}14)$$

Therefore, the lower an object's reflectance of thermal energy, the higher its emissivity, if it is assumed that transmittance is not involved. For example, pure water absorbs almost all thermal energy and so reflects almost none, giving it a very high emissivity, close to one (0.993).

The emissivity of common construction materials used in the construction of man-made targets is shown in Table 4-10.

TABLE 4-10 COMMON EMISSIVITIES*

Material	Emissivity
Concrete, dry	0.71 - 0.88
Glass pane	0.87 - 0.94
Wood, planed oak	0.90
Paint, white	0.91 - 0.95
Paint, black	0.88 - 0.95
Paint, aluminum	0.43 - 0.55
Iron, galvanized	0.13 - 0.28

*Emissivities for some common materials (from Sellers, 1965).

Emissivities for several different types of oil are presented in Table 4-11.

TABLE 4-11 OIL EMISSIVITIES*

Oil Type	Emissivity (at 8-14μm)
100 octane fuel	0.973
Kerosene	0.968
Diesel oil	0.972
SAE 30 oil	0.970
8.6 API residual fuel oil	0.964
44.7 API crude oil	0.973
31.3 API crude oil	0.967
19.5 API crude oil	0.972
Fish oil	0.959

*Emissivities for oil types (from Horvath et al, 1971)

Ultraviolet sensors are primarily dependent upon reflected radiation from the sun for image formation. Their use for sensing oil on water is therefore limited to daylight. Performance in the near UV 0.32-0.4 μm is reduced by atmospheric aerosols.

When oil is exposed to broadband ultraviolet radiation from the sun it reflects and absorbs the incident radiation. In the case of oil slicks on the ocean, the reflectance contrast between oil and sea water is significant due to the fact that oil has a higher reflectance than sea water in the near ultraviolet region (Catoe and McLean, 1979). This is a direct result of the greater indices of refraction for oils as compared to that of water.

4.2.3.3.2 Flight Test Results

Table 4-12 is a summary of the environmental and aircraft parameters existing for the IR/UV ship detection data and Table 4-13 is a summary of environmental and aircraft parameters existing for IR/UV oil, thermal outflow, and kelp data. Many more data runs were made using the IR/UV scanner than run with the SLAR due to the relatively short time required for IR/UV

TABLE 4-12 IR/UV BOAT DETECTION DATA RUN SUMMARY

Vessel Size (ft)	Nominal Altitude	Sun Angle Or Wave Angle: Into	Back (With)	Side	Seas: Calm	Rough	Time: A.M.	P.M.	Night	Gnd Speed: Low	High	Atmos-phere: Clear	Over Cast	Under Cast	Comments
30	⩽ 500		X	X	X			X		X		X			
	1000		X		X		X			X		X			
	2500		X		X			X		X		X			
	5000														
	7500														
	⩾ 10,000														
30-150	⩽ 500	X	X	X	X		X	X		X	X	X			
	1000	X	X	X	X		X	X		X		X			
	2500	X	X	X	X		X(3)	X		X		X			
	5000	X			X			X			X	X			
	7500			X	X			X			X	X			
	⩾ 10,000		X	X	X		X	X (2)		X		X			
150-600	⩽ 500		X	X	X			X			X	X			
	1000		X	X	X		X	X		X	X	X			
	2500	X	X	X	X		X			X		X			
	5000														
	7500														
	⩾ 10,000														
600-1000	⩽ 500			X				X		X		X			
	1000			X	X		X			X		X			
	2500		X		X			X			X	X			
	5000		X		X			X			X	X			
	7500			X	X			X		X		X			
	⩾ 10,000		X	X	X		X			X (1)		X			

Low Speed ≡ < 200kts Nom 150kts
High Speed ≡ > 200kts Nom 250kts
Calm Seas ≡ ⩽ 10kts Wind
Rough Seas ≡ ⩾ 10kts Wind

(1) Right Sun Angle Only
(2) Left Sun Angle Only
(3) Back Sun Angle Only

TABLE 4-13 IR/UV OIL DETECTION DATA RUN SUMMARY

		Sun Angle Or Wave Angle			Seas		Time			Gnd Speed		Atmos-phere			
Target	Nominal Altitude	Into	Back	(Width) Side	Calm	Rough	A.M.	P.M.	Night	Low	High	Clear	Over Cast	Under Cast	Comments
Oil (Day)	500	X	X	X	X		X			X	X		X		
	2500	X	X	X	X		X			X	X		X		
	5000	X	X	X	X			X		X	X		X		
	7500	X	X	X	X			X		X	X	X			
	10,000	X	X	X	X		X			X	X	X			
Oil (Night)	500		X	X		X			X		X	X			
	2500	X	X	X		X			X	X		X			
	5000	X	X	X		X			X		X	X			
	7500		X	X		X			X		X	X			
	10,000		X	X		X			X		X	X			
Thermal Outflow (AM)	500														
	2500														
	5000		X	X	X		X			X	X ①	X			
	7500	X	X	X	X		X			X	X	X			
	10,000	X		X	X		X				X	X			① Sun @ Right Wing Only
(PM)	500			X		X		X		X	X	X			
	2500		X	X		X		X		X	X	X			
	5000														
	7500														
	10,000	X	X	X		X		X		X		X			
Kelp	500			X	X			X		X		X			
	1000		X		X			X		X		X			
	2500														
	5000	X	X	X	X			X		X		X			
	7500														
	10,000														

Low Speed ≡ < 200kts Nom 150kts
High Speed ≡ > 200kts Nom 250kts
Calm Seas ≡ < 10kts Wind
Rough Seas ≡ ⩾ 10kts Wind

885-3927

data runs compared to SLAR runs. Oil data were obtained in the Santa Barbara channel near Platform Holly. Thermal outflow data utilized the hot water discharge from the power plant on the coast at Oxnard. IR and UV imagery of kelp was obtained off the coast north of Santa Barbara.

4.2.3.3.2.1 IR/UV Oil Detection

A detailed analysis of IR/UV oil data from flights of 10 September and 13 September is contained in the UCSB report of Appendix A. This report provides a description of analyses of IR/UV oil detection supported by complete ground truth data. Since the general imagery and characteristics are representative of all the oil data collected using the IR/UV scanner, no further discussion will be included in this report.

Figure 4-8 is an IR/UV image of oil streaming from Platform Holly. The system was set up to display IR1(the higher resolution, less sensitive channel) on the left and UV on the right. In this image, taken at approximately 500 ft, Platform Holly appears as a light spot in the IR image approximately 1/3 down the screen. Oil can be clearly seen trailing from the platform on both the IR and UV. Note that while the IR channel responds to the thicker main trail, the UV channel responds to a large area of thinner oil, some of which appeared to the eye as an oil "sheen."

Figure 4-8. IR/UV Image of Platform Holly

Figure 4-9 is an IR/UV image of a slightly different area. In this image, the data were enhanced in real time using the AIREYE brightness enhancement capability. Again the IR channel is displayed on the left and UV channel on the right. Note that the IR responds to the main thicker oil trail (darker in the image) but data enhancement provides significant definition of smaller temperature variations of the oil over the entire image. The enhanced UV channel also provides significant definition of finer oil structure over the entire image.

Figure 4-10 is an IR/UV image of Platform Holly taken at night. The higher sensitivity channel is displayed on the right and the lower sensitivity is displayed on the right. Oil can be seen streaming from the platform area in both channels but of course is more readily detectable on the high sensitivity channel. Unfortunately brightness enhancement was not used for this sequence, but based on experience during the test program, would have provided a high contrast, easily detectable image on both the IR channels.

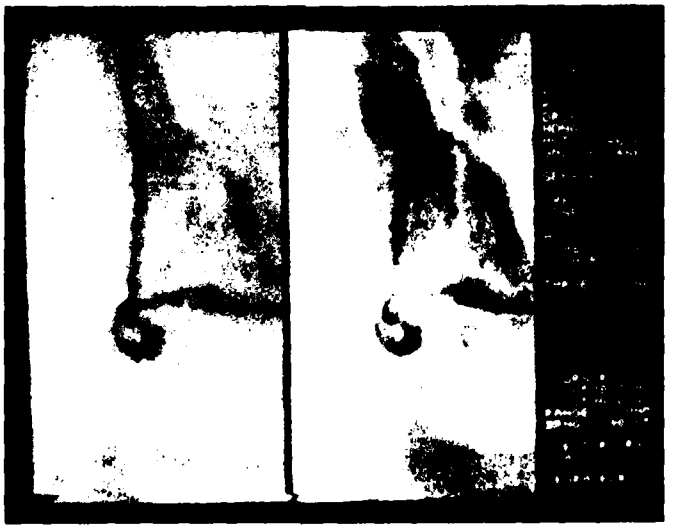

Figure 4-9. IR/UV Image of Platform Holly with Image Enhancement

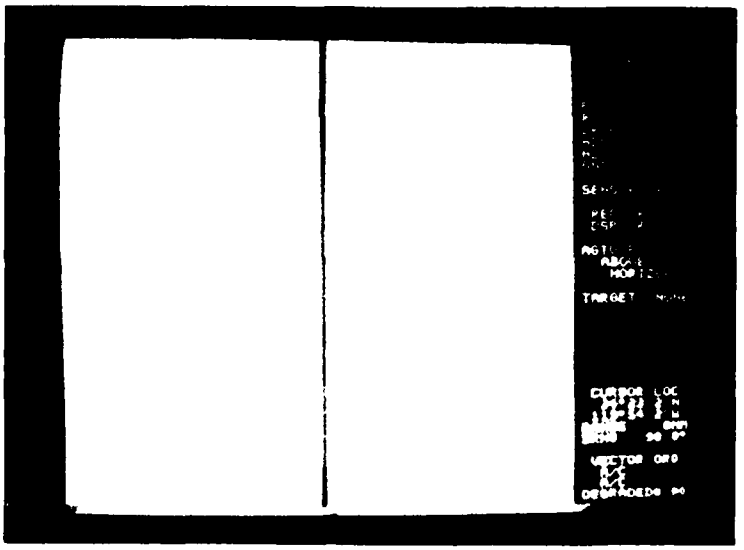

Figure 4-10. IR/UV Image of Platform Holly Taken at Night

A detailed analysis of all IR/UV oil detection data flights yields the following conclusions.

1. There was no discernible effect on oil detection and image quality with air speed variations ranging from <150 knots to >250 knots ground speed.

2. As would be expected the high sensitivity IR channel produced the highest observed detection rate.

3. Because some areas of oil under some circumstances exhibit relatively low temperature contrast, data scaling using the AIREYE brightness enhancement capability greatly enhances detection capability.

4. Utilizing the automatic level selection of the IR/UV line scanner provides best overall oil detection.

5. Although some variation exists in image quality between UV oil detection as a function of sun angle, there were few cases of failure to detect oil in the UV channel caused by poor sun angle. Those cases where sun angle was a factor were extreme cases of sun glint.

6. Even very light clouds cause the UV channel to be saturated and can result in failure to detect oil.

7. The IR channels can detect oil through light clouds with some degraded performance.

8. Oil detection capability is best for low sea state conditions. Very high sea states cause some degradation in detection capability by scattering and breaking up the oil.

9. The optimum altitude range for oil is 500 to 2500 ft although oil was detected up to 11,000 ft.

4.2.3.3.2.2 IR/UV Ship Detection

The IR/UV scanner has adequate resolution to provide some detail of ship structure, direction of travel, etc, as well as ship detection at night. The key factors involved in both the detection of ships and the ability to resolve details are the sensor resolution, the ship's IR or UV signature, and the scanner sensitivity.

The resolution of the RS18C IR/UV line scanner is tabulated below.

	Resolution (mrad)	
Channel	Across Track	Along Track
1, IR Low	2.5	2.5
2, IR High	18	2.5
3, UV	5	5

Figure 4-11a is a plot of the dimension of the ground across track scanner resolution as a function of aircraft altitude. Figure 4-11b shows the dimension of the ground along track resolution as a function of aircraft altitude. Both plots are for sensor resolution directly beneath the aircraft where the best resolution will be obtained.

The thermal resolution or sensitivity of the RS-18C is shown below.

Channel	Sensitivity
1, IR Low	0.2°C (NET)
2, IR High	0.02°C (NET)
3, UV	1.5 mW/m^2 (NEP)

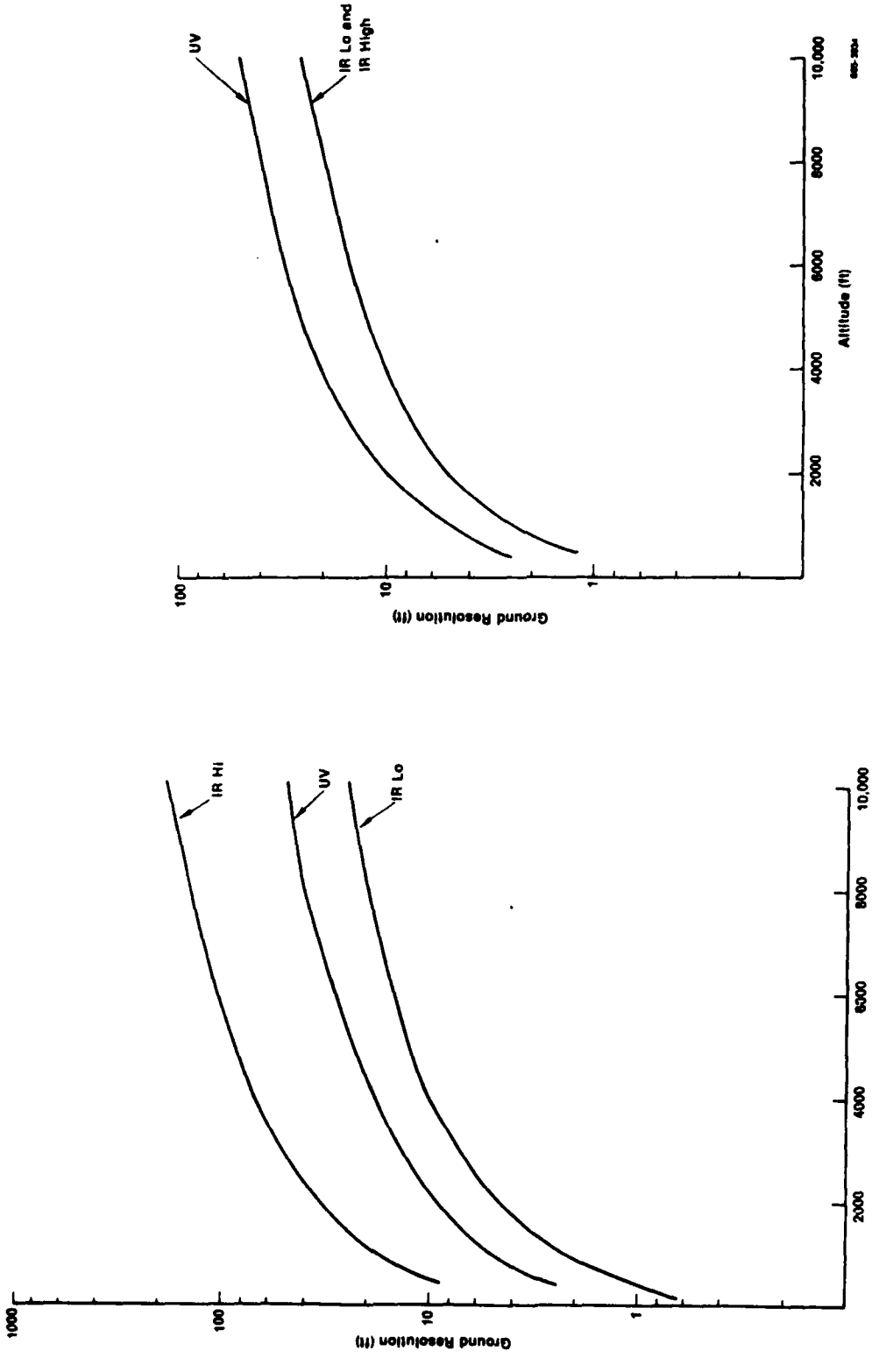

Figure 4-11. RS18C Ground Resolution

Consider the geometry shown in Figure 4-12. The resolution element on the ground is defined by the scanner across-track resolution and the scanner along-track resolution. These dimensions directly define the ability of the scanner to resolve ship deck detail.

The size of the resolution element also limits the ability of the scanner to detect ships. For example, if the target completely fills the resolution element the ability to detect the target is totally defined by the target contrast relative to adjacent resolution elements (neglecting atmospheric effects). If this contrast exceeds the noise equivalent temperature (NET) or sensitivity of the scanner by an adequate signal-to-noise ratio, detection of the target will be possible.

If, however, the target is smaller than the resolution element of the scanner, then for the same target temperature contrast with adjacent elements, detection capability will be reduced by the ratio of the target area to the area of the resolution element. Or stated simply, the net effective temperature contrast of the target is "washed out" by the surrounding background.

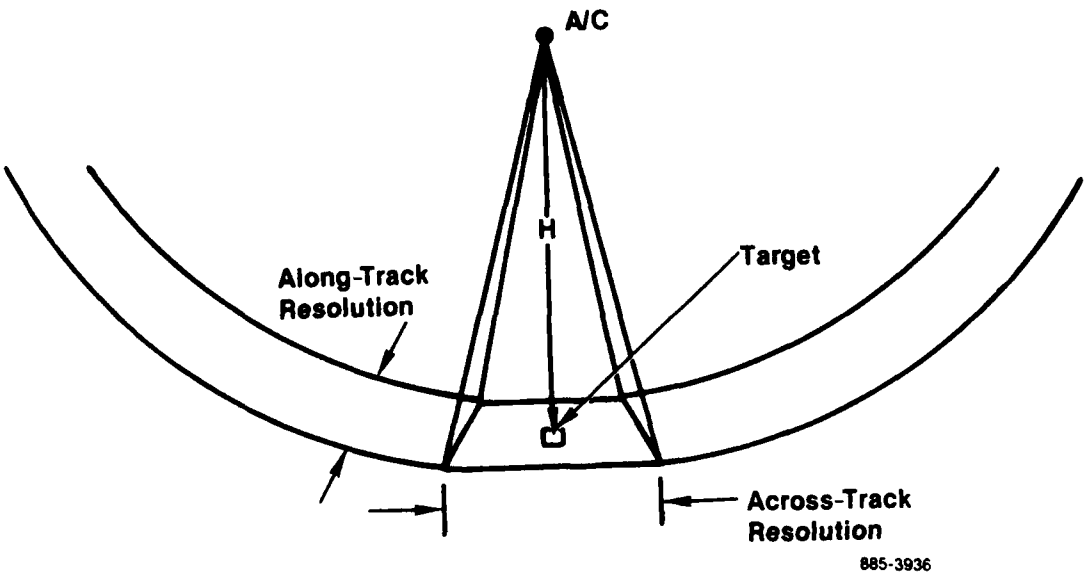

Figure 4-12. IR/UV Scan Geometry

To illustrate the above points, consider the images shown below. Figures 4-13a, b, c, d, e show a sequence of IR/UV imagery taken at altitudes of 214, 599, 1033, 2503 and 11,233 ft respectively. The target was a 110-ft work boat underway. The display was set up to show the high resolution, low sensitivity channel (IR 1) on the left, and the UV on the right. The spatial resolution for the IR 1 channel is approximately 0.5 ft at 214 ft altitude, 1.5 ft at 599 ft altitude, 2.6 ft at 1033 ft altitude, and 6.3 ft at 2503 ft altitude, and 28.1 ft at 11,233 ft altitude. Resolution for the UV channel is exactly twice that of the IR 1 channel.

Figure 4-13a (214 ft altitude) shows some deck detail on the IR and UV channel and a large wake with visible fine structure on the UV channel. Spatial resolution is adequate to determine the direction of vessel travel. Figure 4-13b (599 ft altitude) exhibits little deck detail, but provides enough information to determine the direction of travel, even if the wake were not visible on the UV channel 1. Figure 4-13c (1033 ft altitude) exhibits no deck detail, but still provides enough resolution to determine the direction of travel if the wake were not visible on the UV channel. The bright streak on the left of the UV image is sun glint. In Figure 4-13d, the vessel is barely detectable in the IR image, but readily detectable along with the wake in the UV image. Note that the IR and UV image could have been significantly improved in all data if the AIREYE data scaling function were used.

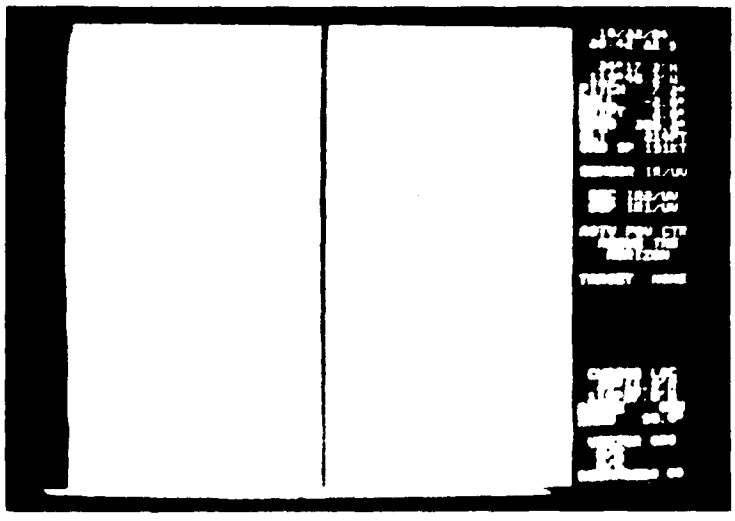

Figure 4-13a. IR/UV Image of 110 ft Work Boat - 214 ft Altitude

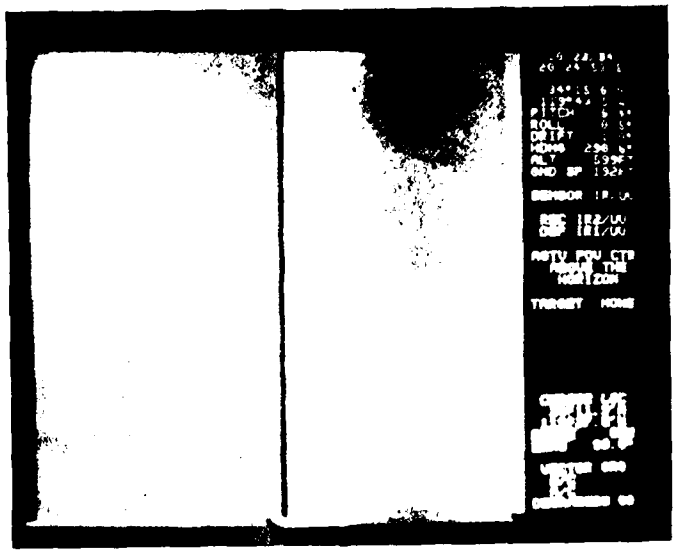

Figure 4-13b. IR/UV Image of 110 ft Work Boat - 599 ft Altitude

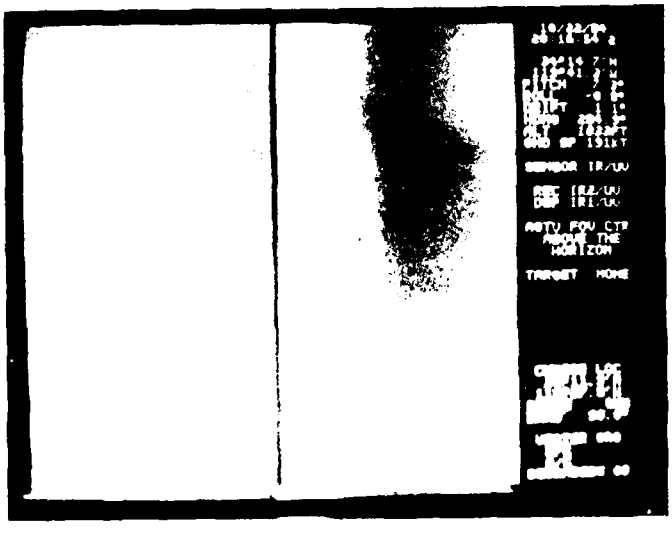

Figure 4-13c. IR/UV Image of 110 ft Work Boat - 1033 ft Altitude

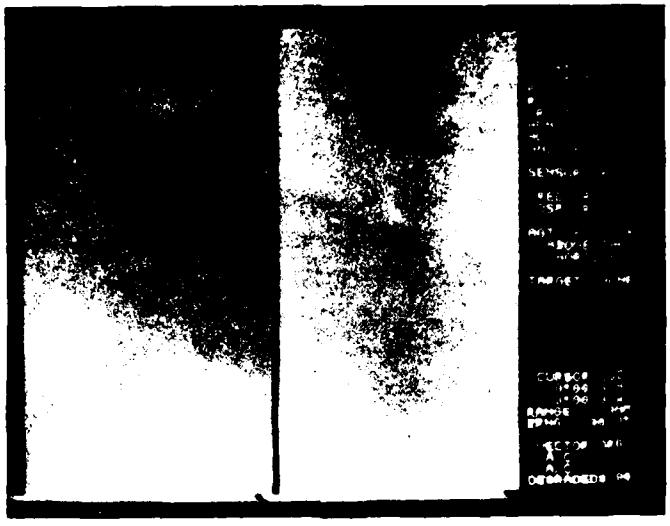

Figure 4-13d. IR/UV Image of 110 ft Work Boat - 2503 ft Altitude

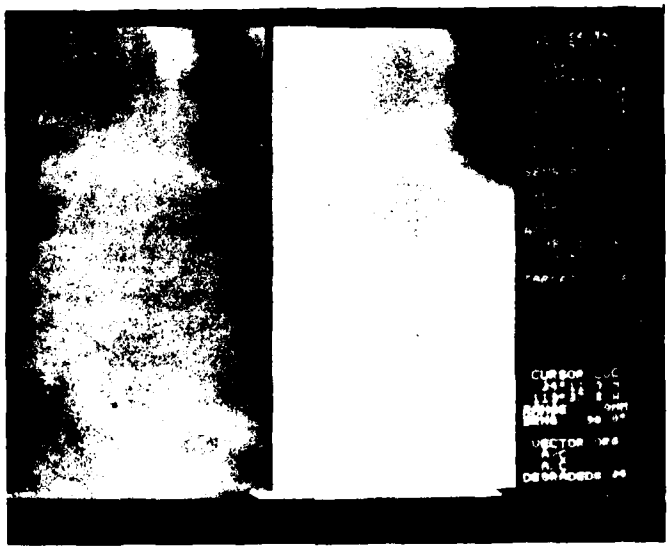

Figure 4-13e. IR/UV Image of 110 ft Work Boat - 11,233 ft Altitude

In Figure 4-13e, the vessel is just barely detectable in both the IR and UV as a small dot. No detail information on vessel characteristics or even direction of travel is possible.

Although ship detection is possible at 11,000 feet, reliable detection will not always be possible and is not recommended. Figures 4-14a, b, c, are taken on the same vessel illustrating the effect of sun angle. All three images were taken at 1000 ft altitude. The sun was off the left wing on Figure 4-14a, behind the aircraft on Figure 4-14b, and directly off the nose in Figure 4-14c. Note that there is no significant difference in the IR images as a function of sun angle. Contrast is best in the UV image for the side sun angle of Figure 4-14a, giving an enhanced wake image and some additional vessel detail. No significant difference can be noted between the other two sun angles on the UV image.

For comparison to the previous smaller ship data, Figure 4-15 is an IR/UV image taken at 600 ft of a large container ship. Note the significant deck and wake detail. The lower resolution IR channel is presented on the left, and the UV channel is presented on the right. As apparent in the UV image, the sun was off the right wing for this data run. This image is discussed in further detail along with an enhancement sequence in Section 4.2.4.

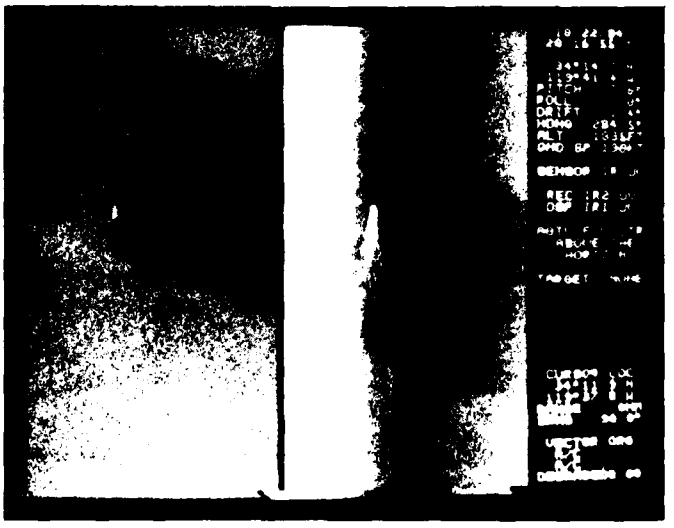

Figure 4-14a. IR/UV Image of 110 ft Work Boat - Sun to Left of Aircraft

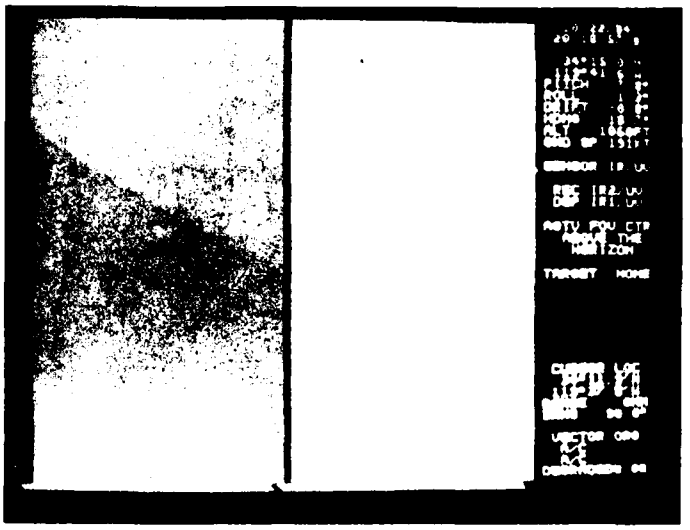

Figure 4-14b. IR/UV Image of 110 ft Work Boat - Sun Behind Aircraft

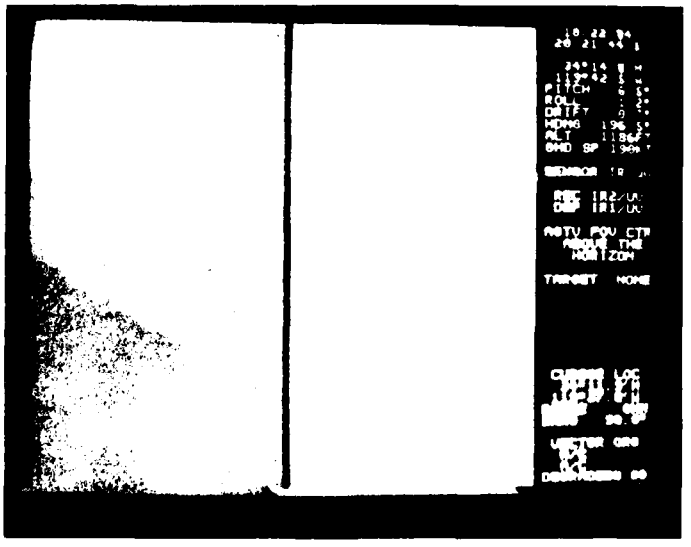

Figure 4-14c. IR/UV Image of 110 ft Work Boat - Sun Ahead of Aircraft

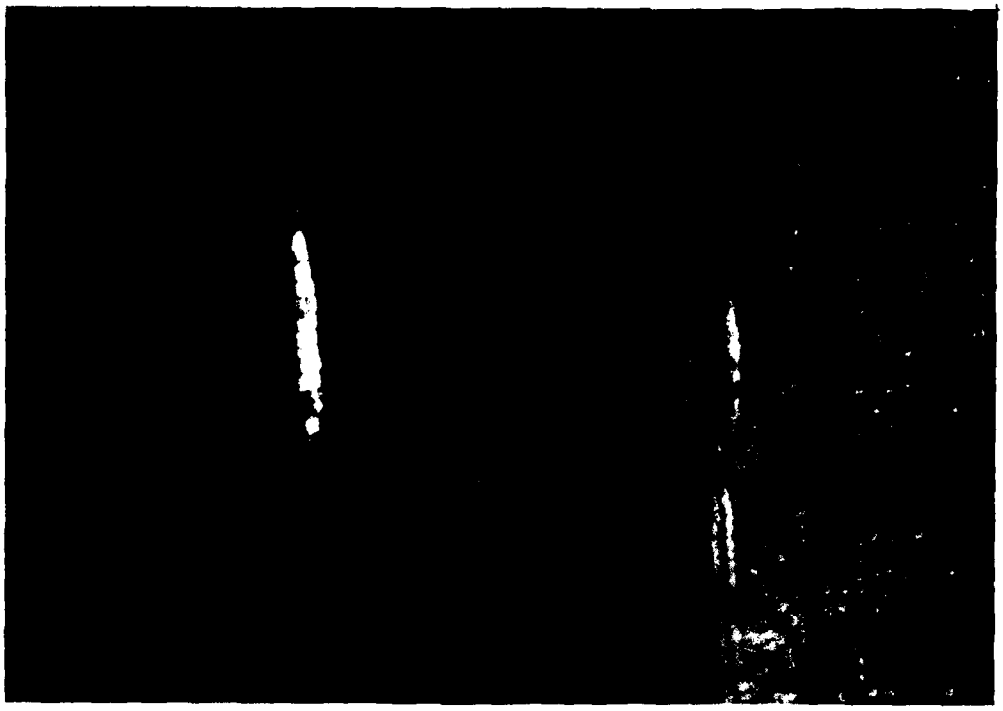

Figure 4-15. IR/UV Image of Large Container Ship

A detailed analysis of all IR/UV ship detection flights yields the following conclusions:

1. There was no discernible effect on ship detection and image quality with airspeed variations ranging from <150 knots to >250 knots ground speed.

2. The high sensitivity channel produced the highest observed ship detection rate.

3. Utilization of the AIREYE brightness enhancement capability greatly enhances ship detection capability.

4. Although some variation exists, an image quality as a function of sun angle, any sun angle not providing excessive sun glint to the scanner will provide essentially the same ship detection capability.

5. Light clouds will mask ship targets in the UV.

6. The IR channel can detect ships through light clouds with some degraded performance.

7. The effect of sea state on ship detection was negligible for the IR channel. Small ship detection in the UV is difficult at most sun angles, with whitecaps present.

8. Altitudes up to 5000 ft provide good ship detection capability during both day and night operations. Ship detection is possible on a 100-ft size vessel up to 11,000 ft. One thousand to twenty-five hundred feet appears to be an optimum tradeoff between ship detection probability and swath width.

9. Useful deck detail requires altitude of ≤500 ft.

10. The UV wake signature provides an excellent measure of vessel direction in daylight conditions.

11. Boats as small as 25 ft were easily detectable with the IR/UV line scanner at low altitudes.

4.2.3.3.2.3 Image Interpretation

The following discussion is summarized from AESC Report No. CG-D-90-75. Since oil represents the most complex target to interpret, this section focuses on oil IR and UV characteristics.

Interpretation of the MPD display and IR/UV film record is based on three key parameters; tone, shape, and texture. By tone, we mean the relative brightness of one object compared to another. Shape is defined as both the overall outline of an object and also the outline of various large regions of differing brightness (tone) within that object. By texture, we mean the small-scale spatial variability in brightness (tone) between adjacent points in the object. The following sections define how the tone, shape, and texture information seen in both the IR and the UV data are used for oil slick interpretation.

The image tone of an object is a relative measure of its brightness, compared to surrounding objects. It was previously noted that UV brightness depends only upon reflectance for any particular condition of solar illumination. On the other hand, IR brightness depends primarily upon temperature.

The tone of an oil slick relative to water in a UV image is a complex function of the oil type, slick thickness, water quality, and solar

illumination geometry. The general effects for the first three of these parameters are shown in Figure 4-16. Both Figures 4-16a and 4-16b show that an oil slick always produces a brighter tone than water if its thickness is small enough, and will generally produce a darker tone than water if its thickness is great enough. The minimum thickness required to change from a brighter tone to a darker tone depends upon oil type, as shown in Figure 4-16a. Lightweight refined products (diesel fuel for example) must be present as extremely thick slicks before their UV tone can be darker than that of the water, whereas heavy crude oil slicks with much less thickness can produce dark tones. This figure also indicates that a very thin slick of heavyweight crude is of brighter tone than a very thin slick of a lighter weight petroleum.

Figure 4-16b shows the effect of water quality upon the UV tone of an arbitrary oil slick. Clear blue waters yield a greater UV brightness than do dirty turbid waters. If the slick is thin enough, its UV tone relative to that of the water is approximately independent of water quality. As the slick becomes thicker, the tendency for its UV tone to become darker than that of the water is more pronounced in clear waters than in dirty water. Thus, a particular intermediate thickness of a particular petroleum type could produce a dark tone if located in clear Caribbean waters and a bright tone if located in dirty harbor waters.

The quality of the solar illumination on an oil slick will affect its UV tone. On a very clear day with the sun high in the sky, the tendency toward darker slick tones will be increased. Conversely, if the sun is very low in the sky, or if cloud cover is present to diffuse the solar radiation, the tendency for brighter slick tones will be increased.

To summarize, the UV tone of an oil slick on water can be characterized by the following:

1. Thin portions of the slick will be brighter than the water. Thus, every slick will have some portions which produce light tones.

2. Thick portions of the slick can become darker in tone than the water. However, the conditions which lead to such tones are not always present.

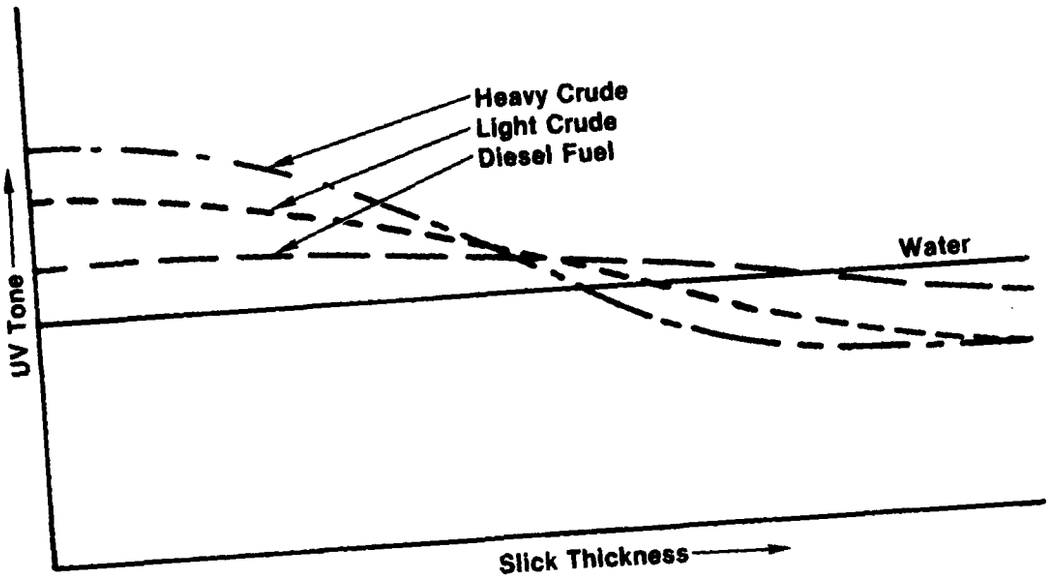

(a) Oil Type Variability

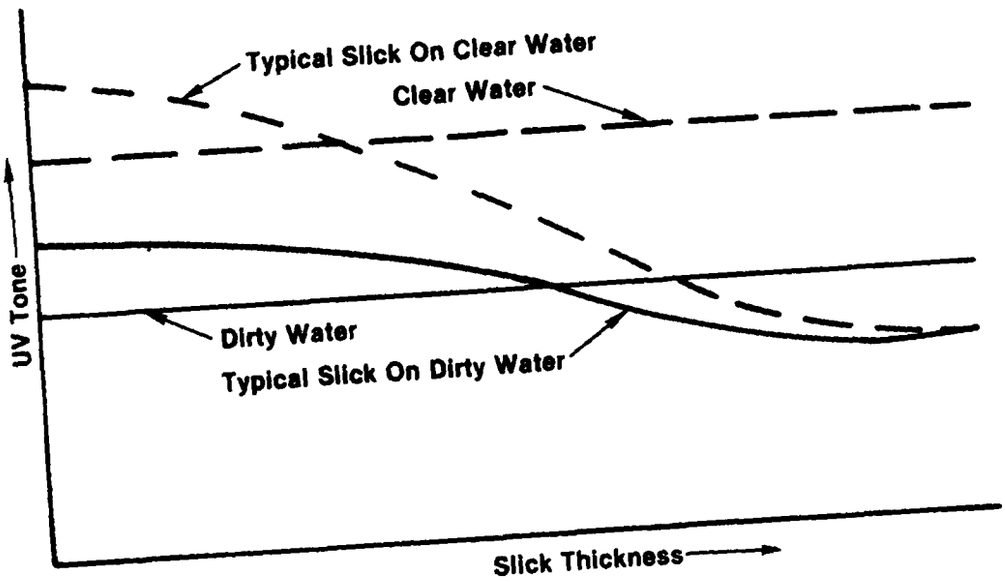

(b) Water Quality Variability

Figure 4-16. Qualitative Variation of UV Tone with Oil Type, Slick Thickness, and Water Quality

3. Slicks composed of heavyweight crudes are capable of exhibiting a wider range of tones than slicks composed of lightweight refined products.

4. Slicks existing in clear waters will show a greater tendency toward dark tones than slicks on dirty waters.

5. Slicks observed during clear weather with a high solar elevation will show a greater tendency toward dark tones than if observed under overcast or low solar elevation conditions.

The tone of an oil slick relative to water in an IR image is a function of oil type, slick thickness, and the environmental conditions. The general parametric effects are shown in Figure 4-17, which focuses on the two conditions of low and high solar illumination. In contrast to the previous discussion of the illumination effects upon UV tone, the question here is merely whether the solar illumination is great enough to produce significant heating in absorbing materials. Figure 4-17a shows that in the absence of such heating, all oil slicks have IR tones less than or equal to that of the water on which they rest. The IR tone decreases to a limiting level as thickness increases. The evaporative cooling present with volatile petroleums leads to their generally colder (darker) tones for any thickness when compared to nonvolatile petroleum products.

The effects of high solar illumination as represented in Figure 4-17b are somewhat more complex. Here, the absorption capability as well as the volatility of the petroleum must be considered. Those petroleum products able to absorb significant quantities of solar radiation can become hotter than the water, and thus produce brightner tones if sufficiently thick. However, the intermediate slick thicknesses of these absorbing petroleums still exhibit dark (cold) tones, while the thinnest regions do not exhibit any IR tonal contrast with the water. Note also in Figure 4-17b that the IR tone of nonabsorbing petroleums, whether volatile or not, is not strongly affected by the level of solar illumination.

Any categorization of petroleum oils into such gross classes as volatile and nonvolatile, and absorbing and nonabsorbing must be somewhat arbitrary. However Table 4-14 presents such a categorization which, based on experience, should provide a reasonable classification of petroleum types in terms of the expected IR tonal respones shown in Figure 4-17.

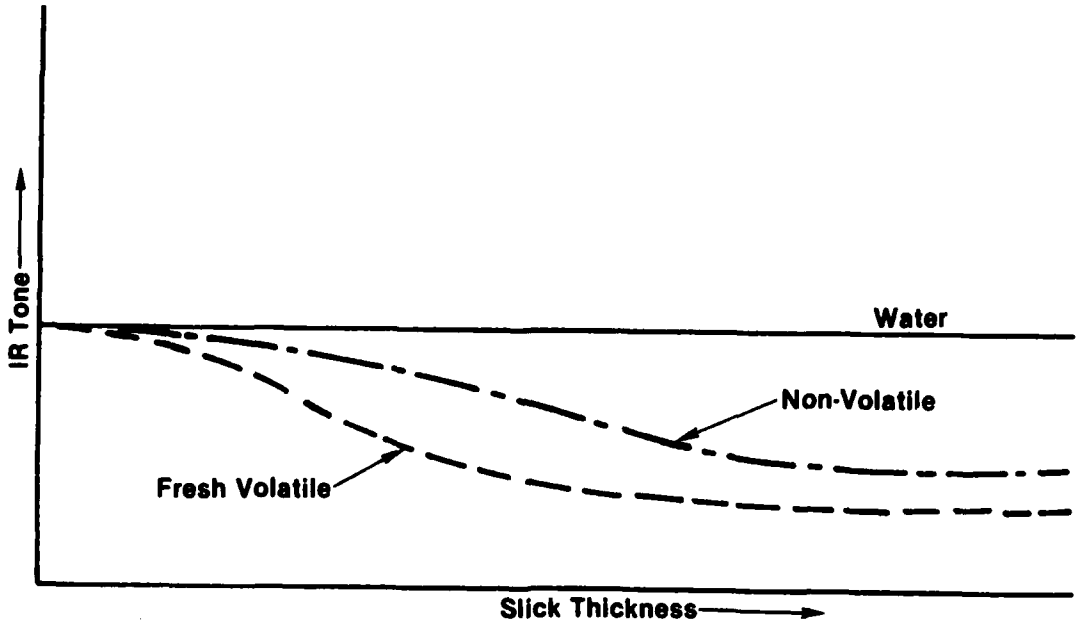

(a) Low Solar Illumination

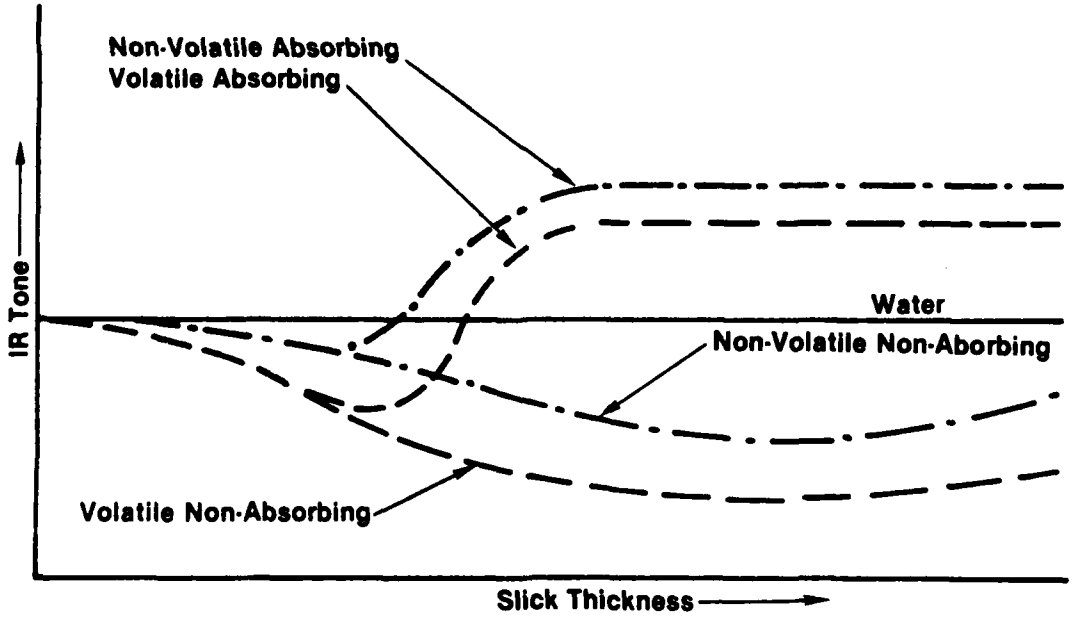

(b) High Solar Illumination

Figure 4-17. Qualitative Variation of IR Tone with Oil Characteristics, Slick Thickness, and Solar Illumination Level

TABLE 4-14 CATEGORIZATION OF PETROLEUM TYPES

Volatility	Absorption	Petroleum Type
High	High	Most fresh crudes
High	Low	Fuels, very light crudes
Low	High	Residuals, very heavy crudes, all aged crudes
Low	Low	Light lube oils

Likewise, it is difficult to define a precise dividing line between low and high solar illumination levels: as the illumination level increases, there is actually a continuous gradation from the IR tonal responses of Figure 4-17a to those of Figure 4-17b. The following criteria, however, are approximately correct:

- If the sky is clear (or contains only a very light cirrus overcast) and the solar elevation above the horizon exceeds 30°, then a high solar illumination condition exists and Figure 4-17a holds.
- If there is a heavy overcast, or if the solar elevation is less than 30°, then a low solar illumination condition exists and Figure 4-17b holds.

Obviously, early morning, late evening, and night are always low illumination conditions. Midday can be a high illumination condition, but only if latitude, season, and cloud cover are appropriate as defined above.

To summarize, the IR tone of an oil slick on water can be characterized by the following:

- Thin portions of the slick will always be similar in tone to the water. Thus, every slick will have some portions which cannot be seen in the IR.
- Under low solar illumination levels, slick regions of intermediate and greater thicknesses will be darker in tone than the water, the darkest tone being associated with the thickest region or the most volatile petroleums.
- Under high solar illumination conditions, slick regions of intermediate thickness will be darker in tone than the water. Thicker regions may be either lighter or darker in IR tone, depending upon whether the petroleum is highly absorbing to solar illumination or not, respectively.

The shape of an oil slick is defined by its overall outline of tonal contrast to the water, and by the outline of regions of contrasting tone within the slick. The shape of a fresh oil slick depends more upon the method by which it was created than upon the type of oil present. In particular, relative motion between the source of oil and the receiving water determines initial shape.

Relative motion between the polluting source and the water produces a linear slick whose length is significantly greater than its width. Such shapes result from ships pumping contaminated ballast while underway, discharge from land-fixed installations into flowing rivers, continuous discharges from offshore drilling rigs or natural oil seeps into shore currents, etc. As the result of the finite rate at which oil spreads out on the surface of the water, the slick width tends to be narrower at the source, widening in the downstream direction to produce a long, narrow, wedge shape. This widening because of lateral surface spread also tends to result in a thinner slick as one moves downstream. The wedge shape tends to disappear after several minutes on the water and the only strong thickness variation is perpendicular to the long axis of the slick.

If there is no relative motion between the polluting source and the water, the oil tends to produce a fairly circular pool. When fresh, this pool is thickest in the center and thins out toward the edges.

A fresh slick usually exhibits very well-defined and smooth boundaries in either the UV or the IR. The UV shows the outer boundary quite crisply due to the bright tone of these thin oil film regions relative to the water. UV tonal variations within the slick resulting from thickness variations tend to be less crisp in outline than the outer boundary. On the other hand, the IR shows crisp tonal outlines resulting from internal thickness variations, while showing none of the outer regions of very thin oil.

After remaining on the water for some time, the slick shape becomes controlled by the wind, sea, and current. The time required for significant alteration can vary from minutes to hours depending upon the intensity of these factors. The effects of waves and currents on slick shape tend to be greatest for linear slicks which tend to become bent into a

crescent. Long narrow slicks are also tended to break up into smaller slicks. Normally, the crispness of the slick boundary, especially as seen in the UV, will tend to diminish after aging.

Texture is produced by tonal fluctuations between adjacent points in an object. The texture of an oil slick in IR and UV imagery tends to increase with slick age.

A fresh oil slick normally consists of fairly coherent regions of uniform or smoothly varying thickness. As a result, tones are also uniform or smoothly varying. This leads to internal tonal structure which we have previously classified as shape information because of its fairly large scale. As the slick ages, smaller scale thickness variations start to occur, especially because of wind and wave action. Usually, the thinnest regions are the first to exhibit increases in texture as these agitations start to overcome the surface tension holding the thin films together. These thin film textural effects are seen only in the UV imagery since thin oil film areas are not detectable in the IR. Texture in the IR images will tend to occur initially through breakup of the relatively thick wind-blown streamers on the lee side of the slick.

Texture in the UV image of a slick can also be produced by waves themselves. Variable reflectance from different wave slopes will produce texture in the UV image in the same manner as it produces texture visually. This sea state effect is enhanced when the slick is observed within an area of high intensity sun glint during clear weather. Texture caused by sea state can usually be identified by the regularity of the tonal variations associated with the regularity of wave trains. In any case, sea state is observable only in the UV, and not in the IR.

Fish oil is similar to certain types of petroleum products in terms of its mechanical and optical properties, i.e., it forms slicks on top of the water similar to petroleum oils and may produce IR and UV tones and shapes characteristic of lightweight, nonvolatile, or nonabsorbing refined products. Fish oil slicks may be differentiated from petroleum slicks if a narrowband IR channel is available as in the case of AOSS. The RS18C line scanner does not have this capability. However, it should be noted that in

the entire AOSS-I, AOSS-II, and AIREYE flight test program, no fish oil slick was ever detected most likely due to the usually small size of fish oil slicks in the Southern California waters.

The motion of ships through water creates two phenomena which could be potentially mistaken for oil slicks in IR or UV imagery by an untrained operator. These waves are regular wave trains and wake scars. Bow and displacement waves are the primary wave trains created by vessel motion. The displacement waves are created directly behind the vessel and move forward along the ship's track. Both types of waves are detectable in the UV imagery, especially when occurring in a region of sun glint. They can be identified by their regularity of texture as being wave trains. Unlike oil, these waves are not detectable in the IR.

The ship motion also leaves a scar directly in its wake as a result of prop wash and breaking of the bow waves. The foam and bubbles in the scar are very bright in the UV, sometimes even brighter than the ship itself. The breaking bow wave forms a halo around the ship and the bright UV tone in the scar can trail out as much as one or two boat lengths behind.

The foam and bubbles which produce the bright UV tone do not produce a detectable IR response. However, if the water has a significant vertical temperature stratification, the ship's passing will bring up the cooler water from below the surface and produce a thermal scar. This dark IR scar can last for many minutes, sometimes hours. Light seas diminish this scar both by destroying the initial temperature stratification and by mixing the water in the wake.

The bright UV tone associated with the scar can be differentiated from an oil slick primarily because it only lasts for a few seconds, and is only visible very close astern. On the other hand, a dark thermal scar trailing far behind can easily look like the dark IR tone of an oil slick. In this case, the UV tone in the scar (far behind the foaming region) can be used to determine whether or not oil is present. At night, of course, no UV data will be available for this discrimination.

Seaweed of any type is readily detected in UV imagery provided it is near the surface and the water is fairly clear. It produces a uniformly dark UV tone which might be mistaken for thick oil except for the absence of the bright border characteristic of a slick. In addition, the seaweed generally does not exhibit the clear shape and outline of an oil slick, but tends to produce a splotchy pattern. If the seaweed is extensive, and if the water is calm, subtle thermal patterns can sometimes be found in the IR imagery during bright daytime conditions. These thermal patterns will tend to have the billowy appearance of clouds, which is quite different from an oil slick pattern. As an example, Figure 4-18 is an IR/UV map of a kelp bed north of Santa Barbara taken at 600 ft.

Changes in water depth, particularly as the result of sandbars and near-surface shoals, are often seen in the UV as areas of brighter tone. They can generally be discriminated from oil slicks by their tonal shape and texture. Unlike an oil slick, a sandbar or shoal will tend to be brightest in the middle, with this bright tone fading toward the edges until it merges with the tone of the deeper water. Also, the edges will not usually be so crisply defined as those of an oil slick.

Figure 4-18. IR/UV Image of Kelp Bed North of Santa Barbara

The thermal outflow from an industrial facility such as a power plant produces an IR signature. Figure 4-19 is an IR/UV image taken at 2500 ft of the power plant on the coast at Oxnard. Note the warmer water pattern streaming from the plant on the left IR imagery. However, the UV image on the right shows only glint from waves breaking near the shore and hence may be easily differentiated from an oil slick based on the UV response.

Figure 4-19. IR/UV Image of Power Plant on the Coast at Oxnard

4.2.3.4 AGTV Data

Due to a multitude of problems associated with the AGTV, only approximately one week (21.3 flight hours) was able to be devoted to actual AGTV mission verification testing. However valuable performance data was also obtained on AGTV engineering evaluation flights performed at various times during mission verification. More than 85 data runs (38 active and 47 passive) were conducted during the AGTV mission verification testing.

4.2.3.4.1 Passive Performance

Flight tests were scheduled so as to arrive on scene approximately 1/2 to 1 hour before total darkness so that the low light (passive) performance of the AGTV could be evaluated prior to active testing on each flight.

In many cases this also allowed both passive and active performance evaluation on the same vessel. Passive performance capability is summarized below.

1. Large lights on ships permitted passive ship detection at ranges exceeding 4 miles.

2. The AGTV demonstrated the ability to read vessel names and observe deck detail after sunset. This was impossible for the flight crew to accomplish.

3. Good deck detail, including personnel activity, was discernible from 0.2 to 0.5 nmi slant range.

4. The best passive imagery was always obtained with the setting sun behind the aircraft.

5. Ship silhouettes were routinely identifiable at ranges exceeding 1 nmi.

6. Twelve-inch letters from known targets (UCSB sign) were readable at 0.25 nmi. Six-inch letters were almost readable at this range.

7. Best letter visibility occurred with a black hull with white letters. The next best was a white hull with black letters.

8. It frequently appeared that although a ship's name should have been readable, it was not. This phenomena appears to be attributable to the narrow spectral response of the AGTV. This phenomena should be further investigated.

9. The best method of obtaining good imagery was to locate the ship initially using the trackball position control in the surface track mode. When the target grew to a few TV lines in height, the AGTV video track mode was selected. As the target further grew in size, the target position was "fine tuned" using the joystick.

10. It was determined that, due to the limitations in the resolution of the AGTV as limited by the narrow field-of-view lens, the best approach in reading the name occurs by a direct overflight with minimum offset. Maintaining a constant radius turn of the required offset proved extremely difficult.

4.2.3.4.2 Active Performance

Due to the AGC action of the AGTV, the active mode could be utilized only when negligible passive return was visible, i.e., essentially total darkness. Almost all of the active mode data runs utilized the AIREYE computer range mode. Following is a summary of observed active performance.

1. Specular glint from large metallic or white objects was observable up to 1.7 nmi.

2. Ship silhouettes were discernible up to 0.7 nmi.

3. "Daylight" deck details were visible at ranges ≤0.32 nmi.

4. It was demonstrated that ship names with letter size ≥1 ft could be read in total darkness at ranges up to 0.32 nmi.

5. The best data runs were performed using straight-in approaches as in the passive mode case.

6. The lock-on technique for active mode imagery is the same as passive mode. However because a narrowband spectral filter is activated in the active mode which, by design, eliminates most of the light except at the laser bandwidth, it is important to wait until the last possible moment to select the active mode or video lock may be lost.

7. As was the case with the passive mode, it frequently appeared that although a ship's name should have been readable, it was not. This phenomenon appears to be attributable to the narrow bandwidth of the laser and spectral filter, and further investigation should be done to establish the limiting criteria.

8. Due to the AGC action, the active mode is effective only after passive mode return is negligible.

9. The AGTV requires more range to be operationally useful in the active mode.

4.2.3.4.3 Sample Imagery and AGTV Limitations

Due to a combination of low laser power, possible optics resolution problems, mismatch of spectral response between the gallium arsenide laser and the second generation intensifier, useful active imagery was limited to less than 0.35 nautical miles and optimum at 0.2 to 0.25 nautical miles. This limitation posed several problems:

1. Imagery was noisy with the rather large "snow" characteristics of the image intensifier.

2. The relative change in features between subsequent TV frames was largely due to the high closing rates.

One effect of these problems that is evident in the AGTV images presented subsequently is that the data appears to be very noisy. This effect is not nearly as apparent when viewing the data in real time. The photographs were taken at 1/30 of a second, which represents only one TV frame. When viewing in real time however, the human eye and brain perform an effective frame-to-frame integration and the resultant data appears substantially less noisy.

One of the image enhancement capabilities of the AIREYE system is the multiframe TV average. This enhancement feature typically averages five frozen sequential TV frames to improve image signal-to-noise ratio. It was generally impossible to apply this technique to the AGTV imagery due to the large changes of features occurring between TV frames with the short range, high closing rates required.

Currently the AGTV is being refurbished to include a more sensitive image intensifier and longer focal length lens for the narrow field of view. Since this will improve the effective range of active operation and thus reduce the very high closing rates currently required, it is expected that the AIREYE multiframe average feature will be able to be utilized when these improvements have been incorporated, which will dramatically improve AGTV image quality.

Figures 4-20a and 4-20b are an example of close range passive performance. Data were taken on a 495-ft overflight. The frames are approximately 0.6 seconds apart with the first frame being at a range of 0.48 nmi slant range and the second frame being at 0.21 nmi slant range. Illumination was provided by a combination of the vessel's own light and very dim natural light. Figures 4-21a and 4-21b are examples of the active performance capability of the AGTV. The first image is at a slant range of 0.63 nmi and the second is at a range of 0.25 nmi. At 0.63 nmi, return from highly reflective portions of the ship are clearly visible including the rails. At 0.25, nmi the deck is lit up as if it were daylight, with significant deck detail visible.

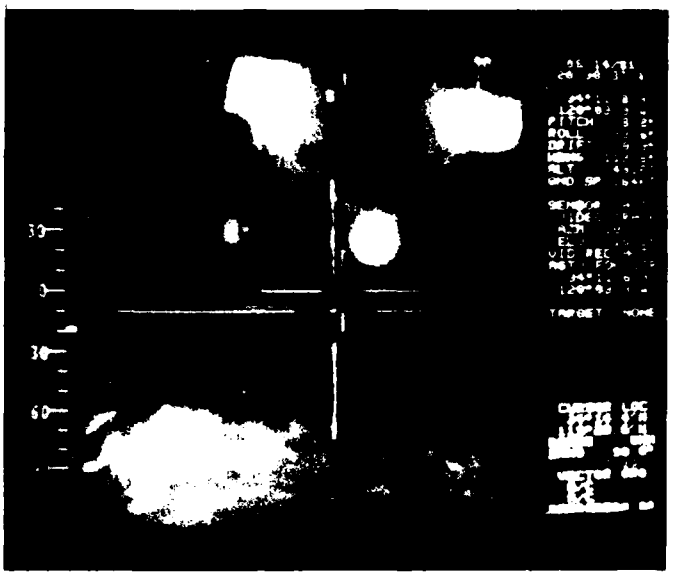

Figure 4-20a. AGTV Passive Ship Examination - 0.48 nmi Range

Figure 4-20b. AGTV Passive Ship Examination - 0.21 nmi Range

Figure 4-21a. AGTV Active Ship Examination - 0.63 nmi Range

Figure 4-21b. AGTV Active Ship Examination - 0.25 nmi Range

A dramatic example of the AGTV low light performance is shown in Figures 4-22a, 4-22b and 4-22c. These images taken at slant ranges of 1.68 nmi, 0.38 and 0.18 nmi respectively are three cigarettes lit on the deck of the Coast Guard Cutter. No other sources of illumination are present.

In this same sequence, light from a cigarette lighter was visible at greater than 3 nmi with enough illumination from the lighter to provide some deck details at 0.3 nmi.

Figure 4-22a. AGTV Passive Detection of Cigarette: Range = 1.68 nmi

Figure 4-22b. AGTV Passive Detection of Cigarette: Range = 0.38 nmi

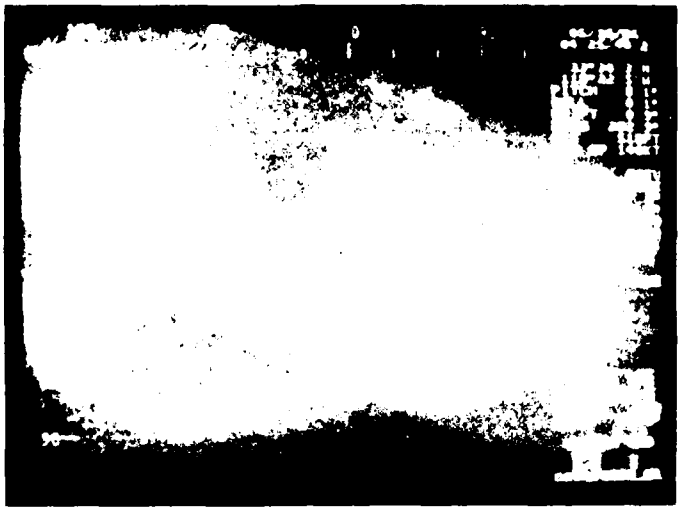

Figure 4-22c. AGTV Passive Detection of Cigarette; Range = 0.12 nmi

4.2.4 Digital Data Enhancement

The AIREYE system provides the capability to perform the following digital image enhancements.

1. Multiframe average (TV or VTR)
2. SLAR full resolution zoom
3. Continuous arithmetic zoom (all sensors)
4. Linear or nonlinear brightness enhancements
5. Single image smoothing
6. Single image sharpening
7. Other special programmable convolution enhancements.

This section illustrates the use of some of these enhancements on actual AIREYE flight test data.

Figure 4-23 is a SLAR image of the Santa Barbara channel. Platform Holly is identified using the AIREYE SLAR overlay capability as well as several other targets in the image. The majority of the small white dots in the image are vessels of various sizes.

Figure 4-23. SLAR Image of Santa Barbara Channel

The next step in the sequence is the selection of an area to be zoomed. The operator accomplishes this by using the trackball to position a zoom box of selected size over the area that he wants to examine more closely as illustrated in Figure 4-24.

The resultant image shown in Figure 4-25 shows some additional detail but is lacking in crispness and is low in contrast. The image is brightness enhanced and sharpened with the result shown in Figure 4-26. Note the significant improvement in boundary delineation or sharpness of the dark areas (oil). As a last step the image is smoothed to give it a more natural appearance as shown in Figure 4-27. Note however that the improvement in detail definition remains even after the smoothing process.

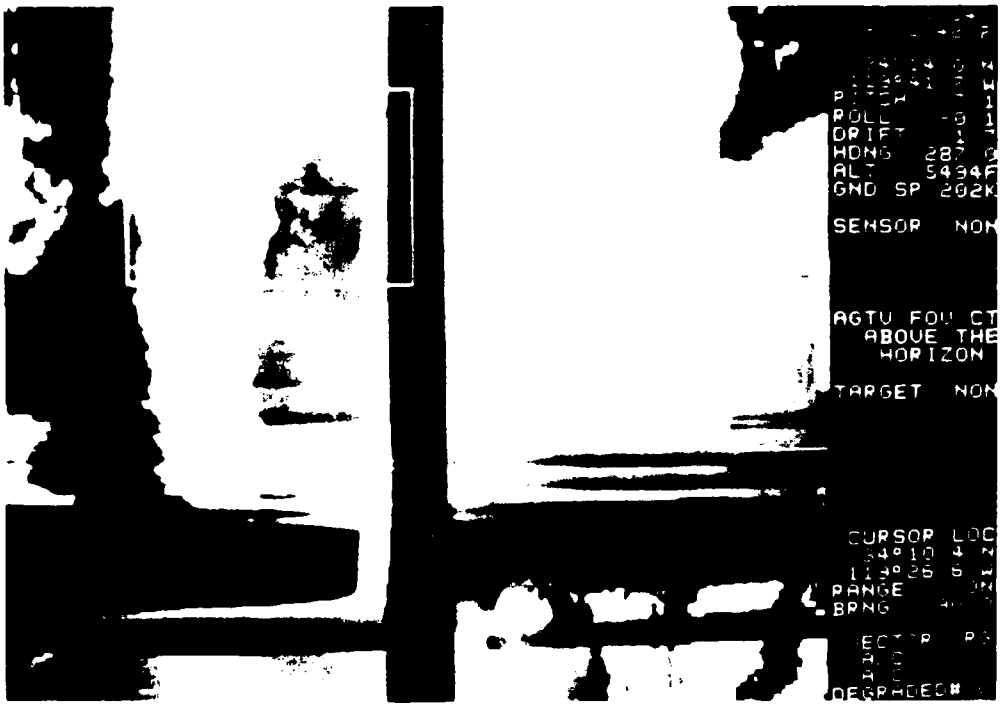

Figure 4-24. Selection of Area to be Zoomed from SLAR Image

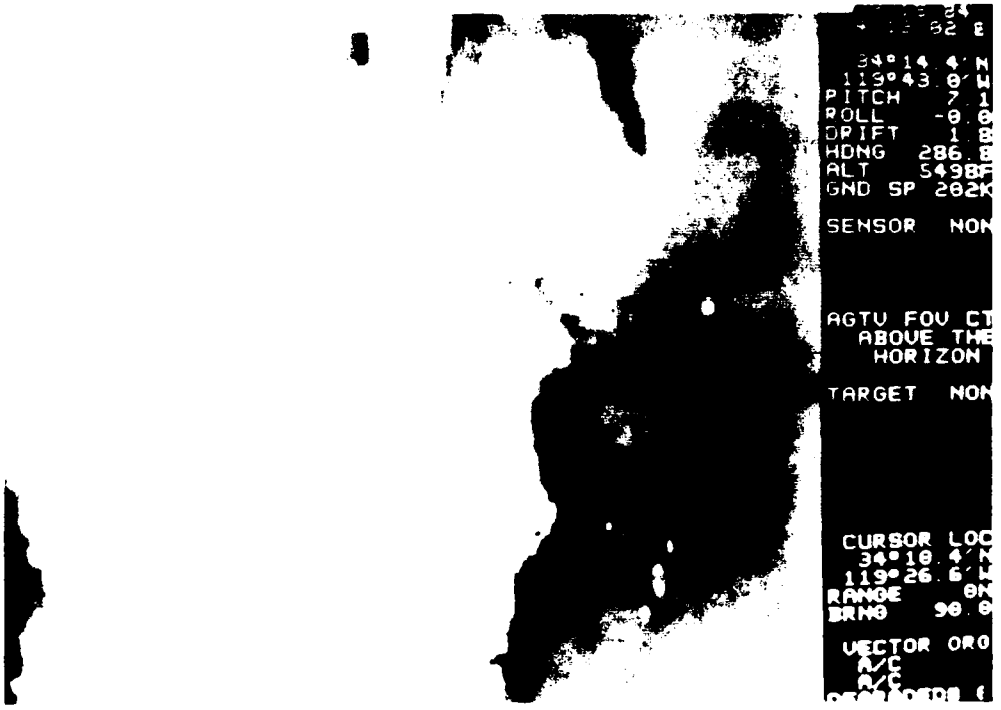

Figure 4-25. Zoomed Image

Figure 4-26. Effect of Brightness Enhancement and Image Sharpening

Figure 4-27. Smoothed Image

Figure 4-28 is an IR/UV image of oil streaming from Platform Holly. The overall image is low in contrast and the area of interest needs to be enlarged for more careful examination. The zoom box is positioned over the area of interest and the size of the box selected to outline the area of interest as shown in Figure 4-29. The image is then zoomed and brightness enhanced with the resultant image shown in Figure 4-30.

Figure 4-31 is another SLAR image of the Santa Barbara channel. The zoom box is set up (Figure 4-32) and the image is zoomed and scaled with the result shown in Figure 4-33.

Figure 4-34 is an IR/UV image of a large containerized cargo ship. The zoom box is positioned (Figure 4-35), zoomed (Figure 4-36) and sharpened (Figure 4-37). Note the detail of the vessel which is not apparent in the original image.

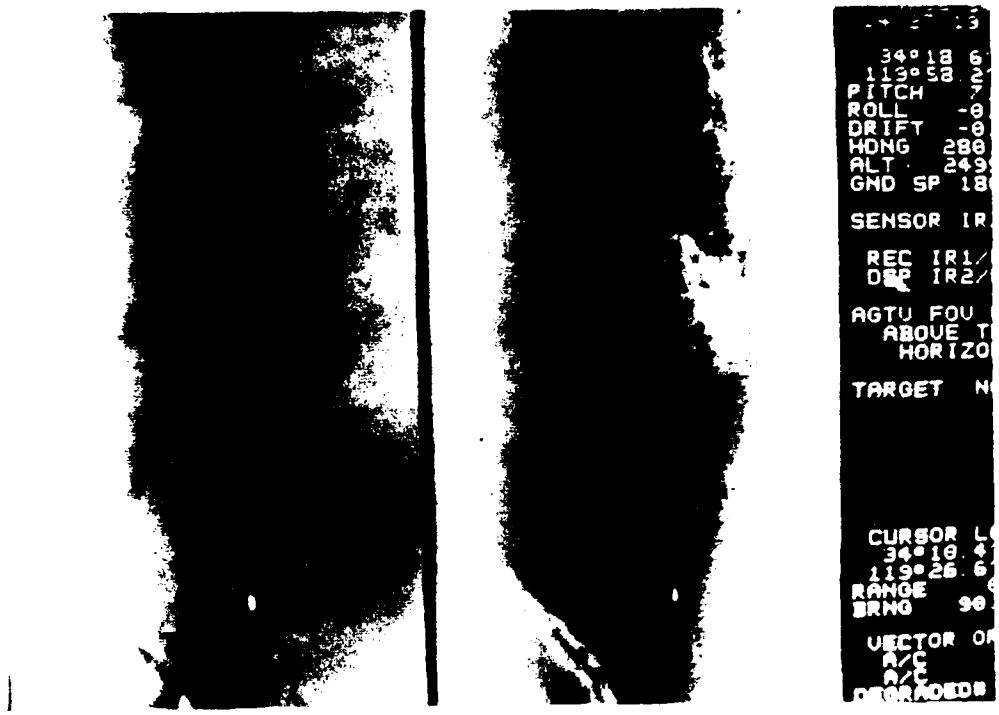

Figure 4-28. IR/UV Image of Oil from Natural Seep near Platform Holly

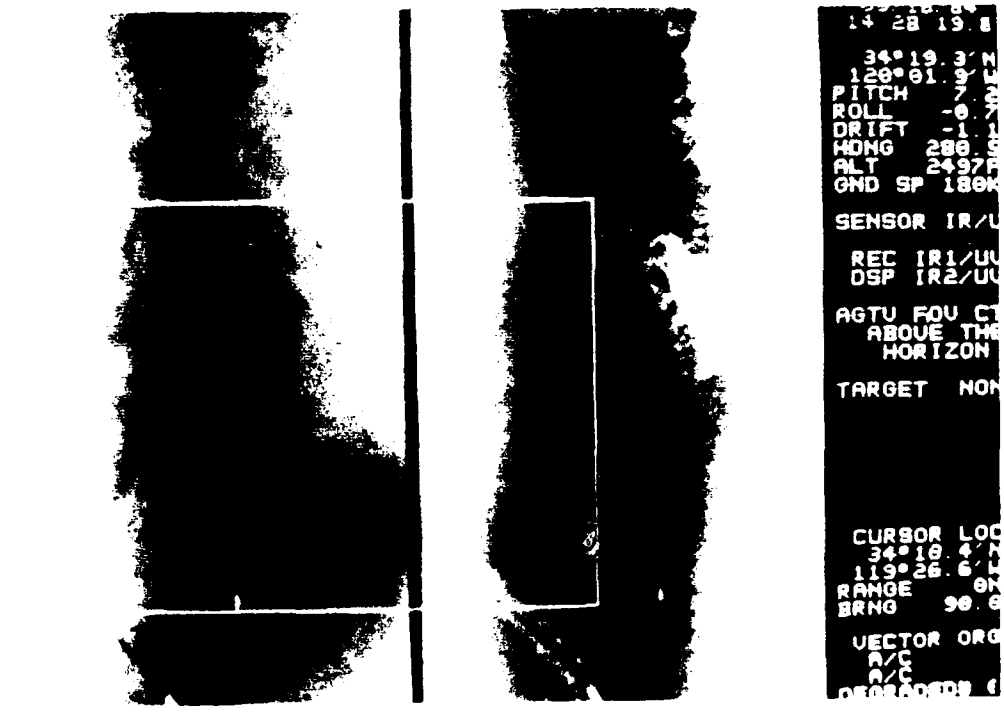

Figure 4-29. Selection of Area to be Zoomed from IR/UV Image

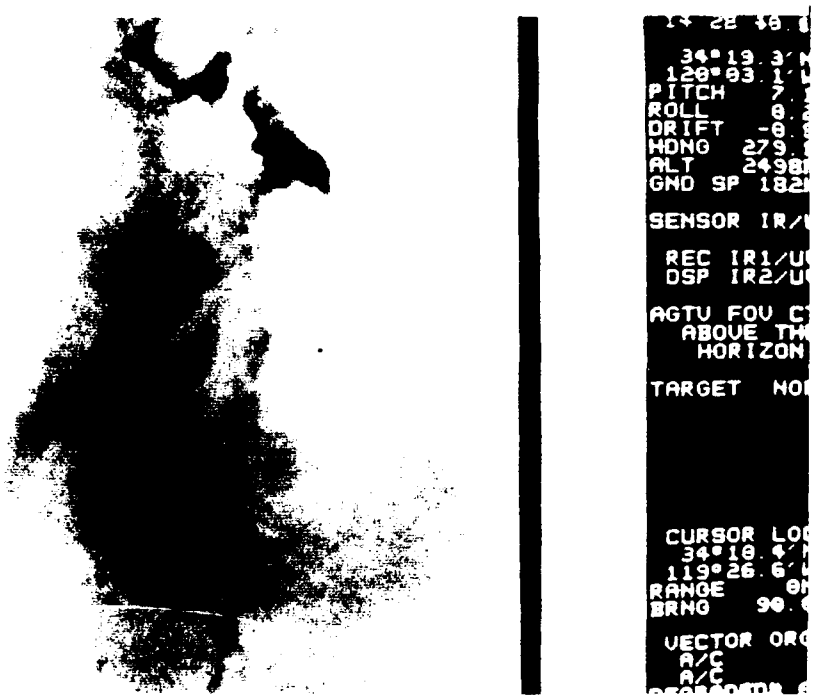

Figure 4-30. Zoomed and Brightness Enhanced IR/UV Image

Figure 4-31. Second SLAR Image of Santa Barbara Channel

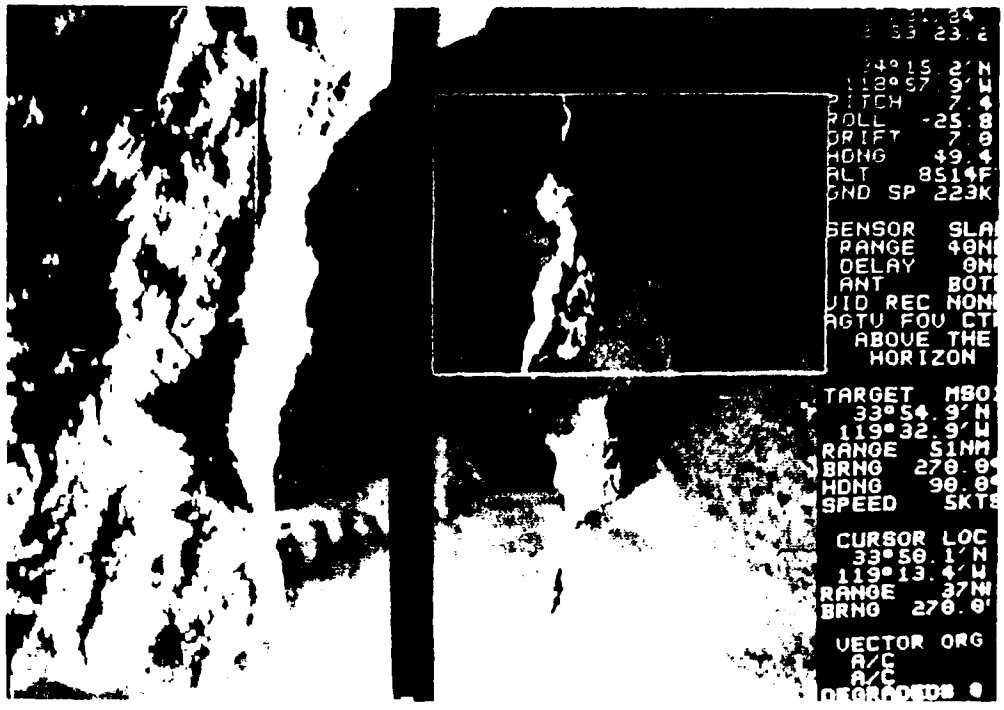

Figure 4-32. Selection of Zoomed Area from SLAR Image

Figure 4-33. Zoomed and Enhanced Image

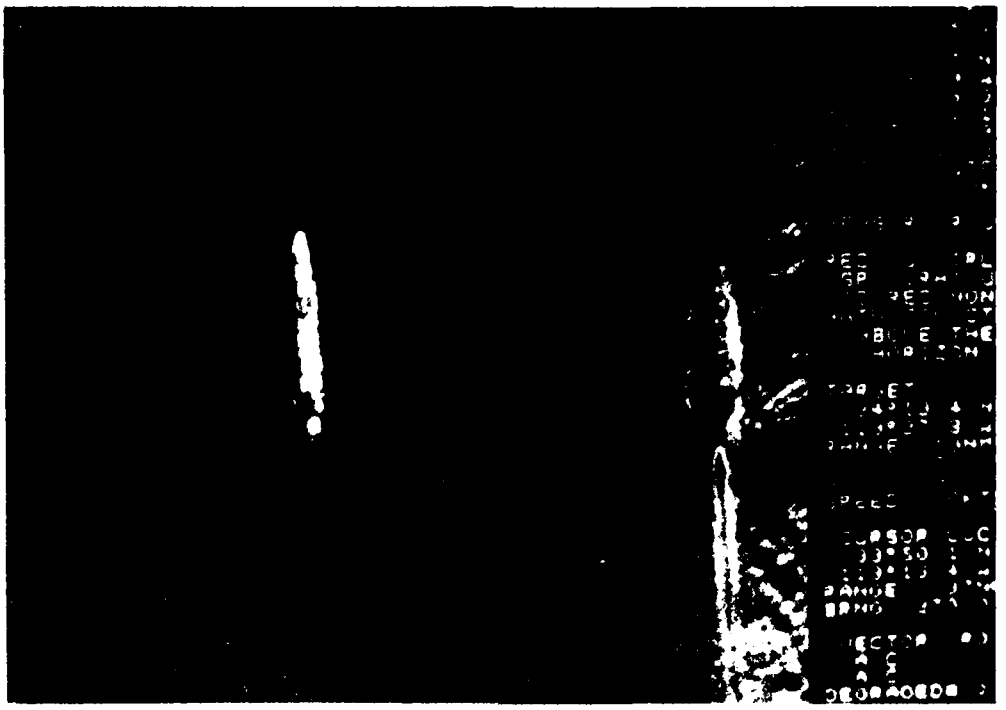

Figure 4-34. IR/UV Image of Container Ship

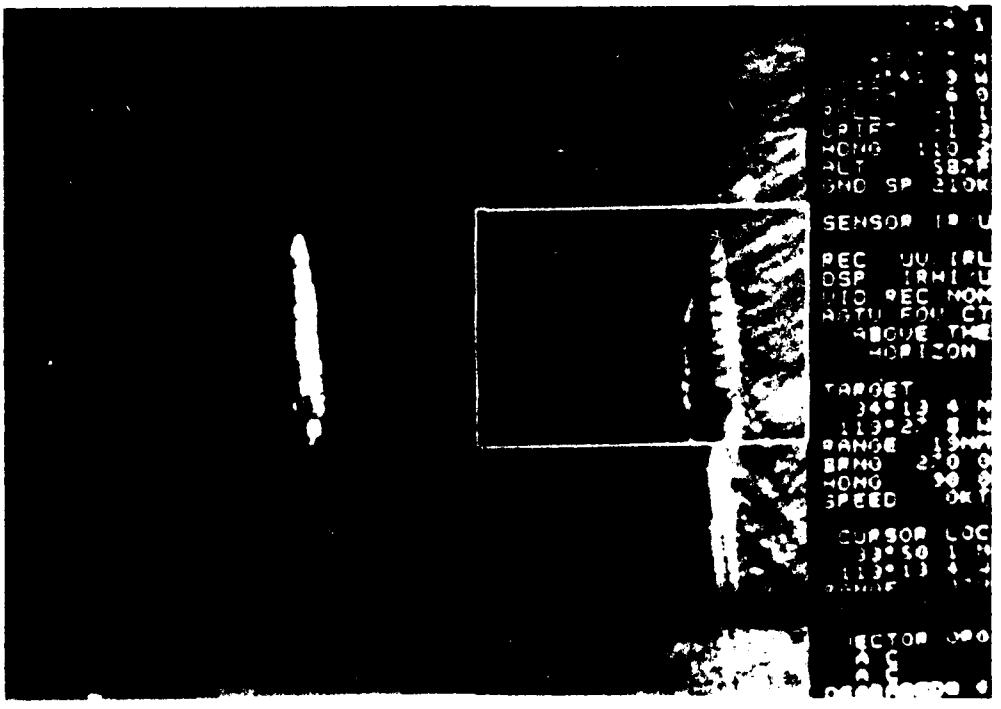

Figure 4-35. Selection of Area to be Examined

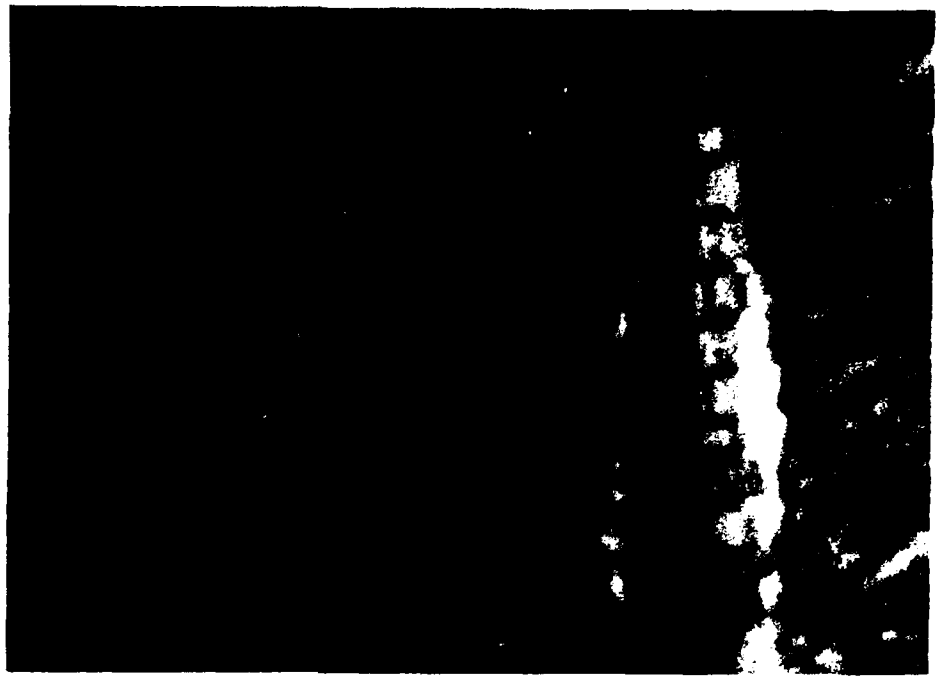

Figure 4-36. Zoomed Container Ship

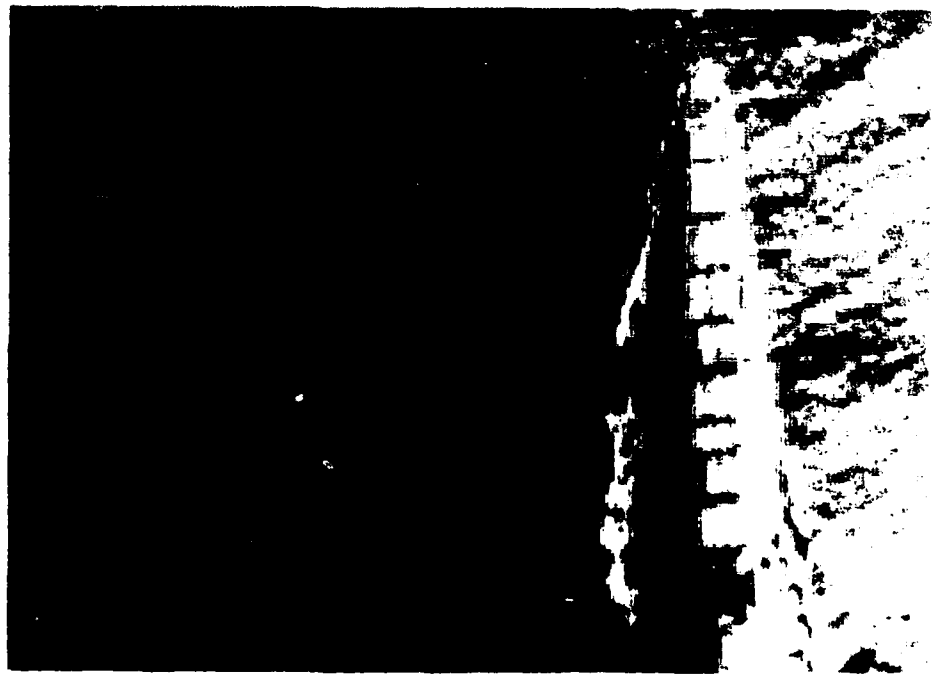

Figure 4-37. Sharpened Image of Container Ship

Section 5

CONCLUSIONS AND RECOMMENDATIONS

5.1 CONCLUSIONS

The prototype AIREYE system met all USCG requirements and has proven to be both reliable and operationally ready except for inadequate operational range and signal-to-noise ratio of the active-gated television. Successful integration of the system into the USCG HU-25A aircraft was completed and total compatibility demonstrated with minimum limitations on aircraft flying qualities and characteristics. Total EMI compatibility was demonstrated during both ground and flight testing.

Extensive flight testing verified system operational readiness and predicted performance capability. Specific conclusions derived from the flight test program follow:

1. The AIREYE system proved to be very reliable throughout the entire test program thus demonstrating operational/production readiness.

2. The AIREYE system can be operated by a single operator. During flight tests the AIREYE operator frequently operated the aircraft forward-looking radar.

3. The AIREYE signal processing system effectively coupled aircraft navigation data and sensor data to the SSO operator, facilitating image and target interpretation that effectively supported the "next step" decision process.

4. The ability to provide on-board hard-copy documentation was demonstrated.

5. The structured menu selection utilized by the AIREYE system enabled system operation by personnel with minimum training.

6. The utility of the AIREYE image enhancement capability under adverse operational conditions was effectively demonstrated.

7. The SLAR and IR/UV scanner performance were as predicted.

8. The AIREYE AGTV performance was lacking in range and signal-to-noise ratio from that predicted and required for operational use. The concept of the utilization of the AGTV in short-range surveillance, including the reading of a vessel's name, was successfully demonstrated. Specifically demonstrated were:

   - The ability of the AIREYE signal processing system, when combined with the AGTV video track mode, to establish and maintain AGTV positioning adequately to allow reading of ship's names and viewing of deck detail.
   - The ability of the AIREYE signal processing system to accurately and reliably position the AGTV range gate for active operation.
   - The ability of the AGTV gimbal to function under wind loading.

   Current improvements being incorporated into the AGTV should provide the required operational range.

5.2 RECOMMENDATIONS

The AGTV requires the following improvements to provide operational capability.

1. The addition of a third generation intensifier and longer focal length optics for the narrow field of view.
2. Additional laser power should be incorporated.
3. The turret and laser optics require an active air dryer/heater to prevent fogging in operational high humidity environment.
4. An investigation should be conducted to verify/establish the spectral performance of the AGTV as it relates to reading of ship's names.

Section 6

BIBLIOGRAPHY

Horvath, R., W. L. Morgan, and S. R. Stewart, 1971. "Optical Remote Sensing of Oil Slicks: Signature Analysis and Systems Evaluation," Report No. 27660-17-F, p 117, Willow Run Laboratories, University of Michigan for the U.S. Coast Guard, Office of Research and Development, Ann Arbor, Michigan.

Sellers, William D., 1965. Physical Climatology, p 272, University of Chicago Press, Chicago, Illinois.

Estes, John E., Rowena M. Carlson, and Joseph Scepan, 1985. "Aerojet ElectroSystems Oil Sampling Test - Final Report," Geography Remote Sensing Unit, University of California, Santa Barbara, for Aerojet ElectroSystems Company.

Catoe, C. E. and J. T. McLean, 1979. "A Multispectral Look at Oil Pollution and Detection, Monitoring, and Law Enforcement," Report No. NASA-TM-80573, p 25, National Aeronautics and Space Administration, Goddard Space Flight Center, Greenbelt, Maryland.

Edgerton, A. T., J. J. Bommarito, R. S. Schwantje, and D. C. Meeks, 1975. "Development of a Prototype Airborne Oil Surveillance System - Final Report," Report No. AESC-1812-1, USCG-D-90-75, Aerojet ElectroSystems Company for Department of Transportation, U. S. Coast Guard, Office of Research and Development, Washington, D.C.

APPENDIX A

AEROJET ELECTROSYSTEMS OIL SAMPLING TEST

FINAL REPORT

14 JUNE, 1985

PRINCIPAL INVESTIGATOR-

DR. JOHN E. ESTES

AUTHORS-

ROWENA M. CARLSON
JOSEPH SCEPAN

TABLE OF CONTENTS

LIST OF FIGURES

LIST OF FIGURES (CONT.)

LIST OF TABLES

ABSTRACT

Field tests were performed to evaluate the United States Coast Guard's AIREYE airborne surveillance system. AIREYE's thermal infrared, ultraviolet and side-looking airborne radar sensors were tested for oil slick and surface vessel detection capabilities in the Santa Barbara Channel, California. Surface samples were acquired to measure oil slick thickness and a variety of sea-surface and meteorologic data were acquired concurrent to a series of AIREYE system test flights.

AIREYE imagery is interpreted and qualitatively evaluated for detection capabilities. In addition, general detection concepts are presented for thermal infrared, ultraviolet and radar systems for oil slick and surface vessel detection.

1. INTRODUCTION

This report describes the participation of the UCSB Geography Remote Sensing Unit (GRSU) in the surface verification of the remotely sensed imagery produced by the United States Coast Guard AIREYE (USGS/AIREYE) system. This project is part of an extensive flight test program being conducted by the AIREYE system developers, Aerojet ElectroSystems Corp. AIREYE is a multisensor, real-time, all weather, day/night remote sensing system flown on a USCG Falcon Fan Jet (military designation HU-25A). The system is used for a variety of USCG missions, including Marine Environmental Protection, Enforcement of Laws and Treaties, and Search and Rescue. The purpose of the GRSU surface verification is to document AIREYE mission performance for the detection of sea surface oil pollutants and violating vessels under a variety of environmental and operating conditions.

The AIREYE sensors evaluated in this study include a thermal infrared/ultraviolet (IR/UV) line scanner, X band, vertically polarized real aperture side looking airborne radar (SLAR), and an Active Gated Television (AGTV). SLAR, AGTV, and IR/UV line scanner data may be viewed in real time on the on-board video screen, recorded on video tape, or recorded on dry silver film or paper tape. SLAR imagery may be continuously recorded on dry silver film. Enhancements of any data may be viewed in real time, recorded on video tape, or recorded on dry silver film or paper.

The series of AIREYE test flights (originally scheduled for June, 1984) were to consist of five days of flights for concurrent testing of the IR/UV line scanner, SLAR, and AGTV. These tests were to be conducted under a variety of atmospheric and sea surface conditions, both day and night. Due to aircraft and sensor problems, the test flights were rescheduled several times until September 1984.

AESC/USCG then conducted two days of IR/UV test flights on September 10 and 13, 1984. Two days of SLAR radar reflector tests were added to the project and conducted on October 18 and 19, 1984. The remaining three days of oil sample verification tests for the IR/UV line scanner and SLAR were dropped from the schedule. No night tests were conducted. The AGTV was not operational during any of the test flights.

The GRSU sea surface verification involved the correlation of environmental data with the imagery produced during the test flights flown over the Santa Barbara channel in the area offshore of Coal Oil Point, Ca. This area usually contains all normal AIREYE targets, such as vessels of various sizes, offshore oil platforms, and continuous natural oil seeps. The data collected for use in evaluating the IR/UV imagery included oil samples, oil sample radiometric temperature, sea state, atmospheric conditions, sea surface temperature, and color aerial photographs.

Sea truth evaluation of the SLAR imagery involved the use of trihedral radar reflectors to provide a reference for the intensity of the backscattered radar signal from the sea surface.

2. BACKGROUND

2.1 Description of AIREYE System

2.1.1 Infrared/Ultraviolet (IR/UV) Line Scanner

The Texas Instruments RS-18C Infrared/Ultraviolet line scanner is used to provide multispectral information on targets of interest. With data from two portions of the electromagnetic spectrum, ship wakes and kelp beds can be differentiated from oil slicks.

The output imagery from the IR/UV line scanner is recorded in real time on 3/4 inch TEAC format video tape, and dry-silver film or rolls of 4 inch wide paper negatives. Table 2-1 lists the principal operating parameters specified for the IR/UV line scanner.

2.1.2 Side Looking Airborne Radar (SLAR)

The SLAR used in the AIREYE system is an AN/APS-131 manufactured by Motorola Incorporated. The main operating characteristics of this system include:

1. X band (9250 MHz), vertical polarization.
2. Display ranges available of 10, 20, 40, or 80 nautical miles.
3. Range resolution of 30 meters (98 feet).
4. All-weather day/night operation - The SLAR can produce imagery in most weather conditions and is unaffected by clouds or darkness.
5. Latitude-longitude grid lines are superimposed onto the film imagery.
6. Antenna with back-to-back dual array allows simultaneous mapping on both sides of the aircraft.
7. Yaw stabilized to +/- 3 degrees.
8. Pulse width of 0.2 microsecond and pulse repetition frequency of 750 or 1500 pulses per second.
9. Depression angle of beam peak of 1.5 degrees.

2.2 Detection Concepts

The oil slick signature is composed of two basic components; its backscatter or emission differential relative to the

unpolluted water and the shape or pattern formed by the slick and superimposed on the ocean background. No single sensor is capable of imaging the backscatter or emission under all atmospheric conditions. IR and UV sensors cannot penetrate clouds or fog which occur in the United States coastal waters more than half the year (Edgerton et al, 1973). Radar is able to penetrate clouds but cannot detect oil slicks on the sea if wind waves are not present. These waves require a minimum wind speed of 3-4 knots which occur 4.2 to 10.8 percent of the year in most United States coastal regions (Edgerton et al, 1973). Thermal IR and UV sensors are not hampered by wind or sea state. The solar reflection dependent UV sensors cannot operate at night, while thermal IR and Radar have both day and night sensing capabilities.

2.2.1 Thermal Infrared (IR)

Thermal infrared imagery (i.e. that which is sensed in the 8-14 um portion of the electromagnetic spectrum) of oil slicks has been found to be an effective tool for the identification of oil on sea water under certain conditions. It is especially useful for locating areas of an oil slick with thickness greater than 2 um (O'Neil et al, 1983). Thermal IR sensors are passive; they image emitted rather than reflected radiation. As a result, the sensor does not depend upon reflected energy from the sun. This gives the system both day and night surveillance capabilities.

A thermal infrared sensor measures thermal radiation, which is electromagnetic radiation in the wavelength range of 4 to 20 um. The intensity of the thermal radiation emitted by a target depends on the kinetic temperature, and on the emissivity of the object. Emissivity ( ) is the ratio of the exitance of a body of kinetic temperature T to the black body (perfect radiator) exitance at the same temperature. The exitance of a blackbody (M_{bb} (,T)) is described by Planck's equation (Equation 1):

$$M_{bb}(\lambda,T) = \frac{2\pi hc^2}{5\left[e^{(hc/k\lambda T)} - 1 \right]} \qquad (1)$$

where:

c = speed of light (ms^{-1}))
h = Planck's constant (js)
λ = wavelength (m)
k = Boltzman constant ($j\ deg^{-1}$)
T = temperature (degrees Kelvin)

The spectral emissivity of a given target can be defined as:

$$(\epsilon) = \frac{M_r(\lambda, T)}{M_{bb}(\lambda, T)} \quad (2)$$

where:

$M_r(\lambda, T)$ = exitance of a real material at a certain wavelength and temperature.

Therefore, the radiant temperature recorded by a remote sensor will be less than the kinetic temperature of the object.

By the Kirchoff Radiation Law, the spectral emissivity of an object equals its spectral absorbtance alpha (lambda). This means that good absorbers are also good emitters. The energy balance equation (Equation 3) can be modified as follows:

$$\alpha(\lambda) + \rho(\lambda) + \tau(\lambda) = 1 \quad (3)$$

where:

α = absorbtance
ρ = reflectance
τ = transmittance

and

$$\alpha(\lambda) = \epsilon(\lambda) \quad (4)$$

Equation (3) becomes:

$$\epsilon(\lambda) + \rho(\lambda) + \tau(\lambda) = 1 \quad (5)$$

Therefore, the lower an objects reflectance of thermal energy, the higher its emissivity, if it is assumed that transmittance is not involved. For example, pure water absorbs almost all thermal energy and so reflects almost none, giving it a very high emissivity, close to one (.993).

In the case of man made targets, the emissivities of materials which these targets are generally constructed of are presented in Table 2-2.

The precise characteristics of different oils and their emissivities are not fully understood (Catoe and McLean, 1979). The emissivity of oil is thought to be a function of oil type, slick thickness, and the environmental conditions (Horvath, 1974). Emissivities for several different types of oil are

presented in Table 2-3.

It has been suggested (Horvath et al, 1974) that thickness variations have an effect on the amount of radiation emitted by oil, in that as oil thickness increases, evaporation losses from volatiles present increase - thereby producing lowered temperatures in the slick. However, as the oil becomes thick enough to absorb significant solar energy, this cooling trend is overcome by solar heating and a "warm" slick results. However, highly volatile and relatively transparent oil products apparently do not absorb sufficient solar energy to compensate for the reduction in temperature due to evaporation. These generally will appear colder than water.

Allen and Estes (1970) suggest that thicker oil causes an apparent emissivity decrease and appears colder, while thin oil allows some penetration of the underlying water radiation and thus becomes a function of an oil/water combination. Since the radiometric temperature of water is a function of the upper 0.02 mm, and since irridescent oil films are typically on the order of 0.0002 mm it may be possible that infrared energy from the sea water is being imaged through the very thin oil slick. As a result, thermal IR imagery is usually only useful for detection of areas of oil slicks with thicknesses greater than irridescent films.

The complex interelationships between oil and water, which affect radiometric temperature, are not fully understood. But, evidence does indicate that emissivity of an oil slick does have some relationship to oil thickness and oil type. Table 2-4 presents a classification of petroleum types in relation to their expected thermal IR tonal response (Horvath, 1974). The petroleum of the natural seeps in the study area are considered to fall into the heavy crude category (personal communication with ARCO, 1984) which would exhibit high absorption (high emissivity) whether fresh or aged.

2.2.2 Ultraviolet

Ultraviolet sensors are primarily dependent upon reflected radiation from the sun for image formation. Their use for sensing oil on water is therefore limited to daylight. Atmospheric haze is another major limitation due to scattering of the near UV wavelengths (.32-.40 um) by atmospheric aerosols (Catoe, 1973).

When oil is exposed to broadband ultraviolet radiation from the sun it reflects and absorbs the incident radiation. In the case of oil slicks on the ocean, the reflectance contrast between oil and sea water is significant due to the fact that oil has a higher reflectance than sea water in the near ultraviolet region (Catoe and McLean, 1979). This is a direct result of the greater indices of refraction for oils as compared to that of water.

The characteristic yellow, brown, or brownish-black colors associated with most oils are related to their strong ultraviolet

absorption, which extends into the visible region. Generally, these colors can be seen in oil slicks only with near- vertical viewing, where sky reflectance is weak.

The tone of an oil slick relative to water in a UV image is a complex function of the oil type, slick thickness, water quality, and solar illumination geometry (Horvath, 1974). The UV band gives excellent demarcation of the thinnest part of a slick (Alfoldi, 1982). An oil slick always produces a brighter tone than water if its thickness is small enough, and will generally produce a darker tone than water if its thickness is great enough. This condition may be explained as follows: The radiance viewed by the observer consists of two components - a specular part related to the oil layer, and a diffuse portion upwelling from beneath. The specular radiance from the oil is essentially constant, whereas the diffuse component is maximum for clean water and thin films, but approaches zero for very thick oil films. The minimum thickness required to change from a brighter tone to a darker tone depends upon oil type.

The quality of the solar illumination on an oil slick will affect its UV tone. On a very clear day with the sun high in the sky, the tendency toward darker slick tones will be increased. Conversely, if the sun is very low in the sky, or if cloud cover is present to diffuse the solar radiation, the tendency for brighter slick tones will be increased.

To summarize, the UV tone of an oil slick on water can be characterized by the following:

1. Thin portions of the slick will be brighter (higher reflectance) than the water. Thus, every slick will have some portions which produce light tones.

2. Thick portions of the slick can become darker in tone (lower reflectance) than the water. However, the conditions which lead to such tones are not always present.

3. Slicks composed of heavyweight crude oils are capable of exhibiting a wider range of tones than slicks composed of lightweight refined products.

4. Slicks existing in clear waters will show a greater tendency toward dark tones than slicks on dirty waters.

5. Slicks observed during clear weather with a high solar elevation will show a greater tendency toward dark tones than if observed under overcast or low solar elevation conditions.

2.2.3 Side Looking Airborne Radar (SLAR)

SLAR is an active remote sensing system which provides its own illumination source rather than relying on illumination from

the sun. This gives the SLAR day/night imaging capabilities. SLAR is also relatively unaffected by weather since the wavelengths used are not attenuated by the water vapor in fog, haze, or moderate rainfall.

The term "side looking" means that SLAR produces imagery of the area to one side of the aircraft flight path instead of directly underneath. The antenna points to the side with a beam that is wide vertically and narrow horizontally. The image is produced by motion of the aircraft past the target as the signal is transmitted. When the pulse strikes the target, a signal is returned. The signal return is used to modulate the intensity of the beam on an oscilloscope, which is then transferred by a lens to a film. The film is in the form of a strip that moves synchronously with the motion of the aircraft, so that as the aircraft moves forward the film also moves. After each line of signal return is recorded, another pulse is transmitted in order to obtain a new scan line. The film speed is proportional to the aircraft speed over the ground.

Radar pulses propagate outward at the speed of light. As they encounter variable reflective surfaces they are returned or backscattered toward the radar antenna. The performance of a radar is described by the radar equation, which relates the received power to the target parameters and to the parameters of the radar. The received power may be written as:

$$P_r = \frac{P_t G_t}{4\pi R^2} \sigma_{rt} \frac{A_r}{4\pi R^2} \qquad (7)$$

where:

P_r = received power at polarization r
P_t = transmitted power at polarization t
G_t = gain of the transmitting antenna in the direction of the target at polarization t
R = distance between radar and target
σ_{rt} = radar cross-section, the area intercepting that amount of incident power of polarization t which, when scattered isotropically, produces an echo at polarization r equal to that observed from the target
A_r = effective receiving area of the receiving antenna aperture at polarization r

In most applications of radar remote sensing, the targets are usually much larger than a resolution cell of the radar. As a result, it is more convenient to define an average differential cross-section or radar cross-section per unit area, and to

consider the average return power. The total average received power is then given by integrating the return from each differential area over the entire irradiated area. The scattering cross section per unit surface area, also known as the scattering coefficient, is commonly denoted by σ^{o}_{rt} in terms of decibels. The scattering coefficient, in general, is a function of polarization, look angle, wavelength, and interaction properties of the target: geometric, dielectric, and conductive (Fung and Ulaby, 1983). The gray tones on a radar image are proportional to the average return signal strength or, σ^{o}_{rt}. The range of target cross-sections which can be displayed on an image is termed the dynamic range of the radar system.

Radar systems detect oil slicks by measuring a reduction in radar backscatter resulting from the calming effect of oil films on small-scale water waves. Oil films significantly damp or attenuate the capillary and small-scale gravity waves which cause much of the normal sea backscatter at radar frequencies. Consequently, in radar images, the oil covered areas appear dark since very little energy is being returned, whereas the oil free, and so wind ruffled, ocean areas appear as grainy grey-white. Radar observations of natural slicks have shown a decrease of three orders of magnitude in the return (Catoe, 1973). The magnitude of the return is dependent on the size of the small scale ocean waves which are in turn dependent on the wind speed. It has been found that a wind speed of at least three knots is necessary to create these wind waves (Edgerton et al, 1973). The wind-speed dependence is strongest for upwind observations, somewhat weaker for the downwind, and weakest for cross-wind observations (Chan and Fung, 1977). Vertically polarized SLAR, in low sea state conditions, is able to detect and map oil slicks as thin as one micron or less (Long, 1975).

Man made objects, such as oil platforms and sea surface vessels, produce very strong radar returns (bright image signatures) because of their geometry and electrical properties. These objects may form corner reflectors which consist of three planar surfaces intersecting at right angles. Regardless of the incidence angle at which a radar wave enters the cavity of a corner reflector, it is reflected directly back toward the antenna and appears as a bright area on the image.

2.2.4 False Targets

There are a number of phenomena which can show up as false targets of oil slicks in IR, UV, and SLAR imagery. These false targets can be distinguished from oil slicks by the methods described in this section. The potential false targets are shown in Table 2-5.

Fish oil is quite similar to certain types of petroleum products in terms of its mechanical and optical properties. It forms slicks on top of the water similar to petroleum oils, and may produce IR and UV tones and shapes characteristic of lightweight, non-volatile, and non-absorbing refined products

(Horvath, 1974).

The motion of ships through water creates two phenomena which may be mistaken for oil slicks in IR or UV imagery. These are regular wave trains and wake scars. Bow and displacement waves are the primary wave trains created by vessel motion. The displacement waves are created directly behind the vessel and move forward along the ship's track. Both types of waves are detectable in the UV imagery, especially when occurring in a region of sun glint. They can be identified by their regularity of texture as being wave trains. These waves are not detectable in the IR.

The ship motion also leaves a scar directly in its wake as a result of prop wash and breaking of the bow waves. The foam and bubbles in the scar are very bright in the UV, sometimes even brighter than the ship itself. The breaking bow wave forms a halo around the ship and the bright UV tone in the scar can trail out as much as one or two boat lengths behind.

The foam and bubbles which produces the bright UV tone does not produce a detectable IR response. However, if the water has a significant vertical temperature stratification, the ship's passing will bring up the cooler water from below the surface and produce a thermal scar. This dark IR scar can last for many minutes, sometimes hours. Light seas diminish this scar both by destroying the initial temperature stratification and by mixing the water in the wake.

The bright UV tone associated with the scar can be differentiated from an oil slick primarily because it only lasts for a few seconds, and is only visible very close astern. On the other hand, a dark thermal scar trailing far behind can easily look like the dark IR tone of an oil slick. In this case, the UV tone in the scar (far behind the foaming region) can be used to determine whether or not oil is present. At night, of course, no UV data will be available for this discrimination. Thermal scars are not associated only with moving ships. If the water is stratified and is being carried by a current, any fixed object can produce a wake and a thermal scar. Thus, offshore drilling rigs, lighthouses, moored ships, and similar structures can produce thermal scars whose IR tone looks similar to an oil slick.

Seaweed of any type is readily detected in UV imagery provided it is near the surface and the water is fairly clear. It produces a uniformly dark UV tone which might be mistaken for thick oil except for the absence of the bright border characteristic of a slick. In addition, the seaweed generally does not exhibit the clear shape and outline of an oil slick, but tends to produce a splotchy pattern. If the seaweed is extensive, and if the water is calm, subtle thermal patterns can sometimes be found in the IR imagery during bright daytime conditions. These thermal patterns will tend to have the billowy appearance of clouds, which is quite different from an oil slick pattern.

Changes in water depth, particularly as the result of sandbars and near-surface shoals, are often seen in the UV as areas of brighter tone. They can generally be discriminated from oil slicks by their tonal shape and texture. Unlike an oil slick, a sandbar or shoal will tend to be brightest in the middle, with this bright tone fading toward the edges until it merges with the tone of the deeper water. Also, the edges will not usually be so crisply defined as those of an oil slick.

2.3 Test Site Description

The AIREYE sensor test site includes a zone of natural oil and gas seepage in the Santa Barbara Channel which has been used for many years as the test site for oil detection sensor experiments. The test site includes the area between Coal Oil Point and Goleta Point and four miles out to sea as seen in Figure 2-1. Major oil seep activity is located within two miles of Coal Oil Point, with several distinct seep areas usually observable within this region.

Although the rate of oil flow from natural seeps in the Coal Oil Point area is somewhat variable, oil slicks derived from natural seepage are generally noted on the ocean surface there year round. The position of these oil and gas seeps is static and well documented (Kraus and Estes, 1977). Surface oil slicks which result from their oil discharge vary through time from narrow streamers of a few hundred meters at one extreme to virtually continuous coverage of a ten to twenty square kilometer area on the other. Estimates of oil flow rates range from 50 to 100 barrels per day (Mikolaj et al, 1972) to 900 barrels per day (Straughan and Abbott, 1971) for the Coal Oil Point area.

3. IR/UV VERIFICATIONT TEST

3.1 Sea Surface Ancillary Data Collection

GRSU collected oil samples during the IR/UV sensor flight time with the use of a 21 ft Boston Whaler. The following information was collected during all AIREYE test flights (specific data may be found in Appendix I):

Sea state - the sea state data recorded includes wave height, swell period, height, and direction. This information was estimated by the GRSU field crew and confirmed or adjusted according to wave staff measurements provided by Neuschel Mariculture, Goleta, California.

Sea surface temperature - the sea surface temperature was obtained from the UCSB Marine Science Institute lab which maintains a temperature recorder off Goleta Point.

Atmospheric conditions - wind speed and direction were obtained from an anemometer mounted on oil platform Holly which is located in the test area. Cloud cover was estimated by the GRSU crew and cloud height was obtained from the AIREYE flight logs.

Oil samples - Sea surface oil samples were collected during the IR/UV test flights for the purpose of measuring oil film thickness in the slick areas. The method which has been developed by the GRSU (Estes et al, 1972 and Kraus et al, 1979) involved the use of an X type sampler which resembles a 39 cm diameter cookie cutter (Figure 3-1). At each sample site, a clean sheet of sorbent material (IBM type 156 sorbent pad) was pulled tightly across the inside of the sampler, which was then lowered onto the water surface. The sorbent pad absorbed and removed the oil from the surface of the water isolated inside the sampler. The oil soaked pads were stored in sealed one liter glass jars until taken to the UCSB Chemistry department for processing. The Gravimetric method used for extracting and measuring the weight of oil collected in the pads, and the calculations necessary to convert the results to thickness are shown in Appendix II.

The radiometric temperature of the oil covered sea surface was measured at each sample site with the use of a Barnes Model 14-220D-1 Instatherm radiometric thermometer. This thermometer has a 2.8 degree field of view which allows it to measure the temperature of an area of 8 cm diameter at a distance of one meter. The temperature is measured without contact with the target by detecting and measuring infrared energy in the range of 6.5 to 20 um which all objects naturally emit.

At each sample site, a hand held compass was used to take bearings to three stationary points. These bearings were used to plot the sample locations. A written description of each sample area was recorded and color photographs taken with a hand held 35 mm camera.

3.2 Airborne Ancillary Data Collection

GRSU personnel in a Cessna 182 light aircraft carried two hand held 35 mm cameras, one equipped with a 55 mm lens and the other with a telephoto lens. Overall views of the test site were photographed each day as well as specifics areas such as oil slicks, the Boston Whaler at oil sample locations, and any surface vessels in the area. The Cessna crew also produced annotated sketches of the study area on base maps with a scale of 1:24000. Features noted on the sketch maps included slicks, surface vessels, oil sample locations, and any other objects of interest seen in the study area.

3.3 Oil Sample Analysis

The oil samples were processed by the UCSB Chemistry department. The Gravimetric method used for measuring the weight of oil in each sample and the calculations used to convert to oil film thickness are described in Appendix II. The calculated sample thicknesses are shown in Tables 3-1 through 3-3.

Seven of the twenty one samples measured the same amount of oil as the blank sorbent pads evaluated for inherent oil. This may be explained in several ways. First, these slick areas may well have been so thin as to not be measurable by this technique. Irridescent oil films are typically on the order of 0.0002 mm (Allen and Estes, 1970), and it is only necessary to have a molecular layer of oil to create a visible sheen on the water (personal communication with Dr. Bruce Rickborne, UCSB Chemistry Department). Second, much of the sample quantity may have been lost by adhering to the inside walls of the sampling device before it could come in contact with the sorbent pad. The inside area of the walls is 1236 cm^2 (194 in^2) which would greatly subtract from the amount of oil adhering to the 1194.6 cm^2 (118.7 in^2) sorbent pad which comes into contact with the water surface.

The areas described as "rainbow" or "sheen" measured the thinnest, around .0008 mm and the areas of "thick skin" or "chocolate mousse" had the thickest measurements. But the "thick" measurements are only relative since these values of 0.0015 to 0.0065 mm (1.5 um to 6.5 um) are considered to be thin slicks according to a recent study where oil film thickness have been categorized as thin film < 10 um, intermediate film = 10 to 150 um and thick film > 150 um (O'Neil et al, 1983).

Oil samples were evaluated with respect to any relationship between thickness and measured radiometric temperature. There seems to be some relationship between temperature and thickness in the 9-10-84 AM samples. The thinnest samples (.0008 mm and 0.0011 mm) have the highest radiometric temperatures (15.1° C and 19.7° C) while the two thickest samples (.0018 gm/ft^2) and (12.3° C and 12.9° C). No relationship between temperature and thickness is apparent in the 9-10-84 PM or 9-13-84 PM samples.

Temperatures of oil samples acquired in the afternoon tests were consistently higher than the set of morning temperatures. Both afternoons were slightly windy, which broke up the oil patches and may have allowed the water temperature to transmit through the broken oil. The oil patches may have also absorbed (and so emitted) more incoming solar radiation over the period of time from morning to afternoon.

The oil sample triangulations were plotted on mylar overlays of topographic maps at a scale of 1:24000. Due to the movement of the Boston Whaler in the waves and swells the bearings contained such large errors that the triangulations were too large to pinpoint the oil sample locations to any useful accuracy. This problem was partially overcome when the IR/UV imagery was obtained. The oil sample locations were obvious along the Boston Whaler wakes which were visible in the low altitude imagery. These wakes were not visible in detail in the high altitude imagery.

3.4 IR/UV Image Analysis Procedures

AESC provided the IR/UV imagery in the form of 3/4 inch U-MATIC format video cassette tapes which had been copied from the original TEAC format tapes, and rolls of 4 inch wide paper negatives. No information was provided as to what-on board image processing,if any, had been done.

It was necessary to create larger forms of hard copy of the imagery than was provided in order to plot sample site locations and compare to the sketch maps created of the area. Several methods for creating hard copy of video tape imagery are available. The optimal method involves the use of a digital freeze frame unit (known as a frame grabber). A video screen image consists of 525 lines by 300 samples and can be digitized in a single frame time of 1/30 sec (Ballard and Brown, 1982). The digital imagery allows a wide variety of image processing to be possible along with the production of high quality hard copy. This equipment was not available for use in this study.

When digital methods are not available, hard copy for analysis of video tape imagery is usually created by photographing a stop frame of the video screen (Meisner, 1985). This method was used and found unsatisfactory for several reasons, including loss of detail and geometric distortion. A major problem with photographing the video imagery occurred when it was found that all copies of the IR/UV and SLAR video tapes showed dark horizontal lines when stop frames were attempted. This problem may have been caused when transferring the original recorded data from TEAC to U-MATIC format.

Positive prints of the paper negatives were created with the use of a COMTAL/3M Vision 1 digital image processing system. This system uses a black and white video input camera (as opposed to the frame grabber technique) to record and transfer an image into a 512 by 512, 24 bit display. With the use of the real time image

processing system, the input negative images were reversed to positive images. This made the paper imagery easier to view in conjunction with the video tapes. Attempts were also made to enhance the frames of the paper film imagery and 35 mm slides of the video tape imagery with the COMTAL. Contrast stretch, color density slicing, and edge detection were done. Hard copy of the enhancements were made by photographing the CRT screen. It is felt that much detail was lost in this process, negating much of the usefullness of the enhancement process.

Another characteristic of the IR/UV imagery which an image interpreter must be aware of is an apparent variation of image tone intensity with across track angle. Many sections of the imagery, especially the UV, displayed an increase in image tone intensity toward the edges of the swath. This may be caused by either a higher sky radiance in that direction or by increased path radiance since the light path is no longer at the edges of the swath (O'Neil et al, 1983). This change in intensity could be misinterpreted as a thin film of oil. O'Neil suggests that this problem can be rectified by conducting an across track normalization of the scanner data over oil free water. This should be repeated for every flight line but would produce an image that has uniform intensity over the water. An increase in intensity would then be properly interpreted as oil.

The video tapes and paper prints were inspected for portions which contained targets of interest within the study area, such as oil sample locations and surface vessels. Images were chosen where the test flight had been flown in a straight line and at constant altitude. Hard copy of these areas were created using the methods described above. The flight lines containing the areas of interest were plotted on mylar overlays of the study area at a scale of 1:24000. The latitude and longitude of the points along the flight lines were obtained from the annotated paper prints.

The images were compared to the air photos and sketch maps in order to identify as many surface targets as possible. These targets included vessels, wakes, oil areal extent and thickness. The images were annotated with sensor altitude, location of oil sample points, atmospheric and sea state conditions, and solar zenith and azimuth angles.

3.5 IR/UV Image Evaluation Results

It is felt that a complete evaluation of the sensor performance under a wide variety of environmental conditions was not possible for this test. The test flights were not conducted under a wide enough variety of oceanographic and meteorologic conditions to fully evaluate the optimum conditions for using the AIREYE system. The test flights were flown on two days with only slightly different environmental conditions. A representative selection of IR/UV imagery is presented with detailed descriptions of the features identified in them.

10 September, 1984 - AM

The sea state and atmospheric conditions remained fairly constant during the entire set of morning and afternoon runs of September 10. The continuous high cloud cover remained throughout the day with the wind increasing from 0 knots in the morning to 8 knots in the afternoon. This caused a slight amount of wind ruffle on top of the consistent 2 foot swell. A detailed description of the meteorologic and oceanographic conditions is found in Appendix I.

Run 5, 9/10/84, 10:52 - Altitude 2500 Feet.

A combination of original paper negative, positive print of paper imagery (Figure 3-2), photograph of the stop frame video screen (Figure 3-4), and moving video tapes, were used to evaluate the imaging performance of the IR/UV line scanner for run 5. Much more detail was visible on the original paper print negative than any other image product. Figure 3-3 shows the locations of oil samples 2 and 3 along the Boston Whaler wake.

Platform Holly stands out as a rectangular bright spot near the bottom of both the IR and UV imagery. Platform Holly is constantly surrounded by an oil slick (Figure 3-5). This slick area gives a very dark return in the IR image and a range of light tones in the UV image. The oval shaped dark spot near the center top of the IR image, (not visible in the UV image), is the natural gas bubble shown in Figure 3-6. The diagonal dark line running from the upper left to lower right corner of the IR image is the wake of the UCSB Boston Whaler. A short portion of the Boston Whaler wake shows up as a dark streak in the UV image. The dark line to the left of Holly in the IR image is the wake of a small boat moving at approximately 8 or 9 knots. The boat was visible as a bright spot at the end of the wake in run 3 imagery at the same heading and altitude. This boat was not visible in the UV band. The wake of this small boat was visible for more than one half hour in sequential IR images.

Figures 3-8 and 3-9 are photographs of oil samples 2 and 3. It was noted in the field that oil slick with these characteristics broke up into brown foam around the Boston Whaler wake.

In the IR image, the area where samples 2 and 3 were taken shows a brighter response (warmer) than the Boston Whaler wake which has one of the darker tones (cooler) in the image. Oil sample 2 had a measured radiometric temperature of 19.6° C. (+/- .1° C.) with sample 3 measuring 19.7° C.

The slick area containing samples 2 and 3 is very bright in the UV image which would indicate from past studies that this is an area of oil films of less than 2 um thick (O'Neil et al, 1983). Samples 2 and 3 had measured thicknesses of less than .8

um. Figure 3-7 is an aerial photograph of the Boston Whaler at the location of sample 3 and illustrates the response of the thin oil slick in the visible wavelengths.

Run 9b, 9/10/84, 11:18 - Altitude 500 Feet.

The area of run 9b described here contains the locations of oil samples 5, 6, and 7. Again, a combination of hard copy imagery was used to evaluate the imaging performance of the sensor. These image forms included the original paper negative print, positive print of the paper negative (Figure 3-10), zoom of the UV positive print (Figure 3-11), zoom of IR positive print (Figure 3-12) photograph of the stop frame video screen (Figure 3-13), and the moving video screen. The original silver paper negative showed the greatest detail.

The dark line which begins at the bottom center of the IR and UV images, circles in the center, and continues up the left edge, is the wake of the UCSB Boston Whaler. The bright spot at the top of the wake in both bands is the Boston Whaler itself. It difficult to tell what IR image tone corresponds to oil samples 5 and 6 due to their proximity to both a light and dark area of the image. These samples have radiometric temperatures of 15.6° C and 14.9° C ,respectively with similar physical descriptions of rainbow and skin combinations. In the fairly homogeneous area where sample 7 was taken, the IR tone is noticeably lighter than the wake. The temperature in this area of rainbow sheen was measured to be 15.1° C.

The locations of samples 5, 6, and 7 all seem to be located in the brighter areas of the UV image. These samples, with their measured thicknesses of less than .8 um, would be expected to give very bright returns.

September 10, 1984 PM

Run 13, 9/10/84, 13:43 - Altitude 4000 Feet.

Figure 3-18 shows the photograph of the stop frame video image of the area around Platform Holly. Due to lack of detail in this form of hard copy, the original paper negatives and moving video tapes were also used to evaluate the imaging performance of the sensors.

The bright spot near the center of the bottom one third of both IR and UV images is Platform Holly. The dark spot barely visible in the upper one third of the IR image is the natural gas bubble which is a possible false alarm problem in natural seep areas. Another feature visible on the video tape and paper negative is the 65 ft. oil rig crew boat "Smith Tide" anchored to the North West of Platform Holly. Another unknown vessel is a bright spot to the South East of the gas bubble. Neither of these vessels are visible in the UV band. The wake of the UCSB Boston Whaler is the dark line down the center of the image, ending just

east of Platform Holly. The Boston Whaler itself is visible as a bright spot at the end of the wake in the UV band. This was the only time the whaler gave a return in any imagery at this altitude.

It was not possible to locate the oil sample sites along the Boston Whaler wake as was done with the lower altitude imagery. The proximity of the sample locations were not compatible with the scale of the imagery created at the 4000 ft altitude.

September 13, 1984 AM

The environmental conditions for the September 13 morning flights remained fairly constant with clear skies along the coast but scattered clouds two miles off shore. Platform Holly was obscured by clouds in most of the imagery. No oil samples were taken during the morning runs due to radio communication problems between the Boston Whaler and the AIREYE aircraft.

Run 6, 9/13/84, 10:26 - Altitude 10443 Feet.

The moving video tape and relatively poor paper film negative print were the only forms of imagery used for interpretation of this run. Figure 3-19 is a photograph of the stop frame video screen.

Thermal patterns along the coast are apparent. But it is not possible to differentiate between thermal sheer lines (caused by opposing currents known to occur along the coast) and oil slicks. Ellwood pier appears bright in the IR image, with some land detail also visible.

The dynamic range of the UV sensor was not broad enough to image the bright reflectance from the cloud tops and reverses the center of the clouds to dark tones as can be seen on the left side of the UV image in Figure 3-19.

A round trip set of crew boat wakes from Ellwood Pier to Platform Holly were apparent in the IR band of the video tape (not visible in the photograph). Since it is a 12-15 minute trip (one way) with 5-10 minute loading time, the wake scars were detectable for at least 35 minute in the IR images.

September 13, 1984 PM

The environmental conditions for the afternoon runs included 10-15 knot winds from the west, with scattered clouds two miles offshore. Two foot swells were also from the west with .25 foot wind waves.

The oil samples taken during the afternoon runs all recorded a higher radiometric temperature than the sea surface. The oil characteristics were very similar everywhere with streamers of brown particulates as shown in Figure 3-20. The wind and current consolidated the slicks into one type of slick, with none of the

usual wide variety of sheens, skins, and rainbows found on the September 10 test.

The moving video screen was the main source of imagery for analyzing the sensor performance for Run 6. Figure 3-21 is a photograph of the stop frame video screen image, but with much loss of detail compared to the moving video image. The poor image quality is apparent, especially in the UV band. High quality paper negative imagery was not available for this run.

The image covers the area from east of Goleta Point to west of Coal Oil Point. Goleta Pier is readily visible as a bright target in both the IR and UV bands. Platform Holly is also visible as a bright spot in the IR video imagery (this feature is not visible in the Figure 3-21 photograph of the video screen due to loss of detail in the photographic process). Clouds near the top of the imagery are the darkest (coolest) targets in the IR band and as bright as the land in the UV band. Good thermal contrast is visible in the IR band but very little sea surface detail is shown in the UV band.

An unidentified sea surface feature located adjacent to the coast east of Coal Oil Point is visible as a bright feature in both the IR and the UV band. Due to the homogeneous return of this feature in both the IR and UV images, this is probably not an oil slick related feature.

The Boston Whaler wake is not visible in the imagery at this altitude. Therefore, it was not possible to locate the oil sample sites along the wake as was done in the lower altitude imagery.

Run 7, 9/13/84, 14:15, Altitude 500 Feet.

Figure 3-22 is a photograph of the video screen image of a 750 ft container ship. The UV band shows the outline of seven square container compartments on deck, and much bow wave and wake detail. The bright area along the left edge of the UV image is sun glint. The outline of the ship is clear in the IR band, but does not show the deck detail of the UV band.

4. SLAR VERIFICATION TEST

4.1 Sea Surface Operations

During the two days of SLAR flights conducted on October 18 and 19, 1984 two UCSB Boston Whalers used as platforms for 1 m^2 and 10 m^2 trihedral radar reflectors. These reflectors were to be used as targets of known cross-section as a reference for the intensity of the backscattered signal from the extended complex target, the ocean surface (Fung and Ulaby, 1983). The geometry of the trihedral reflector is described in terms of the angles and as shown in Figure 4-1 (Robertson, 1947). The radar cross section is maximum along the axis of symmetry ($\theta = 0^o$, $\xi = 0^o$) and is given by Equation 10:

$$\sigma_{max} = \frac{\pi}{3} \cdot \frac{L^4}{\lambda^2} \qquad (10)$$

where L is the length of each edge of the reflector aperture.

The half-power beam width of sigma is about 30 degrees in θ (for $\xi = 0^o$) and about the same in ϕ (for $\theta = 0^o$).

During the October 18 SLAR test the Boston Whalers were positioned approximately one half mile apart near oil platform Holly. The reflectors were located in positions and orientations to the sensor flight lines as directed by the AESC/AIREYE flight crew. On the October 19 flight test it was not possible for the Boston Whalers to reach the desired test area near platform Holly due to high wind and sea state conditions. As a result, the Whalers were positioned in the area approximately one half mile off the beach between Coal Oil Point and Goleta Point. Again, the reflectors were oriented in directions specified by the AESC/AIREYE flight crew.

Air photos were taken from a Cessna 182 to document the sea state and target positions.

4.2 SLAR Image Interpretation Procedures

GRSU personnel photographed rolled transparencies of the SLAR imagery at the AESC Ontario Airport facility. This was done with the use of a portable light table and 35 mm camera. AESC also provided copies of video tapes of the on board enhancements of the radar imagery, which had been done during the AIREYE flight tests.

Photographic prints of the SLAR transparencies and video tape enhancements were annotated with sensor view angle, slant range, atmospheric and sea state conditions. Sea surface features were identified, including oil platforms, vessels, and oil patterns.

4.3 SLAR Image Evaluation Results

The primary objective of the SLAR flight tests was to test the ability of the system to resolve the trihedral radar reflectors. According to AESC, the larger reflector was detected on at least one of the runs on the first generation video tape and on the real time display. Apparently the second generation video tape provided to the GRSU researchers suffered some contrast reduction and the reflector detection was not apparent. The secondary objective was to evaluate the target detection capability for other targets in the area, such as surface vessels, oil platforms, and oil slicks.

The SLAR imagery was obtained only under one set of environmental conditions, with a very limited amount of sensor characteristic variation, such as altitude and range. Therefore the sensor can only be evaluated under a very limited set of conditions.

Figures 4-2 (run 4 AM) and 4-3 (run 3 PM) are photographs of examples of the rolled negative transparencies of the SLAR imagery created on October 19, 1984. All negative transparencies showed similar streaks in the range direction created by aircraft yaw. The transparencies are also streaked lengthwise along the film.

Figures 4-4 and 4-5 show on board zooms and enhancement of the study area extracted from the large radar transparency in Figure 4-2.

The atmospheric and sea state conditions for this day were very rough as described in Appendix I. The wind speed ranged from 19 to 28 knots, 1 to 2 ft wind waves, and swells up to 6 ft as shown in figure 4-6. The wind and swell direction remained fairly constant in the directions annotated on Figure 4-4. Figure 4-7 is an air photo showing the wind and oil slick patterns visible during the morning runs. Note the similar patterns visible in the morning imagery

4.3.1 SLAR Detection of Man Made Targets

Figure 4-8 shows the location of all known surface targets in the area which have acted as strong radar reflectors in past studies (Kraus, et al, 1977) Descriptions of these targets may be found in Appendix 3. Table 4-1 shows the detection or non detection of the targets for each SLAR image which was analyzed. The trihedral radar reflectors carried on the Boston Whalers were never detected by the SLAR during this set of test runs. Bouys in the area were also not detected. The smallest identifiable target detected in the area is the set of pilings near Ellwood Pier. Bright returns in other areas of the images are possibly vessels of unknown size.

The AIREYE flight log describing the sensor settings, aircraft heading and other data may be found in Appendix IV.

4.3.2 SLAR Detection of Sea Surface Oil

The following is a description of each run of SLAR imagery relative to how well it detected ocean contrast caused by wind or oil slicks. The range orientation across the wind and swells showed more ocean return contrast than up or down the swells and wind. Due to lack of surface verification for oil slicks, it is not known if the contrast in sea surface return is due to wind or oil slicks, with the exception of the area surrounding platform Holly.

Run 1 (10/19/84 AM), Sensor orientation - across wind and swell: Some calm areas are apparent on this image, especially around Platform Holly where oil is known to exist on the surface at all times.

Run 2 (10/19/84 AM), Sensor orientation - across wind and swell: The same calm streak seen in run 1 and the Figure 4-7 air photo is also apparent on this run. The entire area round the oil platforms off Carpinteria shows low return (calm water). This could be caused by shelter from the wind or oil on the water.

Run 3 (10/19/84 AM), Sensor orientation - across swell and wind: Very apparent water contrast streaks.

Run 4 (10/19/84 AM), Sensor orientation - across swell and wind: Platform Holly is surrounded by a streak of low return, similar to the pattern shown in the Figure 4-? air photo. A very low return area also surrounds the oil platforms located off Carpinteria.

Run 5 (10/19/84 AM), Sensor orientation - across wind and swell: Showed same low return streak as seen in air photo. Very low return (calm) east of Santa Barbara around Hilda and Hazel.

Run 1 (10/19/84 PM), Sensor orientation - down wind and swell: Film streaks obscure any possible sea surface patterns.

Run 2, not interpretable.

Run 3 (10/19/84 PM), Sensor orientation - down swell and wind: No apparent sea surface contrast.

Run 4, not interpretable

Run 5 (10/19/84 PM), Sensor orientation - up wind and swell: Some slight surface contrast near platforms.

Run 6 (10/19/84 PM), Sensor orientation - across wind and swell: Slight apparent sea surface contrast near Holly.

Run 7 (10/19/PM PM), Sensor orientation - across wind and swell: Showed very, very slight water contrast but the image was obscured with heavy yaw and film processing streaks.

5. CONCLUSIONS

A Quantitative analysis of the imaging performance of the IR/UV line scanner and SLAR was not possible due to the form of the imagery provided. The system was not tested under a variety of environmental conditions; system capabilities are known only for a limited range of conditions.

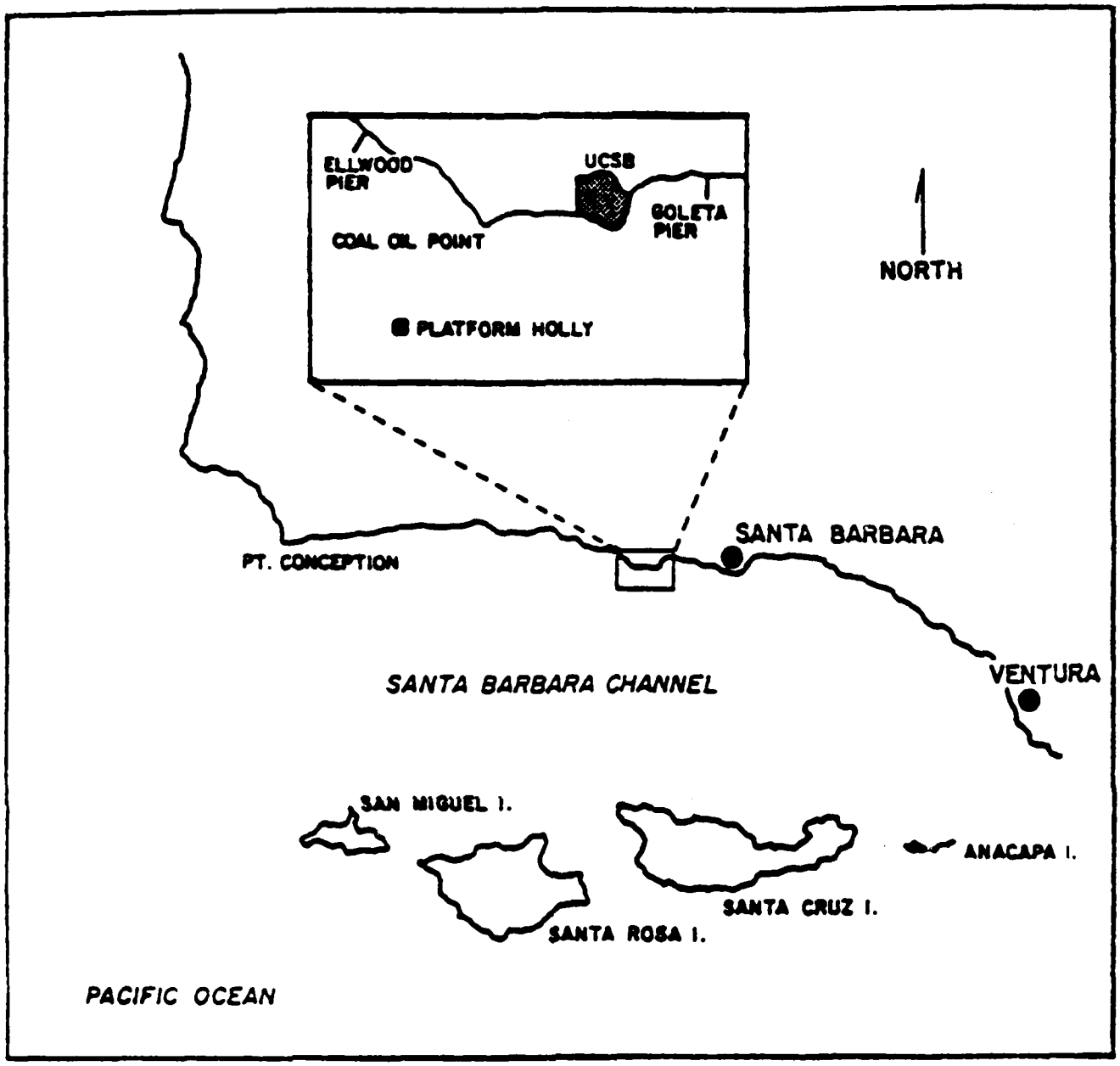

Figure 2-1. Santa Barbara Channel and Coal Oil Point. Location of AESC/USCG AIREYE field tests.

Figure 3-1. Type X oil sampler.

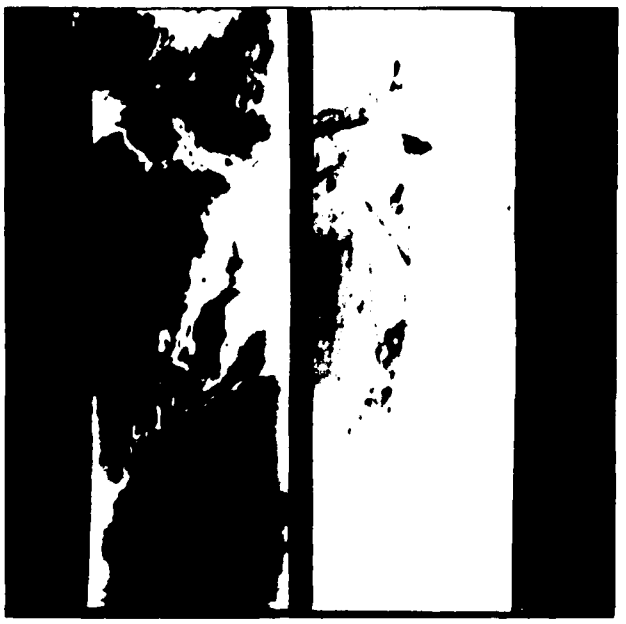

Figure 3-2. Run 5, 9/10/84, 10:52 - Altitude 2500 Feet. Positive print of contrast stretched negative paper print (IR on right, UV on left).

D = DARK IMAGE TONE M = MEDIUM IMAGE TONE L = LIGHT IMAGE TONE

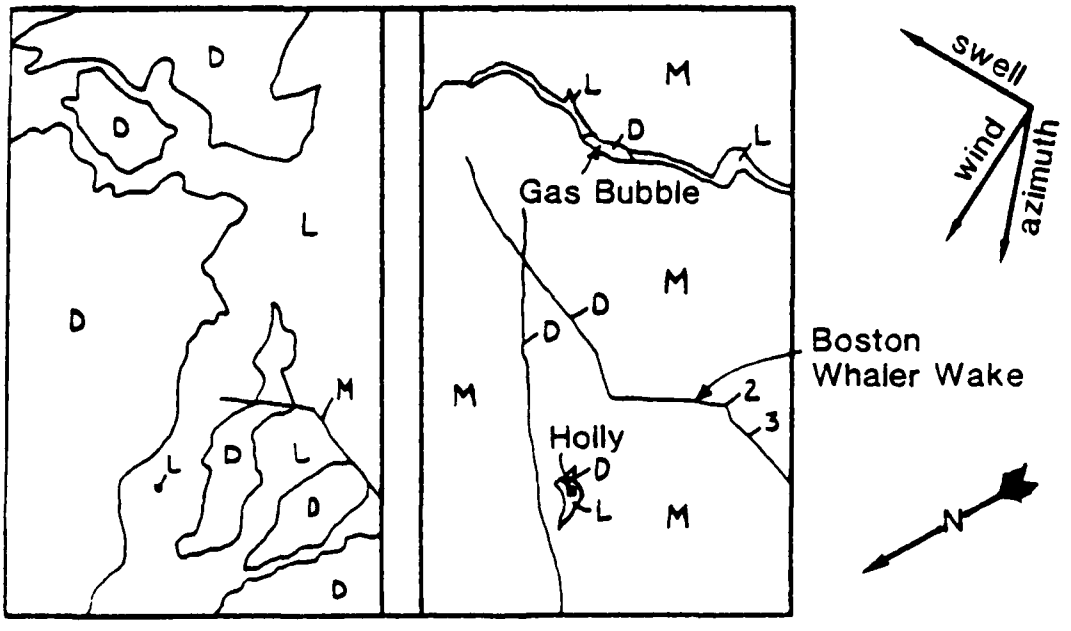

Figure 3-3. Overlay of paper print showing locations of oil samples 2 and 3 (IR on right, UV on left, scale = 1:37989).

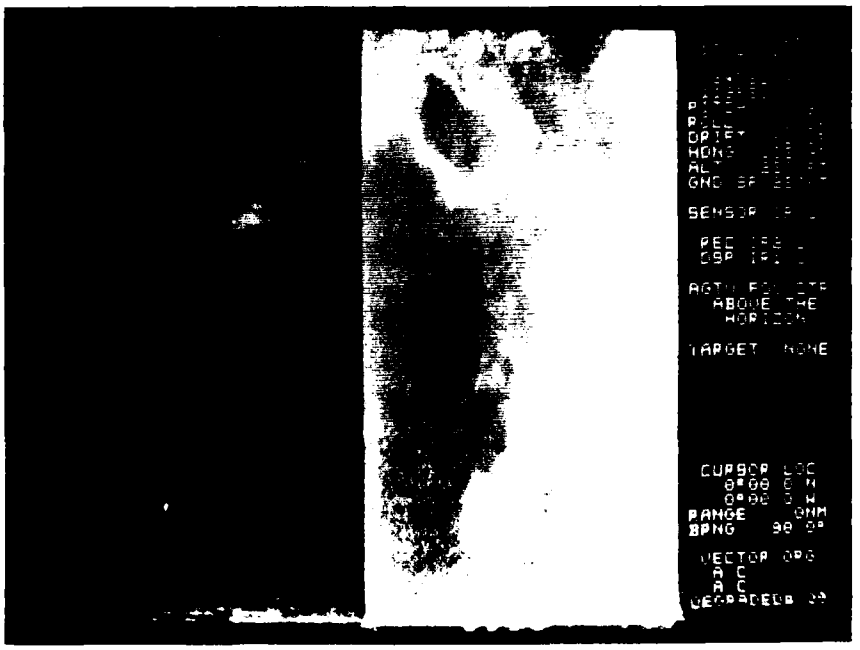

Figure 3-4. Run 5, 9/10/84, 10:52 - Altitude 2500 Feet.
Photograph of stop frame video screen (IR on left, UV on right.)

Figure 3-5. Aerial photograph of platform Holly and surrounding oil.

Figure 3-6. Surface photograph of natural gas bubble.

Figure 3-7. Aerial oblique photograph of Boston Whaler at oil sample location 3, 9/10/84 AM.

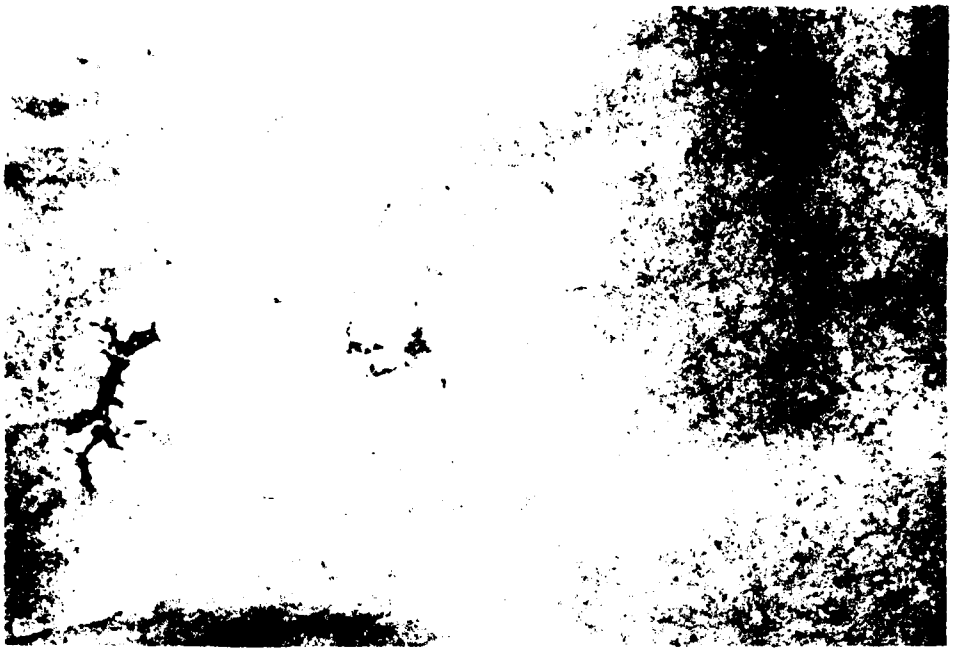

Figure 3-8. Photograph of sea surface characteristics of sample 2 (9/10/84 AM).

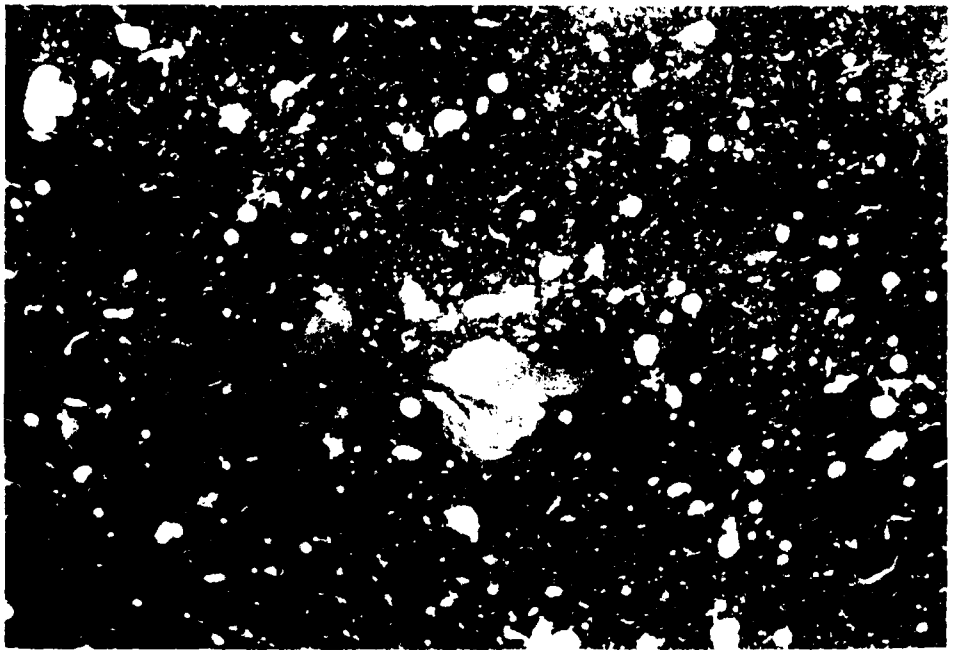

Figure 3-9. Photograph of sea surface characteristics of sample 3 (9/10/84 AM).

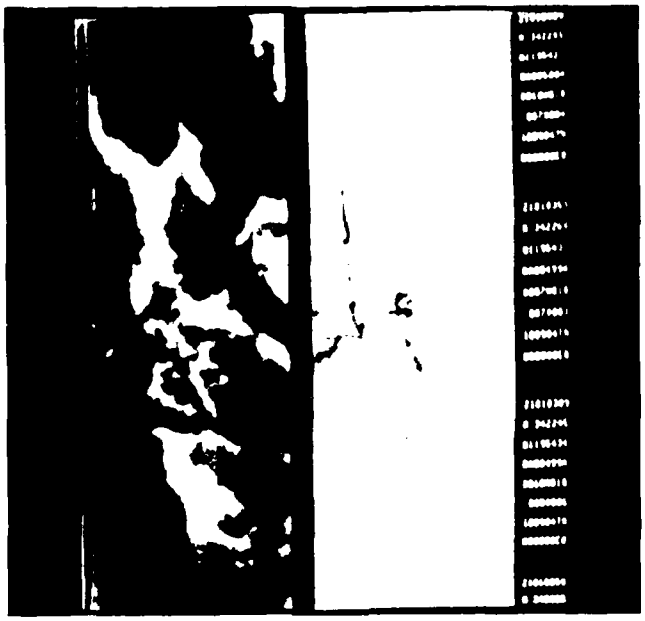

Figure 3-10. Run 9b, 9/10/84, 11:18 - Altitude 500 Feet. Positive print of contrast stretched paper print negative (IR on right, UV on left).

Figure 3-11. Run 9b, 9/10/84, 11:18 - Altitude 500 Feet. COMTAL zoom of UV paper film.

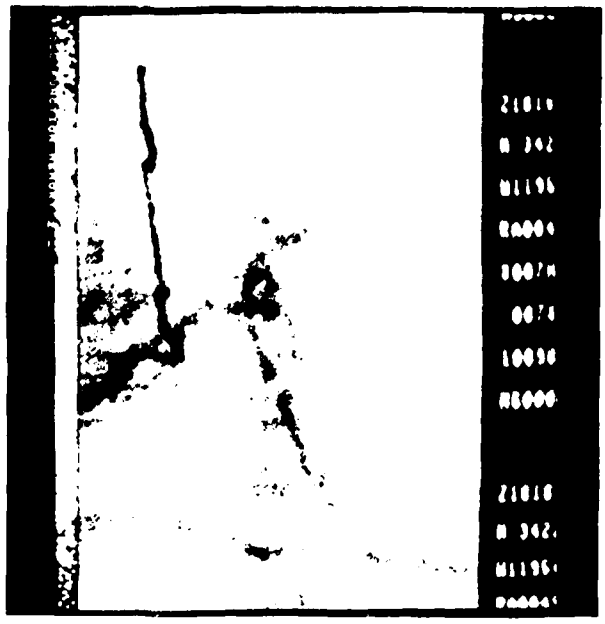

Figure 3-12. Run 9b, 9/10/84, 11:18 - Altitude 500 Feet. COMTAL zoom of IR paper image.

Figure 3-13. Run 9b, 9/10/84, 11:18 - Altitude 500 Feet. Photograph of stop frame video screen (IR on left, UV on right).

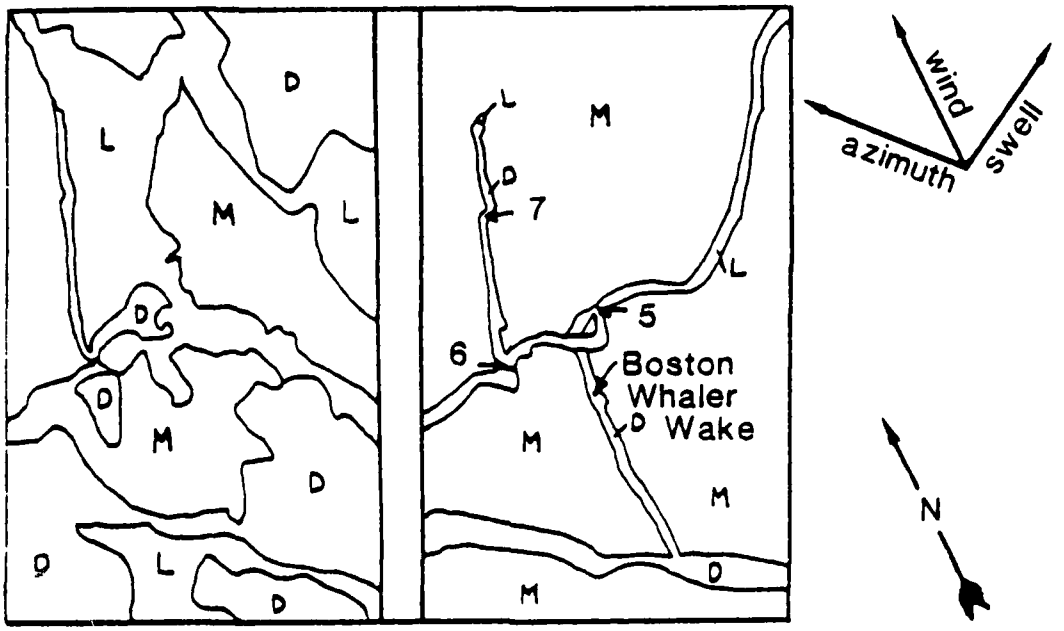

D = DARK IMAGE TONE M = MEDIUM IMAGE TONE L = LIGHT IMAGE TONE

Figure 3-14. Overlay of paper print image showing locations of oil samples 5,6 and 7 (IR on right, UV on left, scale=1:7599)

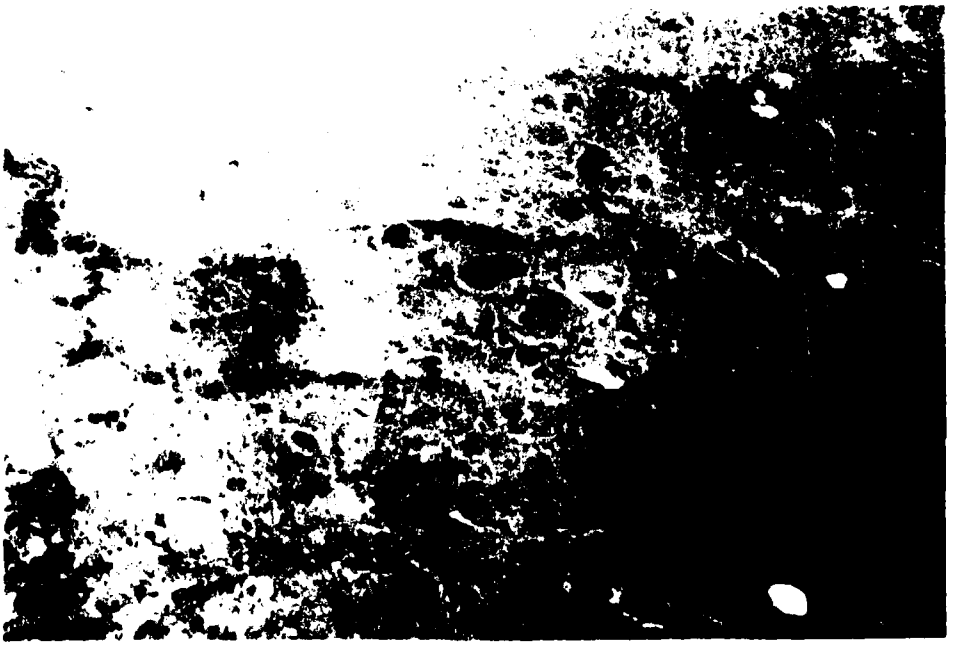

Figure 3-15. Photograph of sea surface characteristics of oil sample 5 (9/10/84 AM).

Figure 3-16. Photograph of sea surface characteristics of oil sample 6 (9/10/84 AM).

Figure 3-17. Photograph of sea surface characteristics of oil sample 7 (9/10/84 AM).

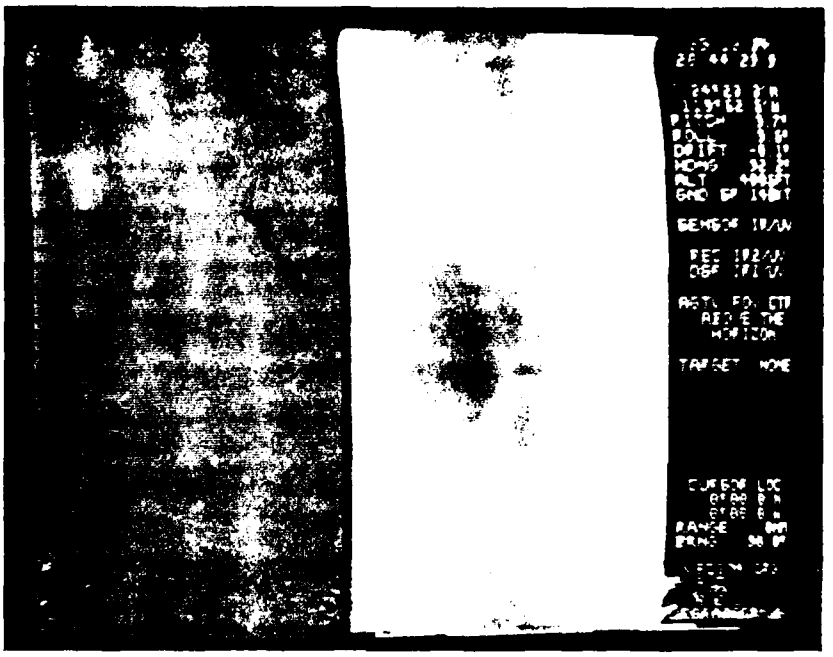

Figure 3-18. Photograph of stop frame video image (IR on left, UV on right).

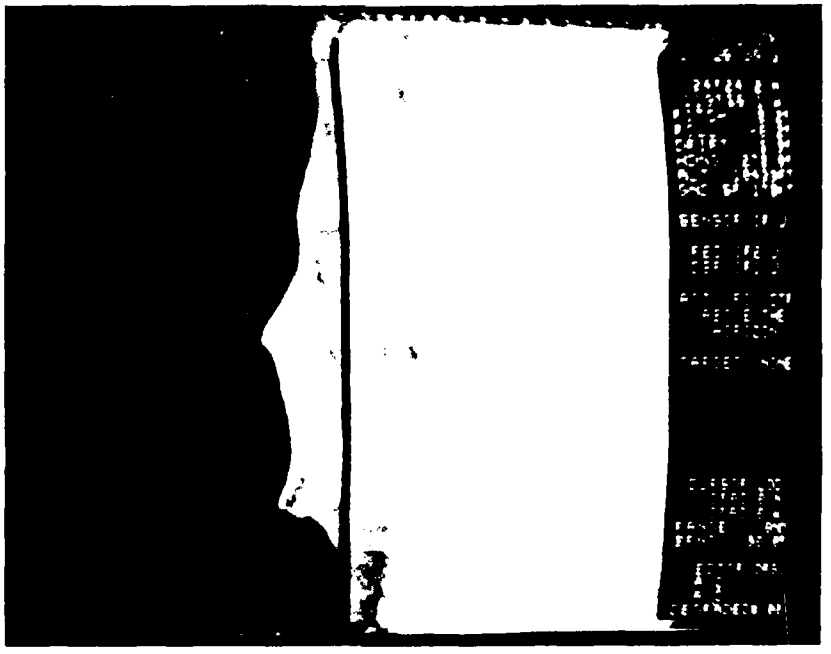

Figure 3-19. Run 6, 9/13/84, 10:26 - Altitude 10443 ft. Photograph of stop frame video screen (IR on left, UV on right).

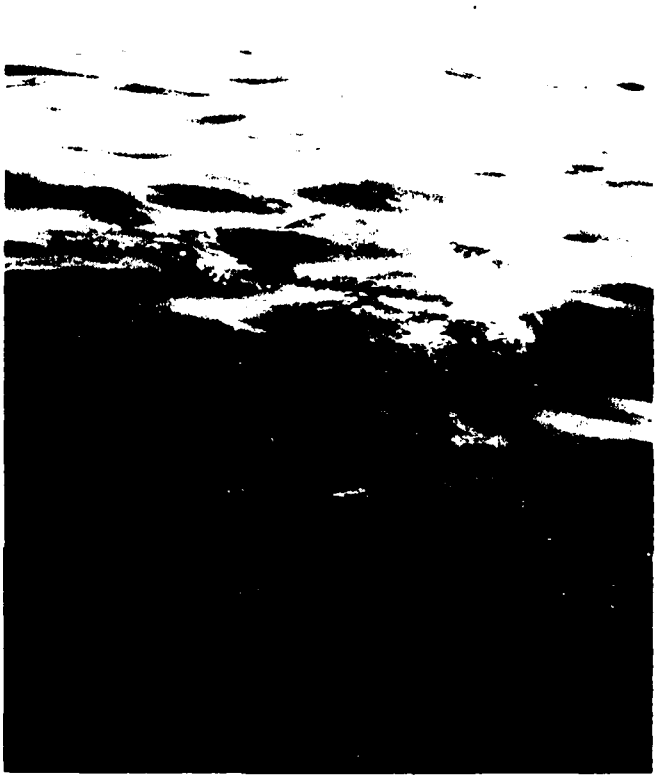

Figure 3-20. Photograph of typical oil slick seen 9/13/84 PM. Run 6, 9/13/84, 14:00 - Altitude 7491 Feet.

Figure 3-21. Run 6, 9/13/84, 14:00 - Altitude 7491 Feet. Photograph of stop frame video screen (IR on left, UV on right).

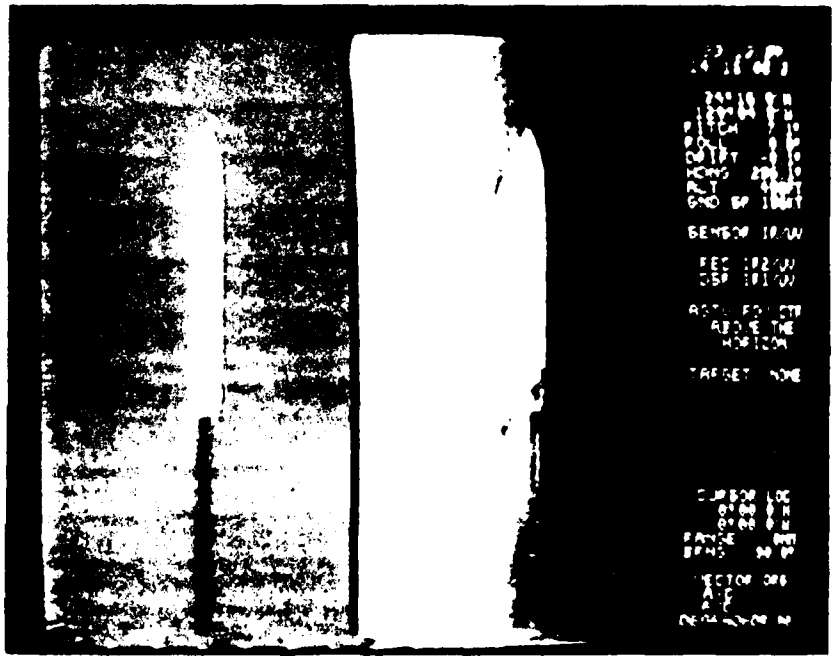

Figure 3-22. Run 7, 9/13/84, 14:15, Altitude 500 Feet. Photograph of stop frame of video screen showing low altitude image of container ship (IR on left, UV on right).

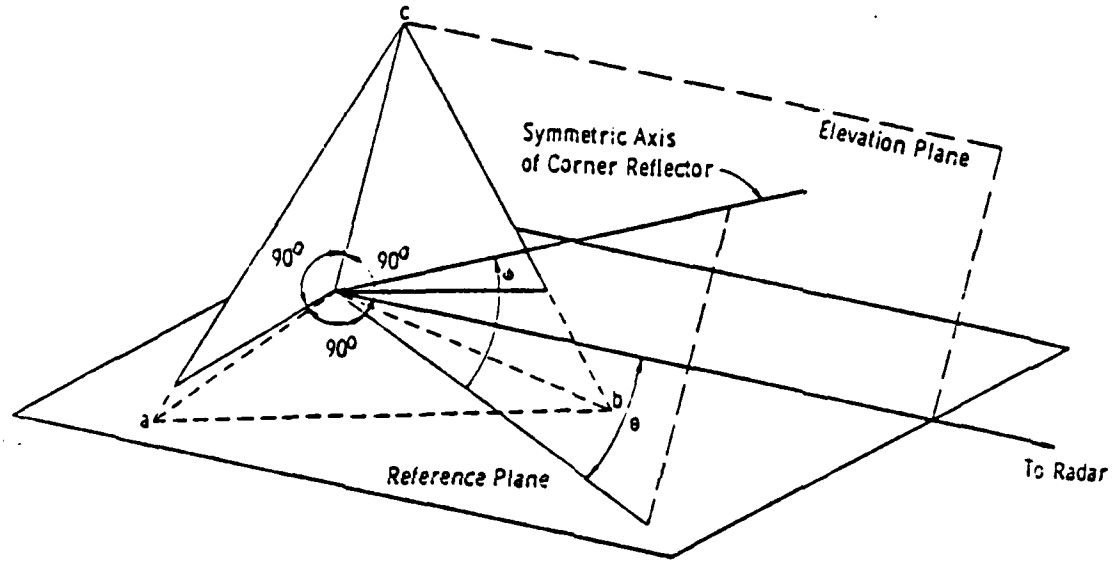

Figure 4-1. Geometry of trihedral radar reflector.

Figure 4-2. Photograph of radar film negative transparency, run 4 AM.

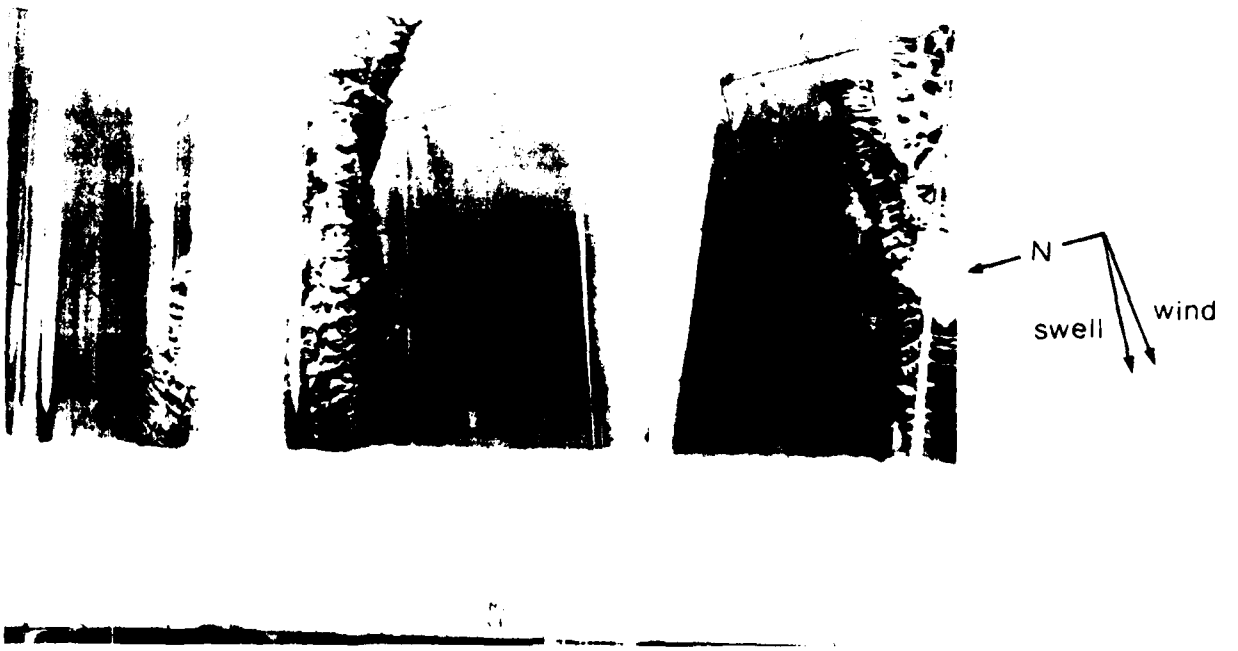

Figure 4-3. Photograph of radar film negative transparency, run 3 PM.

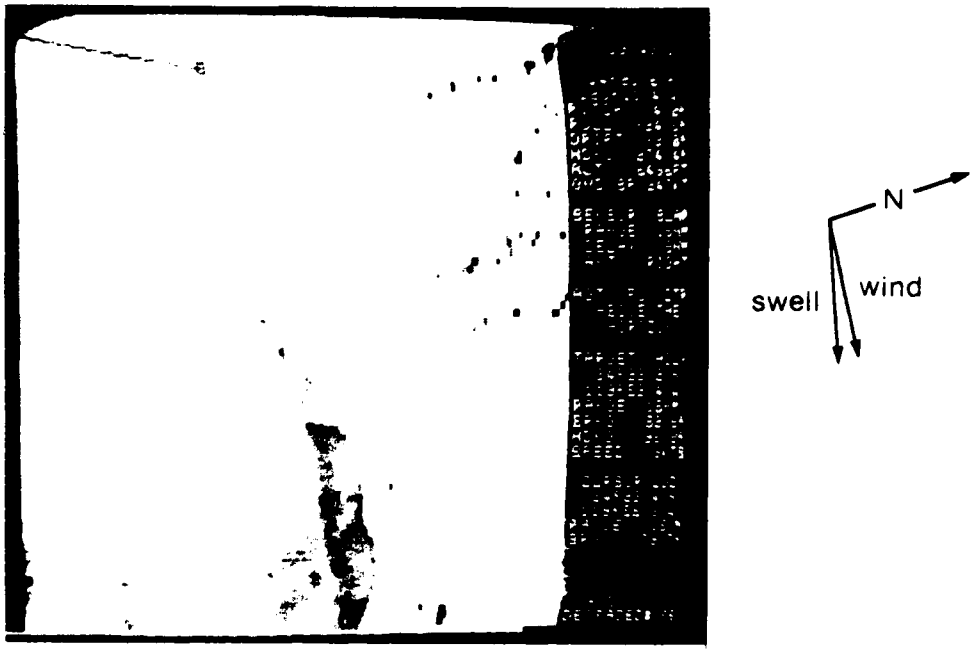

Figure 4-4. Zoom and enhancement of radar image.

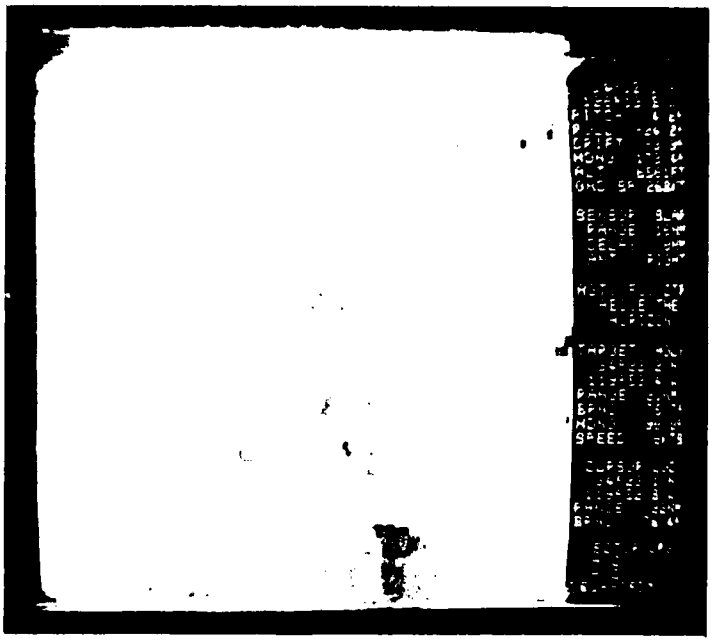

Figure 4-5. Further zoom of radar image.

Figure 4-6. Sea state as seen from Boston Whaler looking toward platform Holly.

Figure 4-7. Air photo of slick conditions on 10/19/84 AM. Note the similar sea surface patterns on the radar imagery.

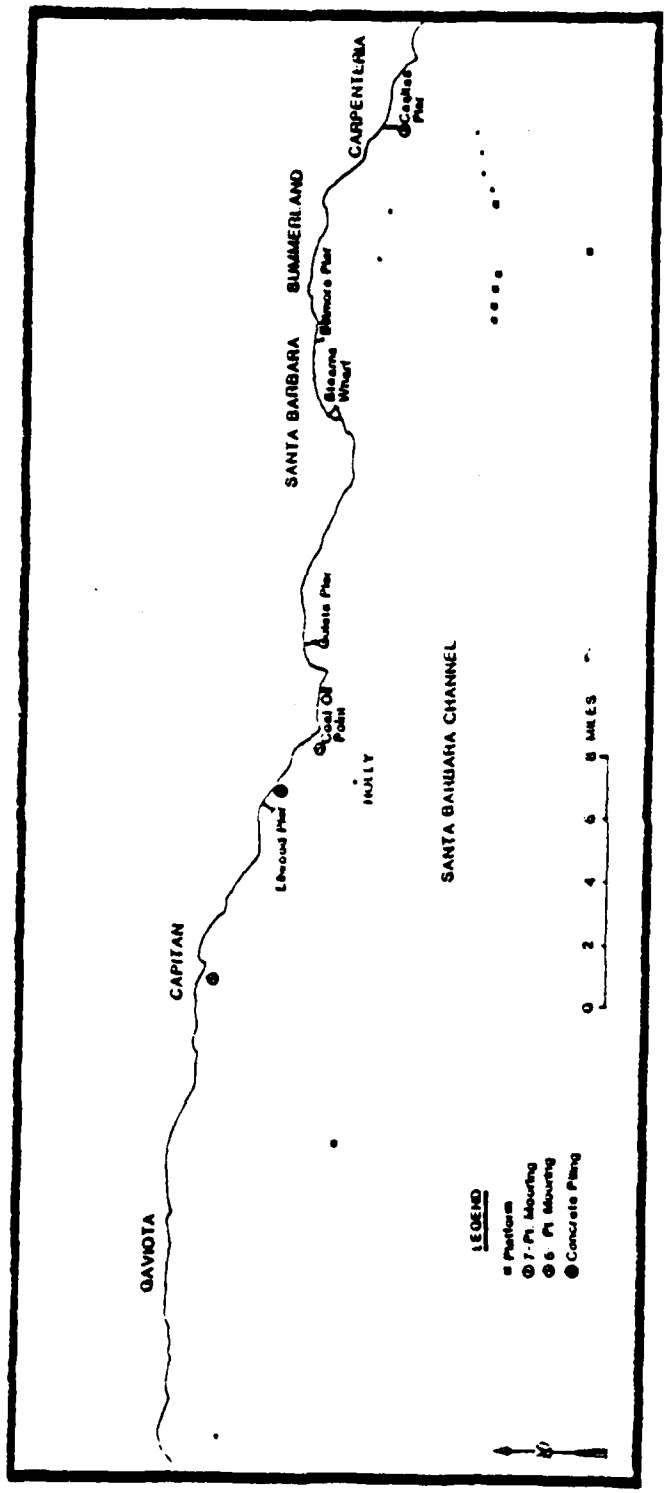

Figure 4-8. Location of surface targets in the study area.

TABLE 2-1

IR/UV LINE SCANNER PERFORMANCE CHARACTERISTICS

CHARACTERISTIC	SPECIFICATION
Field of view	100 degrees
Effective focal length	8.64 centimeters (3.4 inches)
Roll compensation	+/- 15 degrees
Spectral Region	
Infrared	7.8 - 13.8 um
Ultraviolet	.32 - .40 um
Thermal Resolution	
Channel 1, IR low	0.2 deg C
Channel 2, IR high	0.02 deg C
Channel 3, UV	1.5 milliwatt / sq m

Spatial Resolution (milliradians)

Channel 1 (IR low)	2.5	Across-track	2.5	Along-track
Channel 2 (IR high)	18	"	2.5	"
Channel 3 (UV)	5	"	5	"

Table 2-1. Performance characteristics of Texas Instruments RS-18 C IR/UV line scanner.

TABLE 2-2

COMMON EMISSIVITIES

Material	Emissivity
concrete, dry	.71 - .88
glass pane	.87 - .94
wood, planed oak	.90
paint, white	.91 - .95
paint, black	.88 - .95
paint, aluminum	.43 - .55
iron, galvanized	.13 - .28

Table 2-2. Emissivities for some common materials (from Sellers, 1965).

TABLE 2-3

OIL EMISSIVITIES

Oil Type	Emissivity (at 8-14 um)
100 octane fuel	0.973
kerosene	0.968
diesel oil	0.972
SAE 30 oil	0.970
8.6 API residual fuel oil	0.964
44.7 API crude oil	0.973
31.3 API crude oil	0.967
19.5 API crude oil	0.972
fish oil	0.959

Table 2-3. Emissivities for oil types (from Horvath et al, 1971).

AD-A166 755 DESIGN DEVELOPMENT AND INTEGRATE/INSTALL AN AIRBORNE 3/3
REMOTE INSTRUMENTATI.. (U) AEROJET ELECTROSYSTEMS CO
AZUSA CA J J BOMMARITO ET AL AUG 85 7921 USCG-D-27-85
UNCLASSIFIED DTCG23-80-C-20012 F/G 1/3 NL

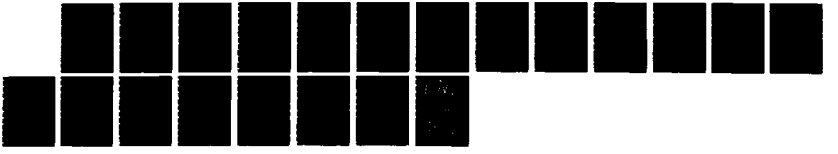

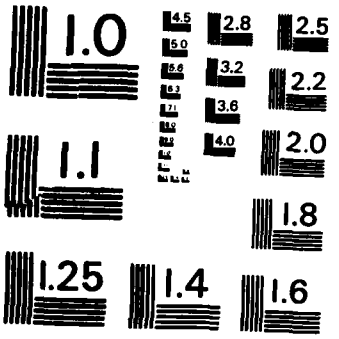

TABLE 2-4

PETROLEUM TYPES

Volatility	Absorbtion	Petroleum Type
High	High	Most fresh crudes
High	Low	Fuels, very light crudes
Low	High	Residuals, very heavy crudes, all aged crudes
Low	Low	Light lube oils

Table 2-4. Categorization of petroleum types (from Horvath, 1974).

TABLE 2-5

POTENTIAL FALSE OIL TARGETS

Spectral Region	False Alarms
Radar (X band)	fish oil slicks wind slicks kelp/debris dense cloud cells
UV (.32-.4 um)	fish oil slicks suspended solids shallow water broken cloud cover
Thermal IR (8-14 um)	fish oil slicks ship wakes effluents upwelling

Table 2-5. Summary of phenomena which are potential false targets (may mistakenly be identified as oil spills) to various sensors (from Edgerton et al, 1973).

TABLE 3-1.

Oil Sample Descriptions for IR/UV Test
9-10-84 AM

Sample #	Thickness (mm)	Radiometric Temp (Deg. C)*	Oil Sample Description
1	<.0008	17.8	rainbow sheen
2	<.0008	19.6	continuous cover, some rainbow
3	<.0008	19.7	rainbow confetti
4	.0011	16.3	marbled sheen
5	<.0008	15.6	rainbow sheen, slight skin
6	<.0008	14.9	very thick skin, marbled rainbow
7	<.0008	15.1	continuous rainbow sheen
8	.0018	12.9	continuous skin
9	.0064	12.3	rainbow, filament, and marbled

* Radiometric temperature is +/- 0.1 degree C.

TABLE 3-2.

Oil Sample Descriptions for IR/UV Test
9/10/84, PM

Sample #	Thickness (mm)	Radiometric Temp (Deg C)*	Oil Sample Description
1	<.0008	20.1	rainbow banding
2	<.0008	20.8	rainbow banding, skin
3	<.0008	19.4	chocolate mousse, rainbow (wide variety)
4	.0015	19.2	patchy sheen, little chocolate mousse
5	.0037	21.0	thick skin
6	<.0008	22.5	small globules and filaments, some sheen

* Radiometric temperature is +/- 0.1 degree C

TABLE 3-3

Oil Sample Description for IR/UV Test
9/13/84 PM

Sample #	Thickness (mm)	Radiometric Temp (Deg C)*	Oil Sample Description
1	.0009	23.1	Brown streamers, light to heavy
2	.0056	22.9-23.6	Continuous streamers, some chocolate mousse
3	<.0008	26.2	Thick sheen, brown filaments, and small light brown clumps
4	<.0008	24.5	Lumpy sheen with light skin
5	<.0008	24.5	Sheen with sprinkles of light brown particulates
6	<.0008	15.1	Very thin rainbow sheen, patches of sprinkled particulates

* Radiometric temperature is +/- 0.1 degree C

TABLE 4-1

SLAR DETECTION TARGETS

OIL PLATFORMS - 10/19/84 AM

PLATFORM NAME	RUN NUMBER 1	2	3	4	5
HONDO	D	OB	#	D	D
HOLLY	D	D	D	D	D
HILDA, HAZEL	OB	D	D	D	D
A,B,C, HILLHOUSE	OB	D	D	D	D
ROW OF 5*	OB	D	D	D	D
HABITAT	OB	D	#	D	D
HELEN	#	#	#	#	D

D = Detected in SLAR imagery.
PD = Possible detection in SLAR imagery.
ND = Target located in area of image but not detected by SLAR.
OB = Obscured by yaw or film streaks, or imagery lat/lon lines.
# = Target not located in area imaged.

* Row of five includes Platforms Henry, Houchin, Hogan, Hope, and Heidi.

TABLE 4-1 (CONT.)

SLAR DETECTION TARGETS

PIERS AND MOORINGS - 10/19/84 AM

	Ellwood Pier	Goleta Pier	Stearns Wharf
Run 1	D	D	ND
Run 2	D	D	D
Run 3	D	D	D
Run 4	D	D	D
Run 5	D	D	D

D = Detected in SLAR imagery.
PD = Possible detection in SLAR imagery.
ND = Target located in area of image but not detected by SLAR.
OB = Obscured by yaw or film streaks, or imagery lat/lon lines.
# = Target not located in area imaged.

TABLE 4-1 (CONT.)

SLAR DETECTION TARGETS

OIL PLATFORMS - 10/19/84 PM

PLATFORM NAME	RUN NUMBER 1	2	3	4	5	6	7
HONDO	D	/	D	/	D	#	OB
HOLLY	D	/	D	/	D	D	D
HILDA, HAZEL	D	/	D	/	D	#	D
A,B,C, HILLHOUSE	D	/	D	/	D	#	D
ROW OF 5	D	/	D	/	D	#	D
HABITAT	D	/	D	/	D	#	D
HELEN	D	/	D	/	D	#	#

D = Detected in SLAR imagery.
PD = Possible detection in SLAR imagery.
ND = Target located in area of image but not detected by SLAR.
OB = Obscured by yaw or film streaks, or imagery lat/lon lines.
# = Target not located in area imaged.
/ = Uninterpretable

* Row of five includes : Henry, Houchin, Hogan, Hope, and Heidl.

TABLE 4-1 (CONT)

PIERS AND MOORINGS - 10/19/84 PM

	Ellwood Pier	Goleta Pier	Stearns Wharf
Run 1	ND	OB	D
Run 2	uninterpretable		
Run 3	OB	ND	D
Run 4	uninterpretable		
Run 5	D	#	D
Run 6	D	D	D
Run 7	D	OB	D

D = Detected in SLAR imagery.
PD = Possible detection in SLAR imagery.
ND = Target located in area of image but not detected by SLAR.
OB = Obscured by yaw or film streaks, or latitude/longitude lines.
# = Target not located in area imaged.

APPENDIX I

Meteorologic Data for IR/UV Test, 9/10/84 AM

Sample #	Time	Cloud Cover (%)	Cloud Height (ft)	Wind Dir/knots	Air Temp (degree C)
1	10:17-10:25	100	4300	135/4	24.0
2	10:33-10:39	98	4300	142/2	24.0
3	10:41-10:44	98	4300	140/2	24.5
4	10:57-11:01	99	4300	155/4	24.5
5	11:03-11:07	99	4300	165/4	24.5
6	11:08-11:11	99	4300	155/4	24.5
7	11:14-11:16	99	4300	165/2	24.5
8	11:26-11:31	100	4300	165/5	25.0
9	11:32-11:36	100	4300	185/5	25.0

Oceanographic Data for IR/UV Test, 9/10/84 AM

Sample #	Time	SST (Deg C.)	Wave Height (ft)	Swell Height (ft)	Swell Direction	Swell Period (sec)
1	10:17-10:25	20.0	0	2-4	225	10-11
2	10:33-10:39	20.0	0	2-4	225	10-11
3	10:41-10:44	20.0	0	2-4	225	10-11
4	10:57-11:01	20.0	0	2-4	225	10-11
5	11:03-11:07	20.0	0	2-4	225	10-11
6	11:08-11:11	20.0	0	2-4	225	10-11
7	11:14-11:16	20.0	0	2-4	225	10-11
8	11:26-11:31	20.0	0	2-4	225	10-11
9	11:32-11:36	20.0	0	2-4	225	10-11

APPENDIX I (CONT.)

Meteorologic Data for IR/UV Test, 9/10/84 PM

Sample #	Time	Cloud Cover (%)	Cloud Height (ft)	Wind Dir/knots	Air Temp (degree C)
1	13:44-13:51	90	4000	210/8	26.5
2	13:52-13:56	85	4000	220/8	26.5
3	14:00-14:04	85	4000	220/8	26.5
4	14:06-14:10	90	4000	230/10	26.5
5	14:18-14:24	90	4000	220/11	26.5
6	14:32-14:40	80	4000	250/11	26.0

Oceanographic Data for IR/UV Test, 9/10/84 PM

Sample #	Time	SST (Deg C.)	Wave Height (ft)	Swell Height (ft)	Swell Direction	Swell Period (sec)
1	13:44-13:51	20.0	0	2-4	225	10-11
2	13:52-13:56	20.0	0	2-4	225	10-11
3	14:00-14:04	20.0	0	2-4	225	10-11
4	14:06-14:10	20.0	0	2-4	225	10-11
5	14:18-14:24	20.0	0	2-4	225	10-11
6	14:32-14:40	20.0	0	2-4	225	10-11

APPENDIX I (CONT.)

Meteorologic Data for IR/UV Test, 9/13/84 PM

Sample #	Time	Cloud Cover (%)	Cloud Height (ft)	Wind Dir/knots	Air Temp (degree C)
1	13:30-13:37	0	-	252/15	24.5
2	13:40-13:44	0	-	252/13	24.5
3	13:49-13:51	5-10	-	245/12	24.5
4	13:54-14:00	10	-	260/12	24.5
5	14:08-14:12	5	-	263/10	25.0

Oceanographic Data for IR/UV Test, 9/13/84 PM

Sample #	Time	SST (Deg C.)	Wave Height (ft)	Swell Height (ft)	Swell Direction	Swell Period (sec)
1	13:30-13:37	21.0	.25	2	225	6-7
2	13:40-13:44	21.0	.25	2	225	6-7
3	13:49-13:51	21.0	.25	2	225	6-7
4	13:54-14:00	21.0	.25	2	225	6-7
5	14:08-14:12	21.5	.25	2	225	6-7

APPENDIX I (CONT.)

Meteorologic/Oceanographic Data for Radar Reflector Test, 10/19/84

Time	Cloud Cover (%)	Wind Direction (kts)	Wave Height (ft)	Swell Height (ft)	Swell Direction	Swell Period
10:31	85	270/19	1-2	3-5	270	5-6
10:35	85	260/20	1-2	5-6	270	5-6
13:26	0	260/28	1-2	5-6	225	5-6
13:30	0	260/26	1-2	3-5	225	5-6
14:10	0	250/24	1-2	5-6	225	5-6

APPENDIX II

GRAVIMETRIC OIL MEASUREMENT TECHNIQUE

The gravimetric oil thickness measurement technique begins with the addition of 500 ml of Mallinckrodt grade A.R. hexane to the jar containing an oil sample soaked sorbent pad. The jar and pad are allowed to stand, sealed, for at least 24 hours. Each pad is then squeezed dry twice (using rubber gloves over a large Buchner funnel with several rinses of both gloves and funnel). The combined extract and rinse is dried with approximately one gram of anhydrous sodium sulfate to remove entrained water. After drying, the solution is gravity filtered through fluted paper into a two liter distillation flask. The majority of the solvent is removed by rapid distillation through a 70 cm vigreux column to a residual volume of approximately 20 ml. Distillation is used rather than the evaporation process used in the past. The distilled solvent is saved for use on subsequent runs which improves the cost efficiency of the procedure and allows a much smaller amount of hydrocarbons to be released into the air. The remaining solution is transferred, along with three 2 ml rinses, to a tared 50 ml round bottom flask. The volume is further decreased by rotary evaporation on a Buchi Rotovapor-R using a water aspirator. The residue is then placed under vacuum (1 torr) until the weight stabilizes (approximately 1 min). The flask is weighed and the weight recorded to the nearest milligram.

The measured weight, W_m, of the oil samples are then converted true weight, W, using a set of correction factors. These factors are W_b, the weight of solvent extractable material in a clean sorbent pad and W_r, the residual weight of oil remaining in a sorbent pad after the extraction process. The W_b correction term is determined by processing three clean sorbent pads with the same process described above. The average value for this term in this study was found to be .38 gm/ft^2 +/- .89 gm/ft^2 (using student t distribution for small sample size).

The W_r correction term is determined by soaking three clean sorbent pads with quantities of paraffin oil, distilled from potassium carbonate, which have been weighed to the nearest milligram in a tared 50 ml Erlynmeyer flask. These pads are processed as described above and the weight of extracted oil compared to the known weight of oil introduced to the pad, with a correction for the weight of extractable material in a clean pad. The average residual weight of extracted oil, W_r, was calculated to be .032 gm/ft^2 +/- .061 gm/ft^2 (using student t distribution for small sample size).

Once the true weight of absorbed oil, W, has been established, the oil film thickness is computed using equation 1.

$$t = \frac{10\,[W_m + (W_r - W_b)A_1]}{dA} \qquad (1)$$

where:

t = average oil film thickness, mm
A_1 = area of sorbent pad, 2.25 ft
A = area of oil slick sampled, 1194.6 cm^2
d = oil density, 0.93 gm / cm^3 which is calculated using equation 2.

$$d = (141.5/131.5) + \text{API gravity} \qquad (2)$$

where:

API(American Petroleum Institute) gravity of Ellwood Crude collected from natural seep in the study area = 20.9 (as measured by ARCO Oil and Gas on September 12, 1984).

APPENDIX III

SLAR SEA-SURFACE TARGET DETECTION

Oil Platforms

Platform Name	Location	Dimensions	Materials
Hazel	Off Summerland	100' x 110' x 95'	Steel
Heidi	Off Carpinteria	100' x 110' x 95'	Steel
Helen	Off Gaviota	80' x 100' x 80'	Steel
Hilda	Off Summerland	110' x 110' x 95'	Steel
Hillhouse	Off Summerland	110' x 125' x 99'	Steel
Hogan	Off Carpinteria	121' x 125' x 99'	Steel
Holly	Off Coal Oil Point	80' x 125' x 84'	Steel
Hondo	Off Gaviota	186' x 76' x 145'	Steel
Hope	Off Carpinteria	110' x 110'x 95'	Steel
Houchin	Off Carpinteria	123' x 125' x 99'	Steel
Union A	Off Summerland	112' x 134' x 99'	Steel
Union B	Off Summerland	112' x 134' x 99'	Steel
Union C	Off Summerland	112' x 134' x 99'	Steel
Henry	Off Carpinteria	unknown	Steel
Habitat	Off Summerland	unknown	Steel

Piers and Wharfs

Name	Location	Dimensions	Materials
Biltmore Pier	SE of Santa Barbara	500'x30'x20'	Wood
Casitas Pier	SE of Carpinteria	750'x40'x25'	Concrete and Wood
Ellwood Pier	S of Ellwood	2000'x160'x25'	Wood
Abandoned Pilings	S of Ellwood	45'x25'x20'	Concrete
Goleta Pier	Goleta Beach	1000'x30'x20'	Wood
Stearns Wharf	Santa Barbara	1445'x76'x16'	Wood

APPENDIX IV

AIREYE Flight Log for 10/19/84 AM SLAR Runs.

Run	Time	Alt. (km)	Ground Speed (kts)	Orientation to Waves	Display Range	Heading	Offset (mi)
1	17:05	5.5	250	up trough	27/10	285	5
2	17:14	6.5	250	up trough	27/20	091	10
3	17:35	6.5	256	up trough	27/10	225	5
4	17:47	6.5	253	up trough	27/20	094	10
5	17:54	6.5	250	up trough	27/10	281	7.5

AIREYE Flight Log for 10/19/84 PM SLAR Runs.

Run	Time	Alt. (km)	Ground Speed (kts)	Orientation to Waves	Display Range	Heading	Offset (mi)
1	20:33	5.5	250	back waves	27/10	2.5	5
2	20:38	5.5	250	front waves	27/10	200	7.5
3	20:46	5.5	250	back waves	27/10	8.8	2.5
4	21:00	5.5	250	into waves	27/10	11	5
5	21:07	5.5	250	back waves	27/10	196	2.5
6	21:13	5.5	250	up trough	27/10	287	5
7	21:24	10.5	250	up trough	27/10	2	5

BIBLIOGRAPHY

Alfoldi, T.T., 1982. "Analysis of Remote Sensing Data Collected for Detection and Mapping of Oil Spills," Report No. NAS 1.26:165886; NASA-CR-165886, INTERA Environmental Consultants Ltd., Ottawa, Canada.

Allen, Alan A. and John E. Estes, 1970. "Detection and Measurement of Oil Films," In Santa Barbara Oil Symposium, ed. Robert W. Holmes and Floyd A. DeWitt, Jr.,pp. 47-74, University of California, Santa Barbara.

Ballard, Dana H. and Christopher M. Brown, 1982. Computer Vision, p. 523, Prentice Hall, Inc., New Jersey

Catoe, C.E. and J.T. McLean, 1979. "A Multispectral Look at Oil Pollution Detection, Monitoring, and Law Enforcement," Report no. NASA-TM-80573, p. 25, National Aeronautics and Space Administration, Goddard Space Flight Center, Greenbelt, Md..

Catoe, Clarence E., 1973. "Remote Sensing Techniques for Detecting Oil Slicks," Journal of Petroleum Technology 267-276

Chan, H.L. and A.K. Fung, 1977. "A Theory of Sea Scatter at Large Incident Angles," Journal of Geophysical Research 82:3439-3444

Edgerton, A.T., J.J. Bommarito, R.S. Schwantje, and D.C. Meeks, 1973. "Development of a Prototype Airborne Surveillance System - System Definitions Studies," Report no. AESC-1812-1; USCG-D-90-75, p. 271, Aerojet ElectroSystems Co. for Department of Transportation, U.S. Coast Guard Office of Research and Development.

Estes, John E., Paul Mikolaj, and Randolph R. Thaman, 1972. Determination of Oil Loss Rates from a High Seas Oil Containment Barrier, p. 71, U.S. Coast Guard Department of Transportation, Washington, D.C..

Fung, Adrian K. and Fawaz T. Ulaby, "Matter-Energy Interaction in the Microwave Region" In Manual of Remote Sensing, ed. D.S. Simonett and F.T. Ulaby, Vol. 2, pp. 115-164, American Society of Photogrammetry, Falls Church, Virginia.

Horvath, R., W.L. Morgan, and S.R. Stewart, 1971. "Optical Remote Sensing of Oil Slicks: Signature Analysis and Systems Evaluation," Report no. 27660-17-F, p. 117, Willow Run Laboratories, University of Michigan for the U.S. Coast Guard, Office of Research and Development, Ann Arbor, Michigan.

Horvath, Robert, 1974. Interpretation Manual for the Airborne Remote Sensor System, p. 99, Dept. of Transportation, United States Coast Guard.

Kraus, S.P., J.E. Estes, and R.R. Vollmers, 1977. "Comparative Evaluation of Real and Synthetic Aperture Radars for the Detection of Oil Pollution in the Santa Barbara Channel," In *Proceedings of the 1977 Oil Spill Conference (Prevention, Behavior, Control, Cleanup)*, pp. 203-208, American Petroleum Institute, New Orleans.

Kraus, S.P. and J.E. Estes, 1977. "Oil Seep Survey over Coal Oil Point and Santa Barbara Channel, California, October 1976," In *California Offshore Gas, Oil, and Tar Seeps*, pp. 323-326, State Lands Commission.

Kraus S.P., R.W. Tennant, and C. Hansen, January, 1979. *Surface Oil Displacement by U.S. Coast Guard 82-Foot Cutters*, p. 76, Geography Remote Sensing Unit, University of California, Santa Barbara.

Long, M.W., 1975. *Radar Reflectivity of Land and Sea*, p. 366, Heath and Co., Lexington, Ma..

Meisner, Douglas E., 1985. "Fundamentals of Airborne Video Technology," *Technical Papers, 51st Annual Meeting, American Society of Photogrammetry* 2:828-843

Mikolaj, Paul G., Alan A. Allen, and Roger S. Schlueter, 1972. "Investigation of the Nature, Extent and Fate of Natural Oil Seepage off Southern California," In *Offshore Technology Conference*, pp. 1365-1376.

O'Neil, R.A., R.A. Neville, and Vince Thomson, 1983. *The Arctic Marine Oil Spill Program Remote Sensing Study*, p. 257, Environment Canada, Ottawa (Ontario), Canada.

Robertson, S.D., 1947. "Targets for Microwave Radar Navigation," *Bell Systems Technology Journal* 26:852-896.

Sellers, William D, 1965. *Physical Climatology*, p. 272, University of Chicago Press, Chicago.

Straughan, D.S. and B.C. Abbott, 1971. *Water Pollution by Oil*, ed. P. Hepple, pp. 257-262, Institute of Petroleum, London.

END

DTIC

5-86